

AN ABSTRACT OF THE THESIS OF

Philipp Keller for the degree of Master of Science in Civil Engineering presented on  
June 13, 2012.

Title: Wind Induced Torsional Fatigue Behavior of Truss Bridge Verticals

Abstract approved: \_\_\_\_\_

Christopher C. Higgins

The Astoria-Megler Bridge is a 6.6 kilometer (4.1 mile) long bridge, connecting Oregon and Washington on US 101, with a continuous steel truss main span of 376 m (1232 ft). It is the second longest main span bridge of this type in the world. Due to vortex shedding, some of the long truss verticals exhibit wind-induced torsional vibrations. These vibrations can create large numbers of repeated stress cycles in the truss verticals and the gusset plate assemblies. The members and connections were not designed for such conditions and the impact of this behavior on the service life of the bridge is uncertain.

A full-scale representation of one of the truss verticals observed to exhibit such wind induced torsional response was fabricated and tested in the Structural Engineering Research Laboratory at Oregon State University. Experimental data of the rotational behavior and the stress distribution along the vertical were collected using inclinometers, an angular rate sensor, and uniaxial and rosette strain gages. The data collected were compared with existing analytical methods and predictions from finite element models. The observed experimental results including twist angle, stress distribution, and stress magnitude were well captured by both the finite element model and the analytical equations. Using analytical expressions, the fatigue lives of the existing bridge verticals were predicted based on assumed storm duration and recurrence.

©Copyright by Philipp Keller

June 13, 2012

All Rights Reserved

WIND INDUCED TORSIONAL FATIGUE BEHAVIOR OF TRUSS BRIDGE  
VERTICALS

by

Philipp Keller

A THESIS

submitted to

Oregon State University

in partial fulfillment of

the requirements for the

degree of

Master of Science

Presented June 13, 2012

Commencement June 2013



Master of Science thesis of Philipp Keller presented on June 13, 2012

APPROVED:

---

Major Professor, representing Civil Engineering

---

Head of the School of Civil and Construction Engineering

---

Dean of the Graduate School

I understand that my thesis will become part of the permanent collection of the Oregon State University libraries. My signature below authorizes release of my thesis to any reader upon request.

---

Philipp Keller

## ACKNOWLEDGEMENTS

I would like to thank Dr. Christopher Higgins for the great opportunity to study in the United States, and for providing exactly the right balance of challenge, advice, and encouragement.

I would also like to thank the Oregon Department of Transportation for providing funding for this research project.

Thanks go to my thesis committee members, Dr. Thomas Miller, Dr. Michael Scott and Dr. Andrew Meigs, for their thoughtful questions, comments and support.

I would like to thank my parents Ursula and Martin, my sister Beatrice and her boyfriend Dominik, my grandparents Lotti and Otto and my grandma Nelly for their never ending love, support, and Swiss chocolate shipments. You have all given me the strength to become who I am today.

Endless thanks to Keely Heintz, my girlfriend, for her great support during the writing process of this thesis and for making my time in the United States one of the best experiences of my life. Also, many thanks to Keely's family for their great friendship and for embracing me in their family.

Special thanks to Thomas Schumacher for convincing me to obtain my master's degree from Oregon State University, and to Lisa Mathews, Tugrul Turan and Mary Ann Triska for their friendship, and for making me feel right at home in Corvallis.

## TABLE OF CONTENTS

	<u>Page</u>
1 INTRODUCTION.....	1
1.1 Background.....	1
1.2 Objectives .....	3
2 LITERATURE REVIEW .....	4
2.1 Aeroelastic Instability .....	4
2.1.1 Strouhal Number of a Bluff Body .....	5
2.1.2 Natural Torsional Frequency of an I-Beam.....	7
2.2 Torsion.....	8
2.3 Fatigue .....	15
2.4 Previous Research Conducted on the Astoria-Megler Bridge .....	17
2.5 Bridges with Wind Induced Torsional Problems.....	17
2.5.1 Commodore Barry Bridge, Delaware.....	17
2.5.2 Dongping Bridge in Guangdong, China.....	18
3 EXPERIMENTAL PROCEDURE.....	20
3.1 Selection of Laboratory Specimen Details .....	20
3.2 Experimental Setup.....	23
3.2.1 Boundary Conditions .....	23
3.2.2 Necessary Changes for the Test-Setup Design.....	23
3.2.3 Drawings and Fabrication .....	24
3.2.4 Connections.....	28

## TABLE OF CONTENTS (Continued)

	<u>Page</u>
3.3 Instrumentation .....	29
3.3.1 Instruments .....	29
3.3.2 Instrumentation Plan (with Initial Configurations) .....	30
3.3.3 Instrumentation by Section.....	33
3.3.3.1 Section 1 .....	33
3.3.3.2 Section 2 .....	34
3.3.3.3 Section 3 .....	34
3.3.3.4 Sections 4 through 6 .....	35
3.3.3.5 Section 7 .....	37
3.3.4 Instrumentation Plan (with Configurations for the Rotation Test).....	39
3.3.4.1 Adaptions Made to Section 7 .....	42
3.4 Load Induction.....	43
3.5 Experimental Results .....	45
3.5.1 Rotational Response of Specimen and Instrument Performance .....	45
3.5.1.1 Time-History Data .....	46
3.5.1.2 Average Peak to Peak Results .....	52
3.5.2 Rotation Testing.....	57
3.5.3 Natural Frequency Testing .....	60
3.5.3.1 Damping .....	61
4 ANALYSIS METHODS .....	63

## TABLE OF CONTENTS (Continued)

	<u>Page</u>
4.1 Finite Element Modeling .....	63
4.1.1 Experimental Vertical Model Development .....	64
4.1.1.1 Boundary Conditions .....	64
4.1.1.2 Parts of FEM Model .....	65
4.1.1.3 Connections .....	68
4.1.1.4 Interaction between the Gusset Plates and Reaction Box .....	69
4.1.1.5 Material Definitions .....	69
4.1.2 Analytical Expressions .....	77
4.1.2.1 AISC Steel Design Guide Series 9 .....	77
4.1.2.2 Boundary Condition: One End Fixed (AISC Steel Design Guide Series 9, Case 9) .....	77
4.1.3 Comparison of FEM and Analytical Methods with Experimental Results .....	80
4.1.3.1 Natural Frequency of Experimental Vertical .....	80
4.1.3.2 Torsional Stiffness of Experimental Vertical .....	82
4.1.3.3 Magnitude and Distribution of Angle of Twist for Experimental Vertical .....	83
4.1.3.4 Angle of twist Comparison for Time History Data .....	84
4.1.3.5 Stresses along Experimental Vertical .....	85
4.1.3.6 Normal Stress along the Length of Experimental Vertical .....	86
4.1.3.7 Normal Stress for the Top Gusset Plate of Experimental Vertical .....	88

## TABLE OF CONTENTS (Continued)

	<u>Page</u>
4.1.3.8 Normal Stress in the Top Flange of the I-Section of Experimental Vertical .....	90
4.2 Prediction of Behavior of Existing Bridge Vertical (L13-M13).....	92
4.2.1 Existing Bridge Vertical (L13-M13) FEM Development .....	92
4.2.1.1 Material Definitions for Model of Existing Bridge Vertical .....	95
4.2.2 Analytical Expressions for the Existing Bridge Vertical .....	96
4.2.3 Comparison of FEM and Analytical Methods for Existing Bridge Vertical.....	99
4.2.3.1 Natural Frequency of Existing Bridge Vertical .....	99
4.2.3.2 Torsional Stiffness of Existing Bridge Vertical.....	101
4.2.3.3 Angle of Twist of Existing Bridge Vertical.....	102
4.2.3.4 Normal Stresses along the Length of Existing Bridge Vertical .....	102
4.2.3.5 Normal Stress in the Top Gusset Plate of Existing Bridge Vertical .....	105
4.3 Further Evaluation of Comparative Results.....	107
4.3.1 Boundary Condition: Both Ends Fixed, Uniformly Distributed Torque (AISC Steel Design Guide Series 9, Case 7).....	107
4.3.2 Comparison of Experimental and Analytical Results .....	109
5 Fatigue Life Development.....	111
5.1 Fatigue Life Calculation .....	112
5.2 Fatigue Life Prediction .....	114
6 Summary and Conclusions.....	116

## TABLE OF CONTENTS (Continued)

	<u>Page</u>
6.1 Further Research .....	119
BIBLIOGRAPHY .....	120
APPENDICES .....	122

## LIST OF FIGURES

<u>Figure</u>	<u>Page</u>
1.1 Continuous steel truss of the Astoria-Megler Bridge .....	1
2.1 Vortex shedding behind a cylindrical bluff body (Figure from [2] and edited) .....	4
2.2 Rectangular bluff body group (values in mm) (Nakamura, 1966).....	5
2.3 Strouhal number ( $St(D)$ ) for different rectangular bluff bodies.....	6
2.4 Location and orientation of different stresses in an I-section with applied torque. (Steel Design Guide Series 9, 2003).....	12
2.5 Distribution of the warping statical moment in the flanges of an I-section. (Steel Design Guide Series 9, 2003).....	13
2.6 Distribution of the normalized warping function in the flange of an I-section. (Steel Design Guide Series 9, 2003).....	13
2.7 Table A-3.1 Fatigue Design Parameters (AISC Steel Manual, 2005) .....	16
2.8 Cracked H-shaped tensile member in the Commodore Barry Bridge (Maher and Wittig, 1980) .....	17
2.9 Cracked H-shaped tensile member in the Dongping arch bridge (Chen <i>et al.</i> , 2012) .....	18
3.1 Length (in feet) and positions of truss bridge members. Vertical L13-M13 is highlighted in red. ....	21
3.2 Original cross-sectional drawings of Member L13-M13 .....	21
3.3 Original gusset plate connecting the vertical truss to the horizontal chord .....	22
3.4 Load application system mounted to the critical truss.....	23
3.5 Critical vertical, orient horizontally in the laboratory .....	23
3.6 Cross-sectional of laboratory vertical representing member L13-M13 .....	24
3.7 Perforations in the reproduced vertical.....	25



## LIST OF FIGURES (Continued)

<u>Figure</u>	<u>Page</u>
3.8 Reproduced laboratory vertical with gusset plate perpendicular to the reaction box .....	27
3.9 Reaction box with head plates welded to the side .....	27
3.10 Experimental vertical with reaction box, gusset plates and fill plates .....	28
3.11 Instrumentation overview of the entire test setup .....	31
3.12 Instrumentation details of the different sections of the specimen .....	32
3.13 Location of displacement sensor (DSP2) for section 1 .....	33
3.14 Location of SG3-10 on the top gusset plate .....	34
3.15 Location of SG17 and 18 on the bottom gusset plate .....	34
3.16 Strain gage (SG16) fixed to the side of the bottom flange .....	35
3.17 Strain rosette (R13) and strain gage (SG13) mounted onto the top flange .....	35
3.18 Strain rosette distribution over top side of the top flange .....	36
3.19 Example inclinometer (INC1) positioned at the neutral axis of the vertical .....	36
3.20 Angular rate sensor (AR1) and inclinometer (INC0) fixed onto the critical vertical .....	37
3.21 Connection between the string potentiometer and the endplate .....	38
3.22 String potentiometer on the strong floor to check the rotations at the endplate .....	38
3.23 Displacement sensor (DSP4) measures displacements of the endplate .....	38
3.24 Inclinometers positioned at a closer distance .....	39
3.25 Instrumentation overview with rotation test configurations .....	41
3.26 Adapted section 7, with new strain rosettes (NR1 and NR2) .....	42

## LIST OF FIGURES (Continued)

<u>Figure</u>	<u>Page</u>
3.27 Torque actuator fixed onto the reaction frame.....	43
3.28 Torque actuator, load cell and vertical assembly.....	43
3.29 RVDT mounted to the torque actuator .....	44
3.30 Rotary variable differential transformer (RVDT) mounted to the torque actuator and connected to the reaction frame .....	44
3.31 Time-history plot of the rotation at the torque actuator (target of +/- 9 degrees) .....	46
3.32 Time-history plot of the torque force ( $T$ ) at the torque actuator (target of +/- 9.0 degrees) .....	47
3.33 Time-history plot of the angular rate sensor (AR1).....	48
3.34 Time-history plot of the inclinometers (INC0-3) and angular rate sensor (AR1) along the vertical .....	48
3.35 Time-history comparison of INC0 (inclinometer) and AR1 (angular rate sensor) at a testing frequency of 1 Hz .....	49
3.36 Time-history displacement response at sensors DSP3 and 4.....	50
3.37 Example time-history plot of a strain gage (SG13) .....	51
3.38 Example time-history plot of strain rosettes (R5 and R7) .....	51
3.39 Rotation along the span .....	57
3.40 Rotation along the span in the region of zero rotation (red line is amplitude of signal noise).....	58
3.41 Rotation along the span with new defined point of zero rotation .....	59
3.42 Example dynamic test with ring down location identified .....	60
3.43 Fast Fourier Transform (FFT) for identifying frequency content of ring down.....	61
4.1 Finite element model of the experimental vertical with regions labeled .....	66

## LIST OF FIGURES (Continued)

<u>Figure</u>	<u>Page</u>
4.2 Finite element model of the experimental vertical region 1 (load induction zone) .....	66
4.3 Finite element model of the experimental vertical region 2 (gusset plate, reaction box detail) .....	67
4.4 Finite element model of the experimental setup region 2 ( reaction box, strong wall detail) .....	68
4.5 Schematic stress-strain diagram of steel .....	72
4.6 FEM rotation angle-torque plot for the experimental setup .....	73
4.7 Location of first yield in the experimental setup FEM .....	74
4.8 FEM predicted normal stress-rotation response at nodal region located near endplate of specimen .....	74
4.9 Location of second yield in the experimental setup FEM .....	75
4.10 FEM predicted normal stress-rotation response at nodal region located near gusset plate of specimen (see Fig. 4.9) .....	76
4.11 Boundary conditions and definitions for Case 9 with an $\alpha$ of 1.0 (Steel Design Guide Series 9, 2003) .....	77
4.12 Rotation along the I-section, calculated from equation [4.1] .....	80
4.13 Comparison of the experimentally measured and analytical predicted angle of twist .....	84
4.14 Comparison of the experimental and FEM predicted time-history of angle of twist at the loaded end of the member .....	85
4.15 Regions of interest in the experimental setup FEM .....	86
4.16 Comparison of the experimentally measured and predicted normal stresses at the tips of the flange .....	88
4.17 Comparison of the experimentally measured and predicted normal stresses in the top gusset plate .....	89

## LIST OF FIGURES (Continued)

<u>Figure</u>	<u>Page</u>
4.18 Comparison of the experimentally measured and analytical predicted normal stresses in the top flange of the I-section.....	91
4.19 Boundary condition and system length of the existing vertical.....	92
4.20 Finite element model of the existing bridge vertical with regions labeled.....	93
4.21 Coordinate system and direction of rotation of the existing bridge vertical .....	93
4.22 Finite element model of the existing vertical in region 1 (load induction zone) .....	94
4.23 Boundary conditions and definitions for Case 6 with an $\alpha$ of 0.5 (Steel Design Guide Series 9, 2003).....	97
4.24 Comparison of the analytically predicted angle of twists for the existing bridge vertical .....	102
4.25 FEM normal stresses ( $\sigma_{w,z}$ ) at the flange tips along the span length (z-axis stresses) for the existing bridge vertical.....	103
4.26 Comparison of the analytically predicted normal stresses at the tips of the top flange for the existing bridge vertical.....	104
4.27 Comparison of the analytically predicted normal stresses in the top gusset plate for the existing bridge vertical .....	106
4.28 Boundary conditions and definitions for Case 7 (Steel Design Guide Series 9, 2003).....	107
4.29 Calculated rotation and normal stress along the I-section for the existing vertical with AISC Steel Design Guide Series, Case 7 (uniform torque along length).....	108
4.30 Summary of experimental and analytical (FEM and calculated) results .....	109
5.1 Fatigue life prediction for critical bridge verticals (Category C) .....	114
5.2 Fatigue life prediction for critical bridge verticals (Category B) .....	115

## LIST OF TABLES

<u>Table</u>	<u>Page</u>
3.1 Steel plate material properties used to reproduce the vertical truss.....	26
3.2 Uniaxial strain gage and strain rosette specifications .....	29
3.3 Strain rosette distances from the edge of the top flange .....	30
3.4 Position and name of the inclinometers in the rotation test .....	40
3.5 Maximum and average peak to peak results for the sensors.....	52
3.6 Maximum and average peak-to-peak results for strain rosettes.....	53
3.7 Maximum and average peak-to-peak results for uniaxial strain gages.....	55
4.1 Overview of the different finite element models .....	64
4.2 General sectional and overall dimensions of the experimental-setup FEA models .....	65
4.3 Material properties and general definitions used in the experimental vertical FEM .....	70
4.4 Steel material properties for the experimental vertical FEM.....	71
4.5 Finite element predicted model frequencies of the experimental setup.....	81
4.6 Natural frequency comparison for the experimental vertical .....	82
4.7 Torsional stiffness comparison for the experimental vertical.....	83
4.8 Displacement coordinates for a 10 degree angle change .....	94
4.9 Material properties and general definitions used in the existing vertical models .....	95
4.10 General sectional and overall dimensions of the existing vertical FEA model.....	96
4.11 Finite element model frequencies of the existing bridge vertical .....	99
4.12 Natural frequency comparison for the existing vertical.....	100
4.13 Torsional stiffness comparison for the experimental vertical.....	101

## LIST OF TABLES (Continued)

<u>Table</u>	<u>Page</u>
5.1 Bridge verticals considered for wind excited response (edited from Higgins and Turan, 2009) .....	111
5.2 Fatigue life prediction, for the L13-M13 (after 1997) bridge vertical.....	113

## LIST OF APPENDICES

<u>Appendix</u>	<u>Page</u>
APPENDIX A – SELECTED ORIGINAL BRIDGE DRAWINGS .....	123
APPENDIX B – FABRICATION DRAWINGS FOR THE EXPERIMENTAL SETUP .....	126
APPENDIX C – SELECTED FABRICATION DOCUMENTS .....	129
APPENDIX D – FINITE ELEMENT MODE SHAPES .....	145
APPENDIX E – SELECTED DESIGN EQUATIONS AND DESIGN CHARTS FROM THE AISC STEEL DESIGN GUIDE SERIES 9 .....	151
APPENDIX F – TORSIONAL STIFFNESS OF AN I-SECTION .....	161

## LIST OF APPENDIX FIGURES

<u>Figure</u>	<u>Page</u>
A.1 Truss dimensions main trusses .....	124
A.2 Truss detail L13.....	125
B.1 New fabrication drawing, parts .....	127
B.2 New fabrication drawing, assembly .....	128
C.1 Fabrication report for the laboratory vertical .....	130
C.2 Welding specifications for the laboratory vertical .....	131
C.3 Welding specifications for the laboratory vertical (continued).....	132
C.4 Welding certifications .....	133
C.5 Welding certifications (continued).....	134
C.6 Material certifications Steel 1.....	135
C.7 Material testing certifications Steel 1 .....	136
C.8 Material testing certifications Steel 1 (continued).....	137
C.9 Material testing certifications Steel 1 (continued).....	138
C.10 Material testing certifications Steel 1 (continued).....	139
C.11 Material certifications Steel 2.....	140
C.12 Material testing certifications Steel 2.....	141
C.13 Material testing certifications Steel 2 (continued).....	142
C.14 Certificate of inspection for the bolts.....	143
C.15 Certificate of inspection for the bolts (continued).....	144
D.1 Laboratory vertical FEM mode shape 1 .....	146
D.2 Laboratory vertical FEM mode shape 2.....	146
D.3 Laboratory vertical FEM mode shape 3 .....	147



## LIST OF APPENDIX FIGURES (Continued)

<u>Figure</u>	<u>Page</u>
D.4 Laboratory vertical FEM mode shape 4 .....	147
D.5 Laboratory vertical FEM mode shape 5 .....	148
D.6 Bridge vertical (L13-M13) FEM mode shape 1 .....	148
D.7 Bridge vertical (L13-M13) FEM mode shape 2 .....	149
D.8 Bridge vertical (L13-M13) FEM mode shape 3 .....	149
D.9 Bridge vertical (L13-M13) FEM mode shape 4 .....	150
D.10 Bridge vertical (L13-M13) FEM mode shape 5 .....	150
E.1 Equation for the rotation of Case 6 (AISC Steel Design Guide Series 9) .....	152
E.2 Design chart for $\theta$ Case 6 (AISC Steel Design Guide Series 9) .....	153
E.3 Design chart for $\theta'$ Case 6 (AISC Steel Design Guide Series 9) .....	153
E.4 Design chart for $\theta''$ Case 6 (AISC Steel Design Guide Series 9) .....	154
E.5 Design chart for $\theta'''$ Case 6 (AISC Steel Design Guide Series 9) .....	154
E.6 Equation for the rotation of Case 7 (AISC Steel Design Guide Series 9) .....	155
E.7 Design chart for $\theta$ Case 7 (AISC Steel Design Guide Series 9) .....	155
E.8 Design chart for $\theta'$ Case 7 (AISC Steel Design Guide Series 9) .....	156
E.9 Design chart for $\theta''$ Case 7 (AISC Steel Design Guide Series 9) .....	156
E.10 Design chart for $\theta'''$ Case 7 (AISC Steel Design Guide Series 9) .....	157
E.11 Equation for the rotation of Case 9 (AISC Steel Design Guide Series 9) .....	158
E.12 Design chart for $\theta$ Case 9 (AISC Steel Design Guide Series 9) .....	158
E.13 Design chart for $\theta'$ Case 9 (AISC Steel Design Guide Series 9) .....	159

## LIST OF APPENDIX FIGURES (Continued)

<u>Figure</u>	<u>Page</u>
E.14 Design chart for $\theta''$ Case 9 (AISC Steel Design Guide Series 9) .....	159
E.15 Design chart for $\theta'''$ Case 9 (AISC Steel Design Guide Series 9) .....	160
F.1 Schematic drawing of the I-section boundary conditions .....	162
F.2 FE model of an I-section without web perforations, used to determine beam stiffness .....	165
F.3 FE model of an I-section with web perforations, used to determine beam stiffness .....	165

## LIST OF APPENDIX TABLES

<u>Table</u>	<u>Page</u>
F.1    Material properties used in the torsional stiffness of an I-section models .....	163
F.2    General sectional and overall dimensions of the experimental-setup FEA models.....	164

# **WIND INDUCED TORSIONAL FATIGUE BEHAVIOR OF TRUSS BRIDGE VERTICALS**

## **1 INTRODUCTION**

### **1.1 Background**

The Astoria-Megler Bridge is a continuous steel truss bridge and was completed in 1966 [1]. It is the second longest bridge of this type in the world. The main span measures 376 m (1232 ft) and the total bridge length is 6.6 km (4.1 miles). The continuous steel truss is shown in Figure 1.1.



Figure 1.1: Continuous steel truss of the Astoria-Megler Bridge

The bridge crosses the Columbia River between Washington State and Oregon on US 101, an important national scenic highway. The nearest adjacent detour highway crossing over the Columbia River is located in Longview, WA, 76 kilometers (47 miles) east of Astoria, OR. Thus, the bridge is a critical lifeline structure for the region.

The bridge has exhibited wind-induced vibrations of some of the longer truss verticals near the continuous support towers. Several of the verticals have been remediated by the Oregon Department of Transportation over many years. However, wind-induced vibrations continue to be observed for some of the bridge verticals and these have raised concerns among the motoring public. The phenomenon which causes this motion is called vortex shedding. Due to vortex shedding, the relatively low torsional stiffness and damping in the verticals results in twisting of some of the verticals. The repeated twisting could produce high-cycle fatigue damage to the member or the attached gusset plates as the vertical member and gusset plate assembly were not designed for such conditions.

Research was undertaken to quantify the interaction between member twisting and the resulting stress magnitudes and distributions in the member and connection. These data, combined with field-measured wind speed and direction along with member twisting amplitude and frequency can be combined to produce estimates of the remaining life of the verticals and connections. The research topic synthesizes wind-induced phenomena, torsional member behavior, and fatigue life prediction.

## **1.2 Objectives**

The following objectives were defined for this research project:

- Develop an experimental model to characterize the relationship between the twist angle and the stresses induced in the member to assess the fatigue vulnerability of truss verticals that exhibit torsional motions.
- Compare experimental results with available analytical methods and finite element models.
- Predict the fatigue life of existing bridge verticals using experimentally validated analytical methods and/or finite element models.
- Use experimental and analytical findings to inform bridge inspectors of the probable fatigue crack locations in bridge verticals that exhibit torsional motions.

## 2 LITERATURE REVIEW

The literature review is divided into four different sections: aeroelastic instability phenomena, torsional behavior, fatigue, and case studies of bridges with fatigue problems associated with torsional excitation of truss verticals.

### 2.1 Aeroelastic Instability

The phenomenon that causes the aeroelastic instability in the existing bridge verticals of the Astoria-Megler Bridge is called vortex shedding. Vortex shedding can occur when wind flows around a bluff body which disturbs the uniform flow of the wind, thereby producing vortices behind the object. Due to the alternating high and low pressure changes behind the body, the vortex moves from one side of the object to the other side. This phenomenon is illustrated in Figure 2.1 for a circular bluff body. If the frequency of the pressure changes is in the same range as the natural frequency of a member, the member can produce relatively large amplitude vibrations.

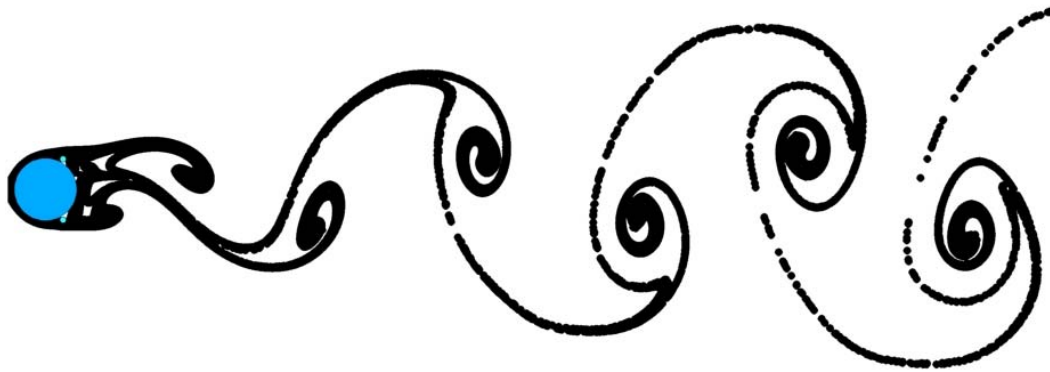


Figure 2.1: Vortex shedding behind a cylindrical bluff body (Figure from [2] and edited)

In the present research, the bluff body is the I shaped cross-section of the truss bridge verticals. The long member length, combined with the open cross sectional shape has a relatively low torsional natural frequency. The combination of vortex shedding in the same frequency range as the natural frequency of some bridge verticals and the unfavorable profile section for this phenomenon is attributed to the visible twisting of some verticals of the Astoria-Megler Bridge.

To determine the frequency for the vortex shedding, the natural frequency and the Strouhal number of the critical section needed to be known.

#### 2.1.1 Strouhal Number of a Bluff Body

Nakamura (1966) derived the Strouhal number for nine different bluff bodies, with different shapes and different  $L/D$  ratios (where  $L$  is the depth and  $D$  is the width of the cross-section), using wind tunnel tests. The nine shapes were split into four groups; the grouping for the rectangular bluff body, the bluff body of interest for this research project, is shown in Figure 2.2.

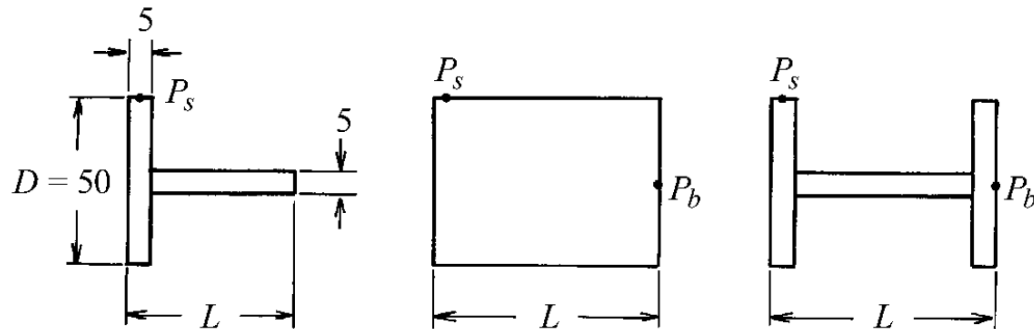


Figure 2.2: Rectangular bluff body group (values in mm) (Nakamura, 1966)



The reported Strouhal numbers for different  $L/D$  ratios are shown in Figure 2.3.

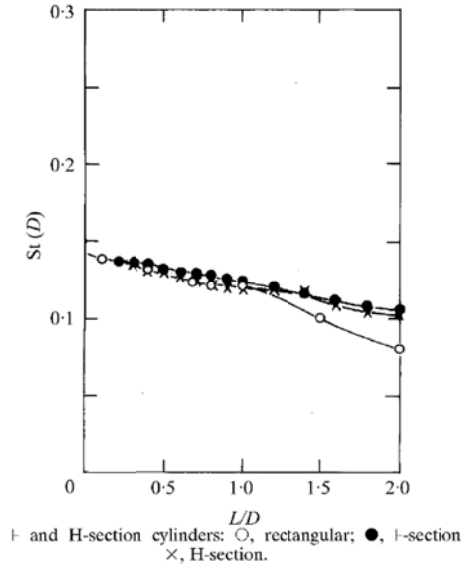


Figure 2.3: Strouhal number ( $St(D)$ ) for different rectangular bluff bodies (Nakamura, 1966)

From the graph shown in Figure 2.3, the Strouhal number for an I-section with a defined  $L/D$  ratio can be determined.

Scanlan (1976) reported that long, slender bridge hangers can start to vibrate due to vortex shedding. The vortex shedding frequency can be determined from the Strouhal relation given as:

$$S = \frac{ND}{U} \quad [2.1]$$

where  $S$  is the Strouhal number,  $N$  is the vortex shedding frequency,  $D$  is the dimension of the section perpendicular to the flow and  $U$  is the mean flow velocity.

### 2.1.2 Natural Torsional Frequency of an I-Beam

Carr (1969) developed approximate torsional frequency equations based on simple beam functions for fixed-fixed and for fixed-simply supported boundary conditions. The equation for the torsional frequency ( $\omega_{torsion}$  with units of rad/sec) for a fixed-fixed boundary condition is given as:

$$\omega_{torsion} = \sqrt{\frac{\frac{EJ_w}{\rho J L^4} * k^4}{\int_0^1 (Cosh(k\xi) - Cos(k\xi) - K Sinh(k\xi) + K Sin(k\xi))^2 d\xi} * \left(1 + \frac{GJ_t L^2}{EJ_w k^3} (Kk - 2K)\right)} \quad [2.2]$$

where  $E$  is the modulus of elasticity,  $G$  is the shear modulus of elasticity,  $J$  is the polar moment of inertia of the cross section,  $J_w$  is the warping constant,  $J_t$  is the torsional constant,  $\rho$  is the mass density of the material used,  $L$  is the length of the beam,  $\xi$  is the non-dimensional length,  $k$  and  $K$  are parameters in the beam function and are given by Carr for fixed-fixed boundary conditions for the first torsional mode as  $k = 4.73$  and  $K = 0.9825$ , respectively.

The equation for the torsional frequency ( $\omega_{torsion}$ ) for fixed-simply supported boundary conditions is given as:

$$\omega_{torsion} = \sqrt{\frac{\frac{EJ_w}{\rho J L^4} * k^4}{\int_0^1 \left( \cosh(k\xi) - \cos(k\xi) - K \sinh(k\xi) + K \sin(k\xi) \right)^2 d\xi} * \left( 1 + \frac{GJ_t L^2}{EJ_w k^3} (K^2 k - K) \right)} \quad [2.3]$$

For the simply supported boundary conditions, the beam parameters  $k$  and  $K$  for the first torsional mode were given as  $k = 3.9270$  and  $K = 1.0$ , respectively.

## 2.2 Torsion

Boresi and Sidebottom (1985) provide equations for torsional beam behavior with different boundary conditions for I-sections with one end restrained to warping. Their approach separates the torque force ( $T$ ) into two parts. The first part ( $T1$ ) is the lateral shearing force ( $V'$ ) in the flanges of an I-section multiplied by the distance between the centers of the flanges ( $h$ ). The second part ( $T2$ ) is the twisting part and is given by multiplying the torsional constant ( $J$ ) with the shear modulus of elasticity ( $G$ ) and the angle of twist per unit length ( $\theta$ ). The final equation for the torque force is:

$$T = JG\theta + V'h \quad [2.4]$$

From this equation, the following equation for the total angle of twist ( $\beta$ ) at the free end of an I-section with a given torque ( $T$ ) was found as:

$$\beta = \frac{T}{JG} \left( L - \alpha \tanh \frac{L}{\alpha} \right) \quad [2.5]$$

$L$  is defined as the total length of the I-section and  $\alpha$  is defined as:

$$\alpha = \frac{h}{2} \sqrt{\frac{EI_y}{JG}} \quad [2.6]$$

Where  $h$  is the total height of the I-section minus one flange thickness,  $E$  is the modulus of elasticity and  $I_y$  is the weak axis moment of inertia of the entire cross section.

The horizontal moment ( $M$ ) in the flanges of the I-section at any point along  $L$  is given as:

$$M = -\frac{T}{h} \alpha \frac{\sinh\left(\frac{L-x}{\alpha}\right)}{\cosh\left(\frac{L}{\alpha}\right)} \quad [2.7]$$

where  $x$  is a distance measured from the fixed end of the beam.

To conclude, Borens and Sidebottom provide an equation for warping stresses at the fixed end:

$$\sigma = \frac{M \frac{1}{2} b}{I_f} = \frac{T}{h} \alpha \frac{\frac{1}{2} b}{\frac{1}{12} t b^3} = \frac{6T\alpha}{h t b^2} \quad [2.8]$$

where  $b$  is the flange width,  $t$  is the flange thickness and  $I_f$  is the strong axis moment of inertia of the flange.

In the Steel Design Guide Series 9 (2003), Torsional Analysis of Structural Steel Members, Seaburg and Carter's approach the torsional problem of different sections with different boundary conditions similar to Boresi and Sidebottom (1985). Seaburg and Carter's basic equation for the torsional moment resistance of an open cross section is:

$$T = GJ\theta' - EC_w\theta''' \quad [2.9]$$

Equations [2.4] and [2.9] are similar, where the first part of the equation describes the torque in a section which is not restrained against warping, and the second part deals with the warping effects. In Eqn. [2.9],  $\theta'$  is the angel of rotation per unit length, which is shown as the first derivative of the rotation ( $\theta$ ) with respect to  $z$ , where  $z$  is the distance measured from the left support along the beam.  $\theta'''$  is the third derivative of  $\theta$  with respect to  $z$ . The equation for the warping constant ( $C_w$ ) is different for different cross sections. The equation for the  $C_w$  of an I-section is given as:

$$C_w = \frac{I_y h^2}{4} \quad [2.10]$$

The torsional constant ( $J$ ), for an I-section, can be calculated with two different equations.

The approximation is given as:

$$J \approx \sum \left( \frac{bt^3}{3} \right) \quad [2.11]$$

A more accurate equation for  $J$  for an I-section is given as:

$$J = \frac{2b_f t_f^3}{3} + \frac{t_w^3 (d - 2t_f)}{3} + 2\alpha_1 D_1^4 - 0.420 t_f^4 \quad [2.12]$$

where:

$$\alpha_1 = -0.0420 + 0.220 \frac{t_w}{t_f} + 0.136 \frac{R}{t_f} - 0.0865 \frac{t_w R}{t_f^2} - 0.0725 \frac{t_w^2}{t_f^2} \quad [2.13]$$

$$D_1 = \frac{(t_f + R)^2 + t_w \left( R + \frac{t_w}{4} \right)}{2R + t_f} \quad [2.14]$$

For these equations,  $b_f$  is the width of the flange,  $t_w$  and  $t_f$  are the web thickness and the flange thickness, respectively.  $R$  is defined as the fillet radius in a rolled cross section.

From the equations shown previously, Seaburg and Carter derived equations for the shear stress due to warping, the shear stress due to pure torsion and the normal stress due to warping along the length of different I-sections and for different boundary conditions. Sign convention and locations of the different stresses are shown in Figure 2.4.

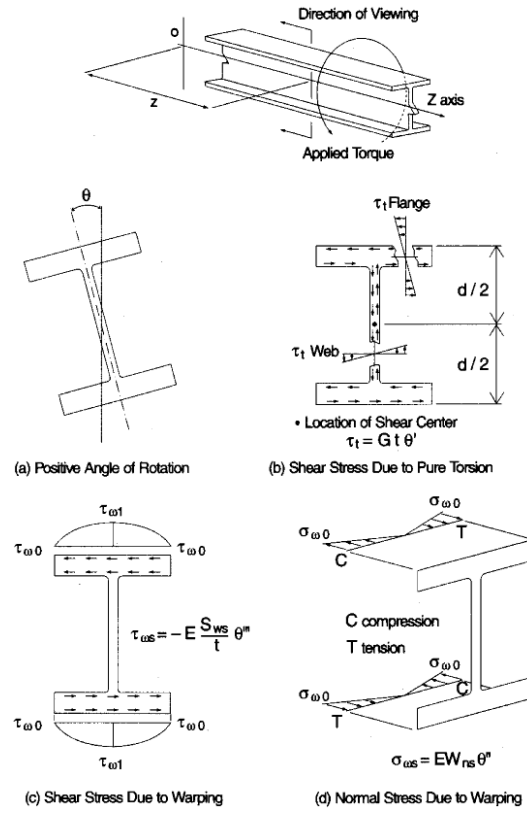


Figure 2.4: Location and orientation of different stresses in an I-section with applied torque.  
(Steel Design Guide Series 9, 2003)

The equation for the pure torsional shear stress ( $\tau_t$ ) is:

$$\tau_t = Gt\theta' \quad [2.15]$$

The variable  $t$  is either the flange thickness or the web thickness (whichever part of the beam is analyzed). To determine the shear stress due to warping ( $\tau_{ws}$ ) at any point in the flanges, the following equation can be used:

$$\tau_{ws} = -E \frac{S_{ws}}{t} \theta''' \quad [2.16]$$

$S_{ws}$  is the warping statical moment at any point  $s$  along the flange as shown in Figure 2.5, and is defined as:

$$S_{ws} = \frac{W_{ns} b_f t_f}{4} \quad [2.17]$$

where  $W_{ns}$  is the normalized warping function located at the same point  $s$  along the I-section flange as shown in Figure 2.6. The equation for  $W_{no}$  for an I-section is given as:

$$W_{no} = \frac{h b_f}{4} \quad [2.18]$$

The variable  $h$  is the total profile height ( $d$ ) minus one flange thickness ( $t_f$ ).

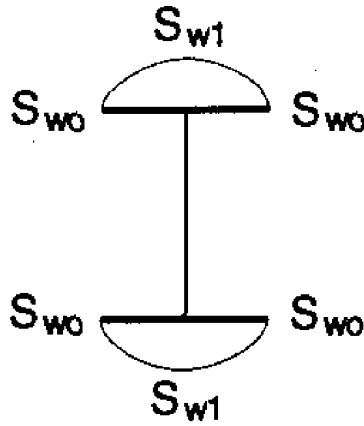


Figure 2.5: Distribution of the warping statical moment in the flanges of an I-section. (Steel Design Guide Series 9, 2003)

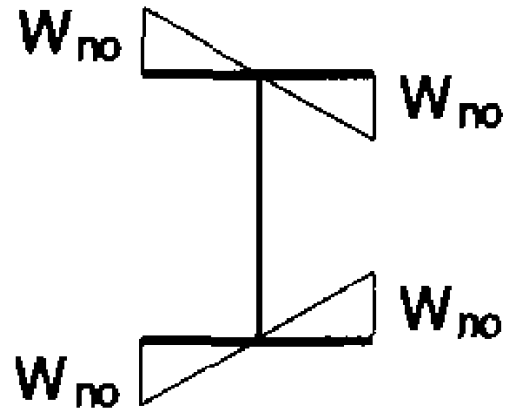


Figure 2.6: Distribution of the normalized warping function in the flange of an I-section. (Steel Design Guide Series 9, 2003)

As shown in Figure 2.6, the normalized warping function is a linear function and therefore any value can be interpolated over the entire flange. With these values, the warping statical moment can be calculated at any point in the flanges.



The values for normal stresses due to warping at any point in an I-section are given as:

$$\sigma_{ws} = EW_{ns} \theta'' \quad [2.19]$$

where  $\theta''$  is the second derivative of  $\theta$  with respect to  $z$ .

Seaburg and Carter give the general equation for the rotation ( $\theta$ ) for a constant torsional moment ( $T$ ) as:

$$\theta = A + B \cosh\left(\frac{z}{a}\right) + C \sinh\left(\frac{z}{a}\right) + \frac{Tz}{GJ} \quad [2.20]$$

where  $z$  is the distance along the  $Z$ -axis from the left support as shown in Figure 2.4.  $A$ ,  $B$  and  $C$  are constants which are determined according to the boundary conditions.

The equation for rotation was presented by Seaburg and Carter for different boundary conditions and graphs corresponding to these results can be found in the appendix of their document. Solutions to this equation, which are used in this research project, can be found in Chapter 4 and the design charts for these boundary conditions are attached in Appendix E.

### 2.3 Fatigue

There are two types of fatigue which typically occur in civil infrastructure applications: low cycle fatigue and high cycle fatigue. The differences between these two regimes are the amplitude of the stress range and the number of cycles.

Low cycle fatigue is characterized by relatively large applied stress range and a correspondingly low number of life cycles, usually less than  $10^4$ . The material accumulates plastic damage as the applied stress range is above the elastic limit. The plastic damage reduces the number of loading cycles required to fracture the material.

High cycle fatigue is characterized by relatively low amplitude applied stresses with corresponding number of life cycles that are usually greater than  $10^4$ . After a crack is initiated at a defect, imperfection, or stress concentration, crack propagation occurs at elastic stress levels until the member fractures.

For this project, high cycle fatigue is the focus of the investigation. The wind induced twisting of the truss members was anticipated to produce elastic stress ranges and the life of the members needs to be evaluated.

The design stress range for fatigue life calculations is given in the AISC Steel Manual (2005) as:

$$F_{SR} = \left( \frac{C_f}{N} \right)^{1/3} \geq F_{TH} \quad \text{AISC Steel Manual: (A-3-1)} \quad [2.21]$$

where  $F_{SR}$  is the design stress range,  $C_f$  is the constant for the governing fatigue category (AISC Steel Manual Table A-3.1 shown in Figure 2.7),  $N$  is the number of stress range fluctuations in the design life and  $F_{TH}$  is the threshold fatigue stress range defined for each fatigue category given in the AISC Steel Manual in Table A-3.1. The detail considered in the present research is the bolt holes in the truss vertical at the gusset plate connection. These are considered as Category B in the AISC Specification.

TABLE A-3.1 Fatigue Design Parameters				
Description	Stress Category	Constant $C_f$	Threshold $F_{TH}$ ksi (MPa)	Potential Crack Initiation Point
SECTION 1 – PLAIN MATERIAL AWAY FROM ANY WELDING				
1.1 Base metal, except non-coated weathering steel, with rolled or cleaned surface. Flame-cut edges with surface roughness value of 1,000 $\mu$ in. (25 $\mu$ m) or less, but without reentrant corners.	A	$250 \times 10^8$	24 (165)	Away from all welds or structural connections
1.2 Non-coated weathering steel base metal with rolled or cleaned surface. Flame-cut edges with surface roughness value of 1,000 $\mu$ in. (25 $\mu$ m) or less, but without reentrant corners.	B	$120 \times 10^8$	16 (110)	Away from all welds or structural connections
1.3 Member with drilled or reamed holes. Member with reentrant corners at copes, cuts, block-outs or other geometrical discontinuities made to requirements of Appendix 3.5, except weld access holes.	B	$120 \times 10^8$	16 (110)	At any external edge or at hole perimeter
1.4 Rolled cross sections with weld access holes made to requirements of Section J1.6 and Appendix 3.5. Members with drilled or reamed holes containing bolts for attachment of light bracing where there is a small longitudinal component of brace force.	C	$44 \times 10^8$	10 (69)	At reentrant corner of weld access hole or at any small hole (may contain bolt for minor connections)
SECTION 2 – CONNECTED MATERIAL IN MECHANICALLY FASTENED JOINTS				
2.1 Gross area of base metal in lap joints connected by high-strength bolts in joints satisfying all requirements for slip-critical connections.	B	$120 \times 10^8$	16 (110)	Through gross section near hole
2.2 Base metal at net section of high-strength bolted joints, designed on the basis of bearing resistance, but fabricated and installed to all requirements for slip-critical connections.	B	$120 \times 10^8$	16 (110)	In net section originating at side of hole
2.3 Base metal at the net section of other mechanically fastened joints except eye bars and pin plates.	D	$22 \times 10^8$	7 (48)	In net section originating at side of hole
2.4 Base metal at net section of eyebar head or pin plate.	E	$11 \times 10^8$	4.5 (31)	In net section originating at side of hole

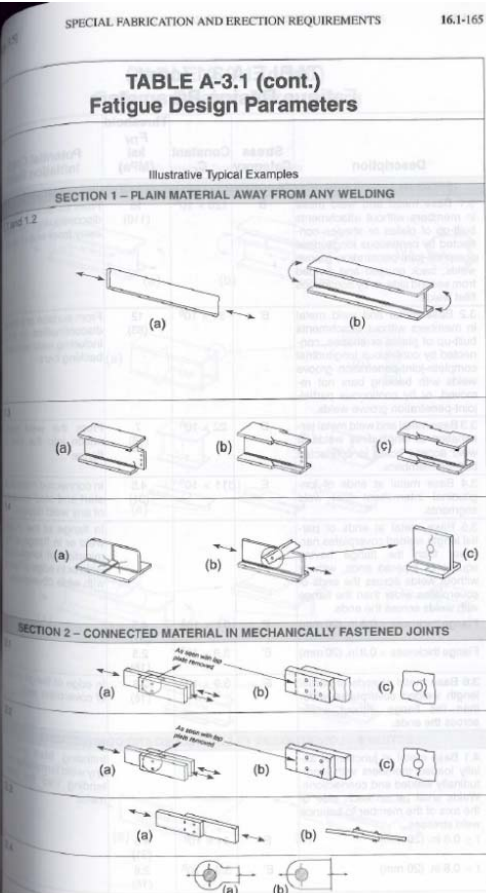


Figure 2.7: Table A-3.1 Fatigue Design Parameters (AISC Steel Manual, 2005)

## 2.4 Previous Research Conducted on the Astoria-Megler Bridge

Higgins and Turan (2009) conducted analytical studies of the overall structure of the Astoria-Megler Bridge, as well as individual verticals, using finite element analyses. The main focus of this study was to find the natural frequency of the overall structure and for selected individual members throughout the bridge. From the computed natural frequencies, the critical wind speeds that excite the torsional natural frequencies of the long truss bridge verticals were determined.

## 2.5 Bridges with Wind Induced Torsional Problems

### 2.5.1 Commodore Barry Bridge, Delaware

Maher and Wittig (1980) investigated wind induced torsional problems of long H-shaped tensile members in the Commodore Barry steel cantilever bridge after several of these hangers cracked during construction of the bridge as shown in Figure 2.8.

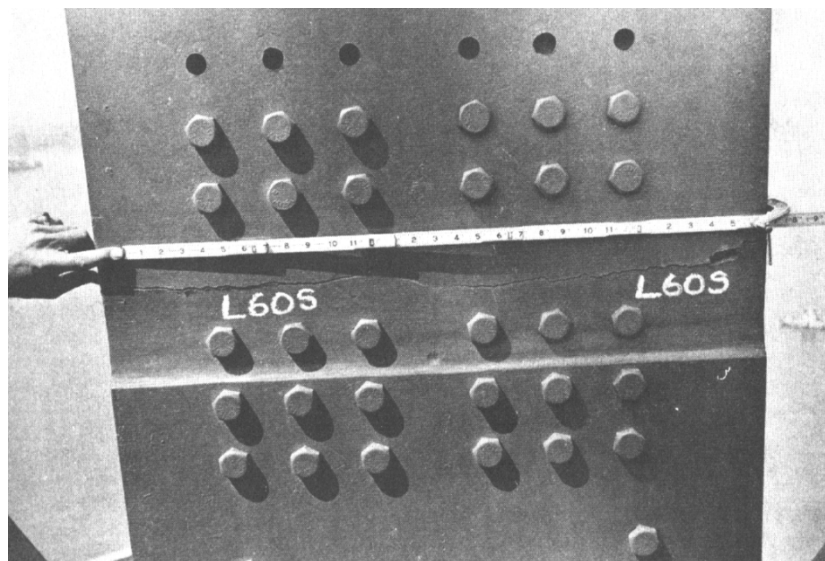


Figure 2.8: Cracked H-shaped tensile member in the Commodore Barry Bridge (Maher and Wittig, 1980)

Maher and Wittig conducted wind tunnel testing of selected H-sections, one with a scale of 1 to 6.25 and one with a scale of 1 to 8.35. For both models aerodynamic coefficients and angle of rotations were determined.

### 2.5.2 Dongping Bridge in Guangdong, China

Chen, *et al.* (2012) completed a study of the Dongping arch bridge located in China. The 13 longest vertical hangers in the bridge showed cracking after a single strong wind event, as shown in Figure 2.9.



Figure 2.9: Cracked H-shaped tensile member in the Dongping arch bridge  
(Chen *et al.*, 2012)

Chen, *et al.* conducted wind study tests on a sectional 1 to 4 scale model and on an aeroelastic 1 to 16 scale model of the cracked hanger. The overall behavior, as well as the influence of web and flange perforations, were reported.

Based on review of the technical literature, no previous structural tests have been conducted on twisting induced response of large I sections to characterize fatigue performance of the members. To fill this gap, the present research was undertaken.

### **3 EXPERIMENTAL PROCEDURE**

#### **3.1 Selection of Laboratory Specimen Details**

To determine which member to investigate in detail under laboratory conditions, past performance observations from the bridge were reviewed. Key vertical hangers were identified by analyzing a video file which was filmed in 2002 on the Astoria-Megler Bridge. The movie showed several of the open section hangers twisting at a relatively low reported wind speed of 10.7 m/s (24 mph). The locations of the vibrating I-sections were found with the help of the original bridge drawings and pictures of the bridge.

Each of the verticals that exhibited twisting response under wind excitation was evaluated and one was chosen for the full-scale experiment. One of the main criteria was a low torsional stiffness of the vertical. The torsional stiffness is governed by member length, boundary conditions and cross sectional properties. In the actual bridge, there are two different types of web design: solid web plate and web plate with perforations. I-sections fixed at the flanges with web openings have a lower torsional stiffness than ones without perforations as shown in Appendix F. The other important criterion was the connection detail (gusset plate) between the vertical and horizontal truss members. Since the research project was first concerned with possible gusset plate fatigue, identifying a gusset plate connection that joins only the vertical to the truss chord was desirable.

Higgins and Turan (2009) suggested that member U12-L12 should be instrumented, since this member had the lowest reported critical wind speed (17.0 m/s (38mph)). This member was initially considered, but later abandoned due to the following factors. The gusset plate

connecting the vertical and the horizontal truss at L12 also connects two diagonals to the horizontal truss, making this connection detail unfavorable for this study. This member was also not chosen due to the web design, which does not include any perforations.

The vertical finally selected for this research project was member L13-M13. The location of this member in the bridge is shown in Figure 3.1.

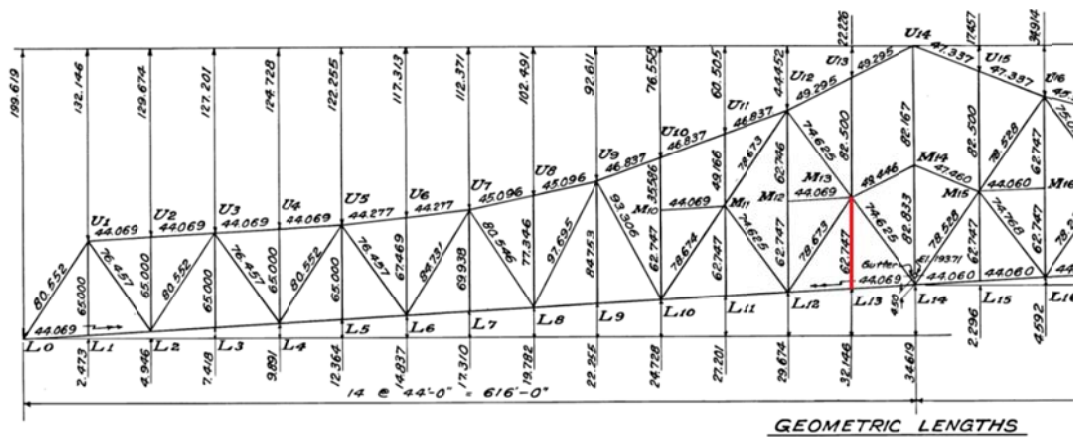


Figure 3.1: Length (in feet) and positions of truss bridge members. Vertical L13-M13 is highlighted in red.

The total length of vertical L13-M13 is approximately 19.2 m (63 ft). The cross sectional dimensions are shown in Figure 3.2.

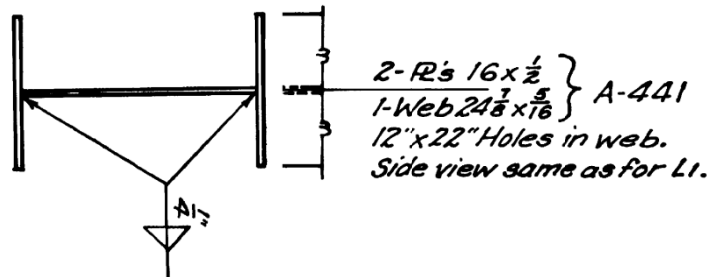


Figure 3.2: Original cross-sectional drawings of Member L13-M13



This I-Section has web perforations, and the gusset plate connection joins only the vertical to the truss lower chord as seen in Figure 3.3.

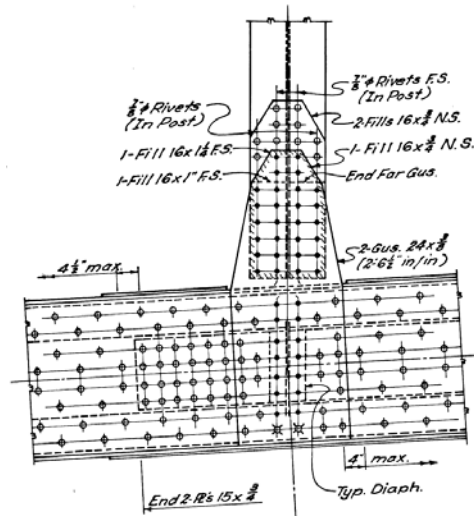


Figure 3.3: Original gusset plate connecting the vertical truss to the horizontal chord

## 3.2 Experimental Setup

### 3.2.1 Boundary Conditions

The experimental setup was designed to represent the boundary conditions and a full-size portion of the vertical hanger in the Astoria-Megler Bridge. Due to limitations in the height of the structural laboratory, the vertical was oriented in a horizontal position. This orientation also simplified the fixation of the load application system and access to the member for instrumentation and observation as shown in Figure 3.4 and Figure 3.5, respectively. The experimental length of the member was half the actual vertical length due to the symmetric behavior of the vertical. The resulting length was modified to the laboratory floor hold-down locations (finite locations where a reaction frame can be fixed to the strong floor) which gave the final length of 10.3 m (33.6 ft).



Figure 3.4: Load application system mounted to the critical truss



Figure 3.5: Critical vertical, orient horizontally in the laboratory

### 3.2.2 Necessary Changes for the Test-Setup Design

As described above, only half the vertical length was reproduced in the laboratory. To produce twisting moment into the vertical, an endplate was welded onto the end as shown in Figure 3.4. This location would typically be the center of the vertical truss in the actual bridge. Adding this plate detail altered the stress distribution in the vertical in the location





Table 3.1: Steel plate material properties used to reproduce the vertical truss

<b>Part name:</b>	<b>Position no.:</b>	<b>Thickness: (mm) [in]</b>	<b>Average <math>f_y</math>: (MPa) [ksi]</b>	<b>Average <math>f_u</math>: (MPa) [ksi]</b>	<b>Average <math>\epsilon_u</math>: [%]</b>
Reaction box	<i>P.3</i>	50.8 [2.0]	262.35 [38.05]	482.29 [69.95]	33
Reaction box	<i>P.4</i>	19.05 (3/4)	275.79 [40]	481.25 [69.8]	26
Reaction box	<i>P.5 / P.6</i>	25.4 [1.0]	293.37 [42.55]	490.22 [71.1]	25
End plate	<i>P.12</i>	19.05 (3/4)	275.79 [40]	481.25 [69.8]	26
Web	<i>P.2</i>	7.9 [5/16]	326.12 [47.3]	437.82 [63.5]	29
Flanges	<i>P.1 / P.1A</i>	12.7 [1/2]	304.06 [44.1]	427.47 [62]	39
Gusset Plates	<i>P.7 / P.8</i>	9.5 [3/8]	289.58 [42]	489.53 [71]	30
Fill Plates	<i>P.9 / P10 / P11</i>	19.05 (3/4)	275.79 [40]	481.25 [69.8]	26

A few changes were made for practical fabrication considerations and are described here.

The gusset plate in the actual bridge was not perpendicular to the horizontal truss as can be seen in Figure 3.3. This feature was neglected to simplify the experimental setup as shown in Figure 3.8.

The reaction box, which acts as the horizontal chord of the truss, was also modified.

Instead of using multiple layers of steel plates per side, as used in the actual structure, one side plate with the same overall thickness was used. To keep the box as rigid as possible, head plates were welded onto the reaction box as shown in Figure 3.9.

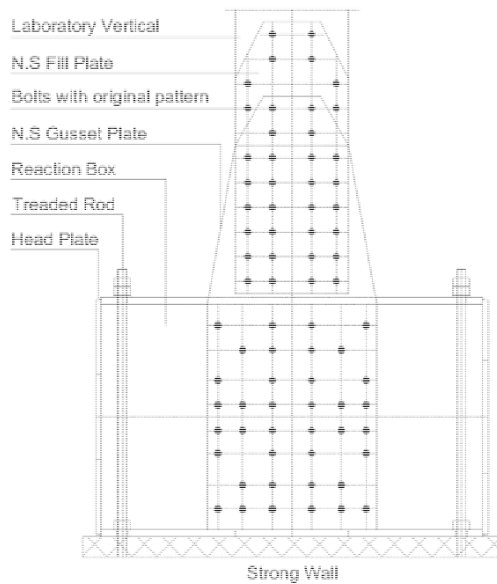


Figure 3.8: Reproduced laboratory vertical with gusset plate perpendicular to the reaction box

Figure 3.9: Reaction box with head plates welded to the side

Four fill plates were used in the existing bridge connection as shown in Figure 3.3. These plates were necessary to adapt the distance between the width of the horizontal chord and the vertical. Since both the reaction box and the vertical were reproduced with the original dimensions, similar fill plates were also used for the experimental specimen.

Two different gusset plates were used for both the near side (N.S) and far side (F.S) connection between the reaction box and the flanges of the I-section as shown in Figure 3.10.

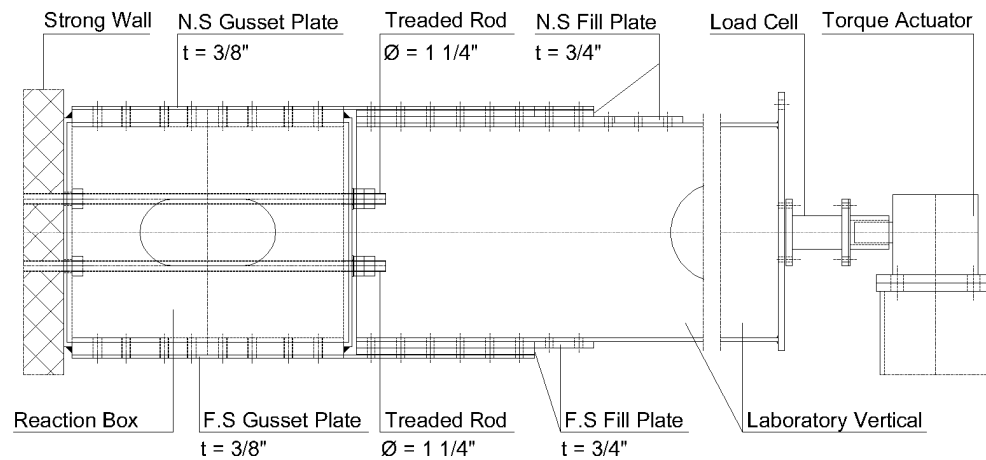


Figure 3.10: Experimental vertical with reaction box, gusset plates and fill plates

The bolt pattern and bolt diameters were reproduced from the existing drawings and adapted to the new gusset plate orientation as shown in Figure 3.8. The original connection used rivets, but the laboratory specimen used A325 structural bolts with identical diameters  $\phi 25.4$  mm (1 in) and  $\phi 22.2$  mm (7/8 in).

All steel assemblies for the experimental setup were produced by a local fabricator and delivered to the structural laboratory on the campus of Oregon State University.

#### 3.2.4 Connections

The reaction box was connected to the strong wall in the structural laboratory as shown in Figure 3.10. The connection consisted of 4 x  $\phi 31.8$  mm (1 1/4 in) threaded rods of ASTM A193-B7. As discussed previously, the reaction box and the vertical specimen were connected with two gusset plates using the original hole pattern and bolt diameters. The vertical specimen was connected to the reaction torque load cell with 8 x 14.3 mm (9/16 in) A574 bolts.

### 3.3 Instrumentation

#### 3.3.1 Instruments

The specimen was instrumented with different strain, displacement, and angular sensors. To measure strains in the laboratory vertical, uniaxial strain gages and strain rosettes were installed. Uniaxial strain gages measure strains only in one direction, whereas strain rosettes measure strains in three different directions. The strain gage sizes used in this experiment are listed in Table 3.2.

Table 3.2: Uniaxial strain gage and strain rosette specifications

<b>Description:</b>	<b>Length: (mm) [in]</b>	<b>Width: (mm) [in]</b>	<b>Angle between gages: (degrees)</b>
Uniaxial strain gage	6.99 [0.28]	3.05 [0.12]	N/A
Strain rosettes	6.1 [0.24]	7.6 [0.30]	45

Using data from each gage, the stress at its location was calculated. Using data from the strain rosettes, stresses in every direction could be calculated at the specific measuring point, by applying the principle of Mohr's circle.

To check boundary conditions and change in the angle of twist along the specimen, five displacement sensors were installed along the length of the vertical. To check the results of the inclinometers, an angular rate sensor, which is being used in as part of a field monitoring installation on the bridge, was installed at the loaded end of the vertical.



### 3.3.2 Instrumentation Plan (with Initial Configurations)

The critical regions of the vertical specimen were at the gusset plate connection location, therefore, strain gages were concentrated in this area of the member (Sections 2 and 3) as can be seen in Figure 3.11 and Figure 3.12. However, to capture the stress distribution over the entire vertical, strain rosettes were distributed over the length of the vertical specimen as shown in Figure 3.11 and Figure 3.12. The locations of the strain gages from the edge of the I-section top flange are shown in Table 3.3.

Table 3.3: Strain rosette distances from the edge of the top flange

<b>Section name:</b>	<b>Gage name:</b>	<b>Distance from edge of the flange: (mm) / [in]</b>
3	R 13	38.89 / [1.53]
4	R 11	26.19 / [1.03]
4	R 9	23.02 / [0.91]
5	R 7	24.61 / [0.97]
5	R 5	27.78 / [1.09]
6	R 3	23.81/ [0.94]
6	R 1	23.81/ [0.94]
7	NR 2	28.58/ [1.125]
7	NR 1	27.78/ [1.09]

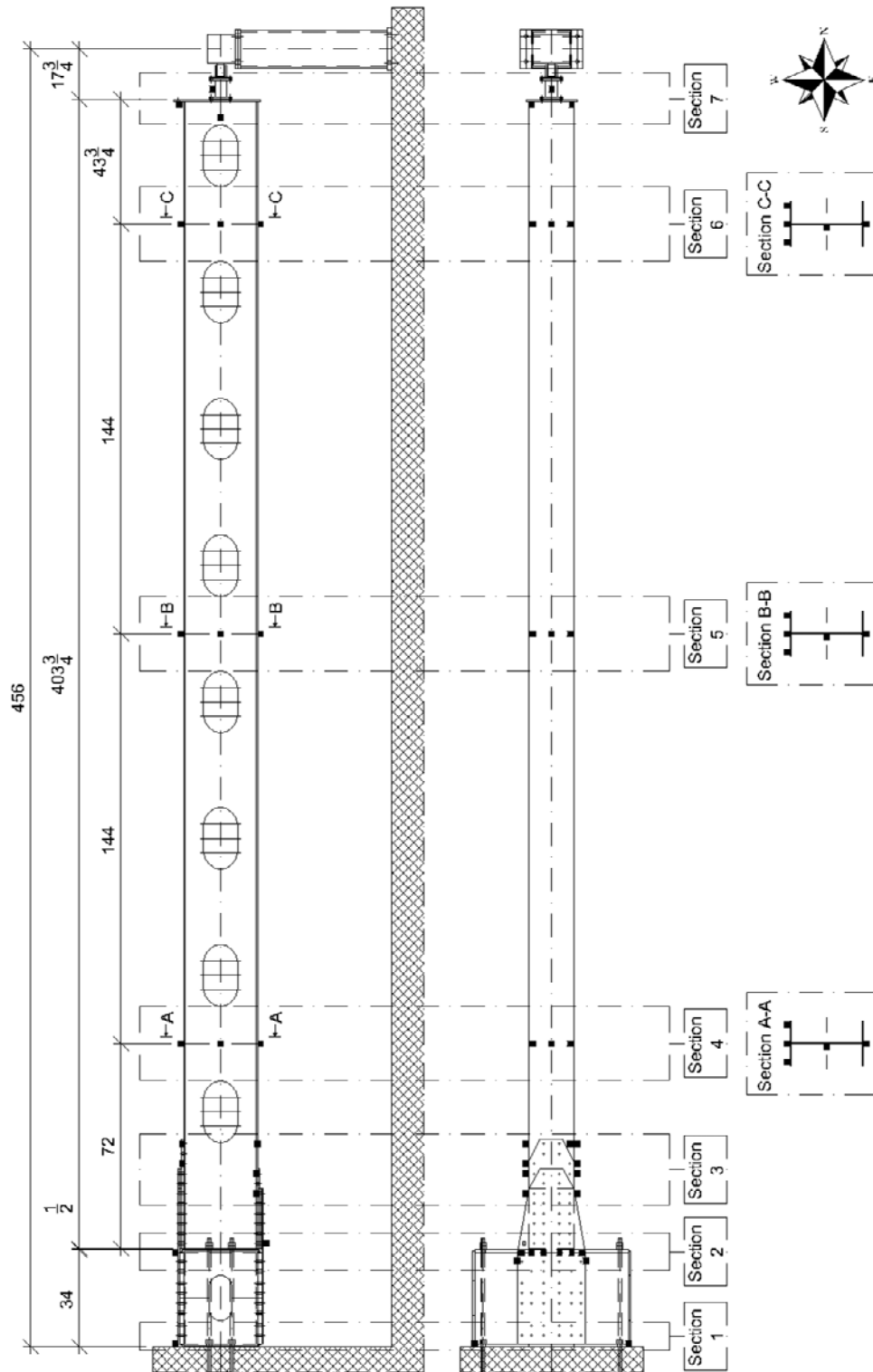


Figure 3.11: Instrumentation overview of the entire test setup

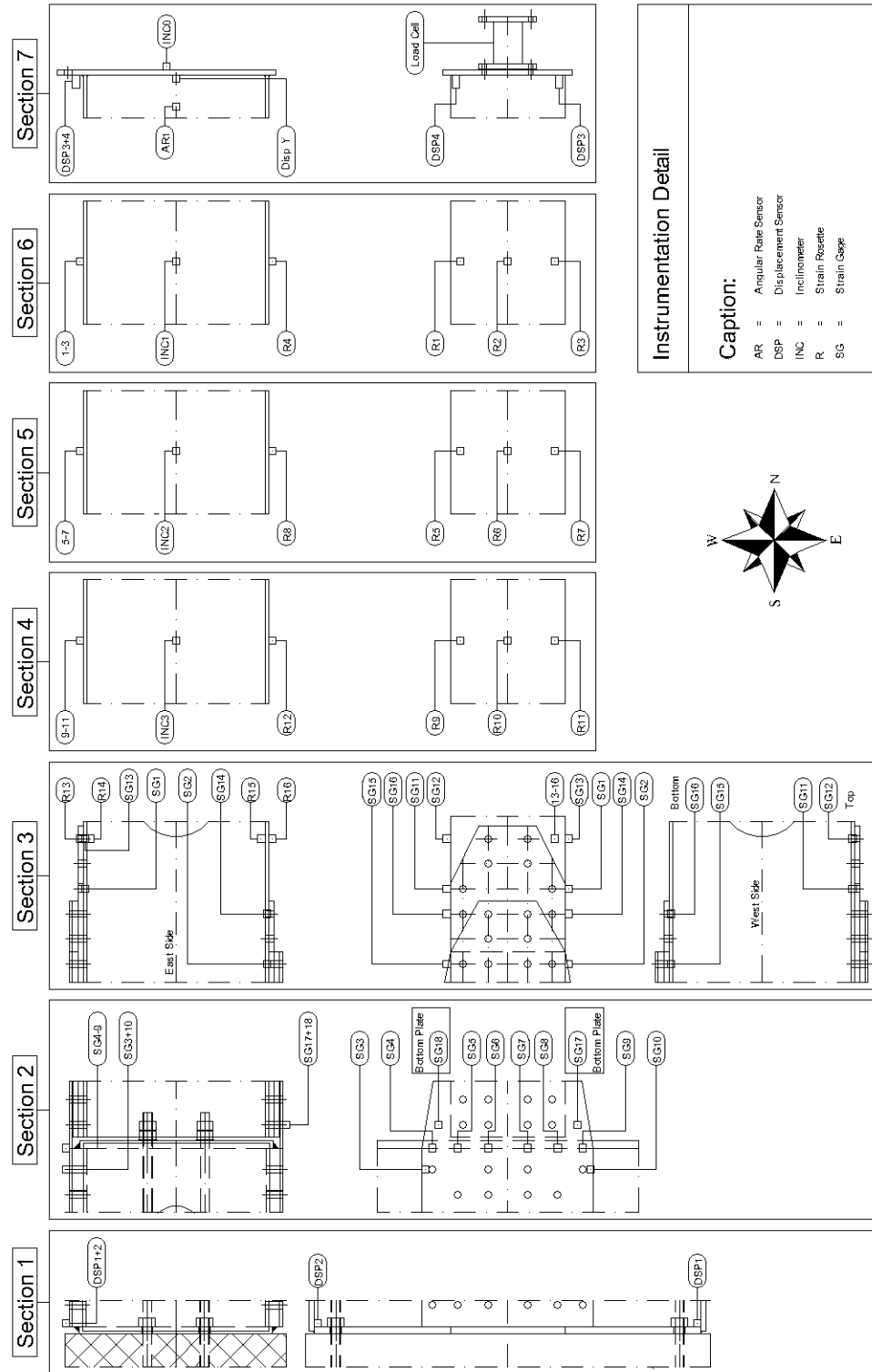


Figure 3.12: Instrumentation details of the different sections of the specimen

### 3.3.3 Instrumentation by Section

The instrumentation of the vertical was separated into seven different sections along the length of the specimen. The instruments placed within each of the different sections and their purpose is explained in the following sections.

#### 3.3.3.1 *Section 1*

Section 1 is the section closest to the strong wall. In this section, measurements were taken from two displacement sensors (DSP1 and DSP2) bonded to the strong wall as shown in Figure 3.13. These sensors were used to monitor relative slip between the reaction box and the strong wall.

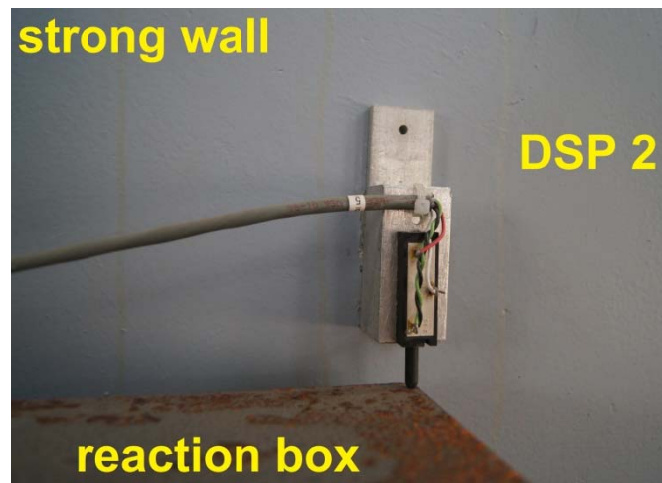


Figure 3.13: Location of displacement sensor (DSP2) for section 1

### 3.3.3.2 Section 2

Section 2 is where the reaction box ends and the vertical specimen begins. The main interest in this section was the stress distribution in the gusset plate along the reaction box edge. To monitor these stresses, strain gages (SG) 4-9 were installed on the top gusset plate. SG3 and SG10 were installed to show stresses between edge bolt and the top edge of the gusset plate. The instrumented top gusset plate is shown in Figure 3.14.

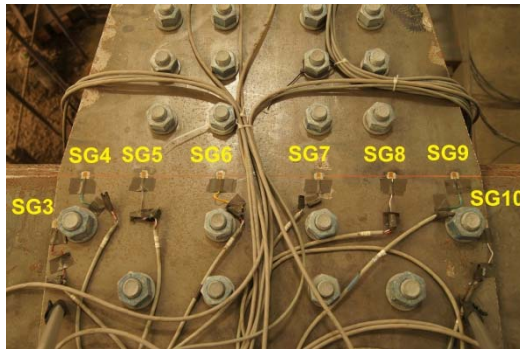


Figure 3.14: Location of SG3-10 on the top gusset plate



Figure 3.15: Location of SG17 and 18 on the bottom gusset plate

In addition, two strain gages (SG17 and SG18) were placed onto the underside of the bottom gusset plate to capture the stress magnitude and distribution in the bottom plate. These gages are shown in Figure 3.15.

### 3.3.3.3 Section 3

The transition zone between the vertical and the gusset plate was instrumented in section 3. Strain gages were installed on the edges of both the top and bottom flanges, as shown in Figure 3.16.



Figure 3.16: Strain gage (SG16) fixed to the side of the bottom flange

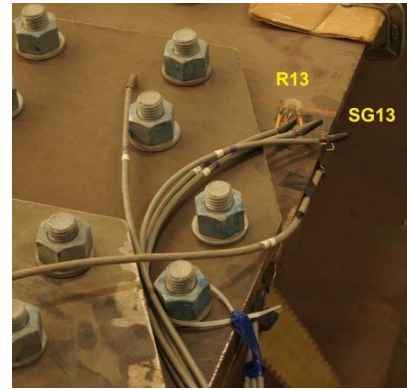


Figure 3.17: Strain rosette (R13) and strain gage (SG13) mounted onto the top flange

Four strain gages (SG1, SG11, SG12 and SG13) were placed onto the side of the top flange whereas four others (SG2, SG14, SG15 and SG16) were placed onto the side of the bottom flange of the vertical. To monitor the stress distribution within the top and the bottom flange in this area, strain rosettes were installed onto the top and bottom side of both flanges as shown in Figure 3.17. The top flange top side rosette is R13, the top flange bottom side rosette is R14, the bottom flange top side rosette is R15 and the bottom flange bottom side rosette is R16.

#### 3.3.3.4 Sections 4 through 6

These three sections were instrumented identically to monitor the stress distribution in the vertical specimen at locations along the length. On the top side of the top flange, three strain gages were installed (Section 4: R9-R11; Section 5: R5-R7; Section 6: R1-R3) as shown in Figure 3.18.

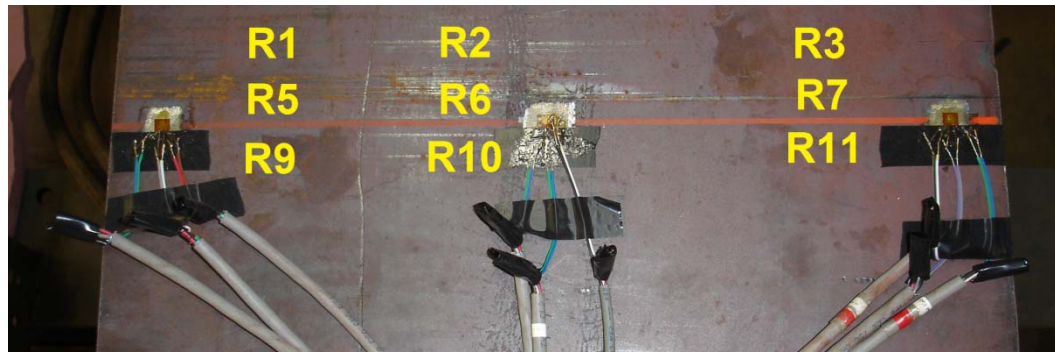


Figure 3.18: Strain rosette distribution over top side of the top flange

The rosettes located near the edge of the flange were placed approximately 25.4 mm (1 in.) from the edge (exact locations are listed in Table 3.3) whereas the other rosettes were placed along the centerline of the top flange.

To compare stresses between the top and bottom flanges, strain rosettes were placed onto the bottom side of the bottom flange (Section 4: R12; Section 5: R8; Section 6: R4). To capture the angle of twist for the vertical specimen, inclinometers were positioned at the neutral axes in each of these sections (Section 4: INC3, Section 5: INC2; Section 6: INC1) as shown in Figure 3.19.



Figure 3.19: Example inclinometer (INC1) positioned at the neutral axis of the vertical

### 3.3.3.5 Section 7

Section 7 is located at the end of the vertical specimen, where the I-section was welded to the endplate and the reaction torque load cell was connected. The load cell was used to measure the torsional moment induced by the torque actuator. To monitor the rotations in that section, an inclinometer (INC0) and an angular rate sensor (AR1) were placed onto the endplate and onto the web of the I-section, as shown in Figure 3.20.



Figure 3.20: Angular rate sensor (AR1) and inclinometer (INC0) fixed onto the critical vertical

To verify the accuracy of the rotation measure sensors (INC0 and AR1), a string potentiometer (Disp Y) was connected to the endplate to measure the centerline displacement relative to the strong floor as shown in Figure 3.21 and Figure 3.22. With this data the rotation angle of the I-section could be independently verified.





Figure 3.21: Connection between the string potentiometer and the endplate



Figure 3.22: String potentiometer on the strong floor to check the rotations at the endplate

To measure the relative displacement of the endplate, two displacement sensors (DSP3 and DSP4) were mounted onto a special fixture that elevates them from the top flange and fixes them to the center line of the top flange, where the movement of the flange was assumed to be zero. This setup is shown in Figure 3.23.

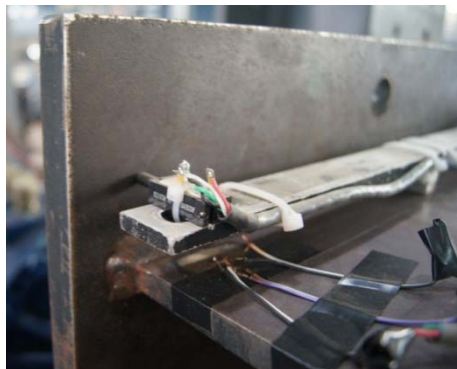


Figure 3.23: Displacement sensor (DSP4) measures displacements of the endplate

### 3.3.4 Instrumentation Plan (with Configurations for the Rotation Test)

To obtain a finer detail of the angle of twist along the vertical specimen, the inclinometers (INC1-INC3) were mounted onto magnets and positioned closer to each other than in the regular tests done previously, as shown in Figure 3.24. These tight grouping of sensors were then moved along the length of the vertical specimen and the input motions repeated.



Figure 3.24: Inclinometers positioned at a closer distance

As a reference, the angular rate sensor (AR1) and one inclinometer (INC0) were left at their initial positions. In each test, three inclinometers were moved to a new location; therefore eight test runs were needed to collect the data that could precisely describe the rotation along the length of the vertical specimen. To align the overlapping data sets, one of the sensors in each test group was left at its previous position and only two of the three sensors were shifted to a new position. The positions of each inclinometer as well as their specific labels are shown in Table 3.4 and Figure 3.25.

Table 3.4: Position and name of the inclinometers in the rotation test

<b>Distance from the end of the vertical: (mm) / [in]</b>	<b>Inclinometer:</b>	<b>Inclinometer Label for Rotation test:</b>	<b>Test run:</b>
10255.25 / [403.75]	INC 0	INC0	All
10188.58 / [401.13]	AR 1	AR1	All
9144 / [360]	INC 1	# 1	1
7924.8 / [312]	INC 2	# 2	1
6705.6 / [264]	INC 3	# 3	1 / 2
5486.4 / [216]	INC 2	# 4	2
4267.2 / [168]	INC 1	# 5	2 / 3
3048 / [120]	INC 2	# 6	3
1828.8 / [72]	INC 3	# 7	3 / 4
889 / [35]	INC 2	# 8	4
762 / [30]	INC 1	# 9	4 / 5
635 / [25]	INC 2	# 10	5
508 / [20]	INC 3	# 11	5 / 6
381 / [15]	INC 2	# 12	6
254 / [10]	INC 1	# 13	6 / 7
177.8 / [7]	INC 3	# 14	7
101.6 / [4]	INC 2	# 15	7 / 8
38.1 / [1.5]	INC 3	# 16	8

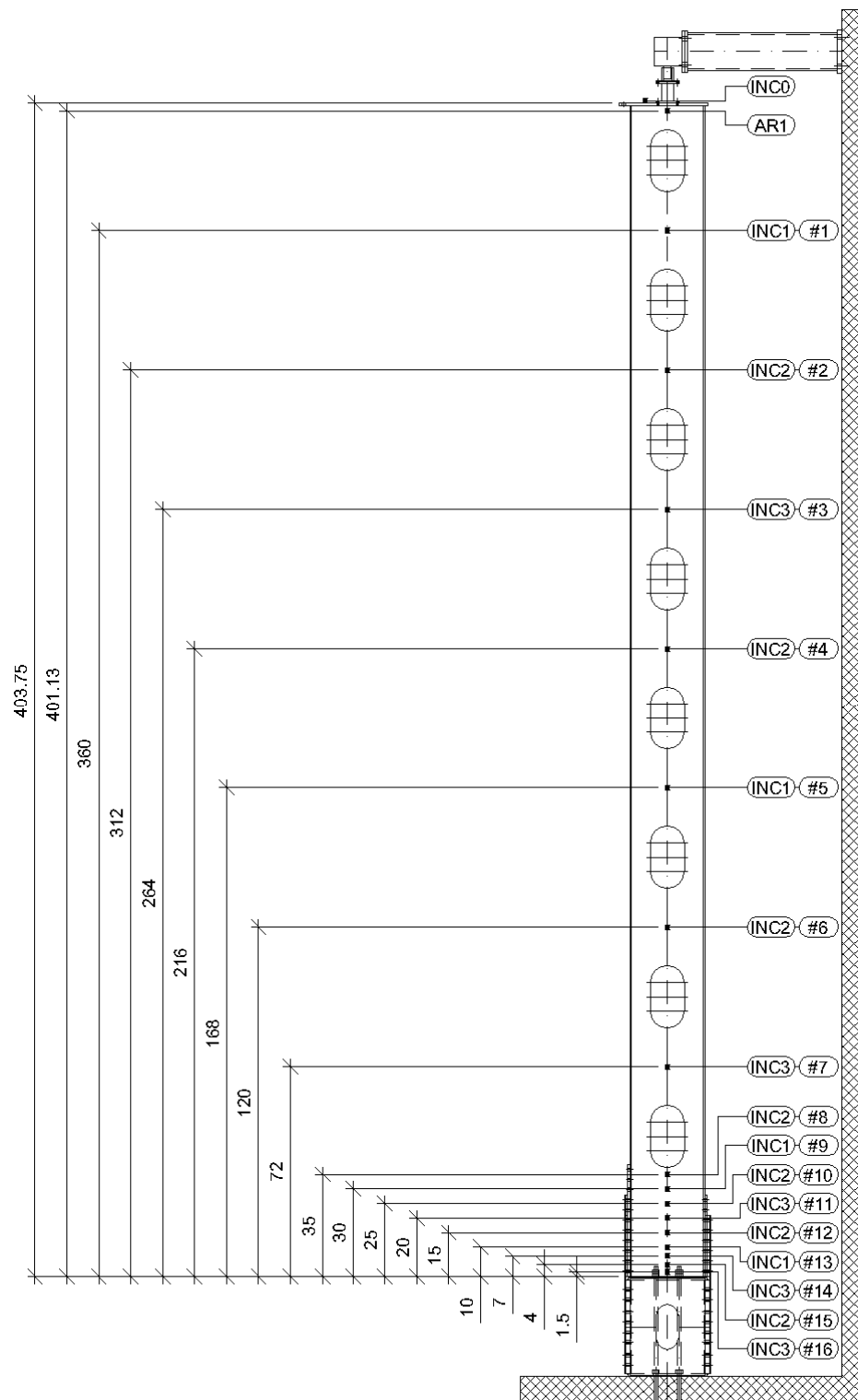


Figure 3.25: Instrumentation overview with rotation test configurations

#### 3.3.4.1 *Adaptions Made to Section 7*

To get a better understanding of the stress distribution close to the endplate, the sensors in Section 7 were adapted. The displacement sensors (DSP3 and DSP4) and their fixture were removed and strain rosettes were placed onto the top side of the top flange, as shown in Figure 3.26. Their distances from the flange edge are listed in Table 3.3.

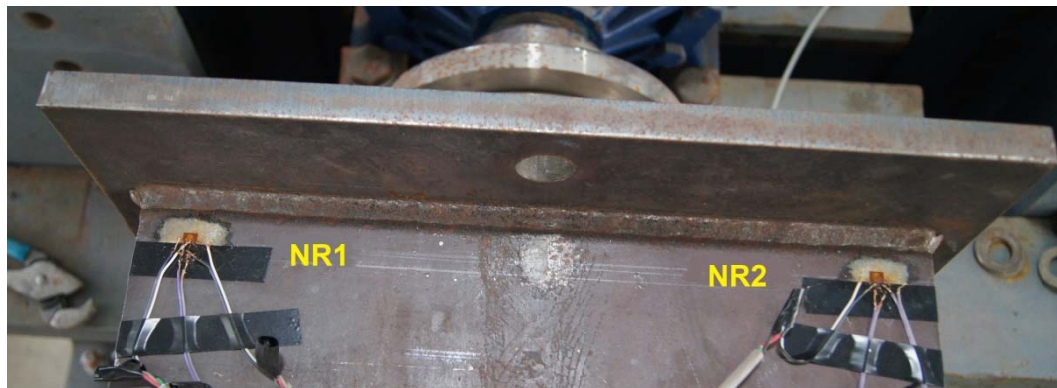


Figure 3.26: Adapted section 7, with new strain rosettes (NR1 and NR2)

### 3.4 Load Induction

To simulate the angle change in the vertical, a servo-hydraulic torque actuator with a torque capacity of 12.2 kNm (108 kip-in) was used. The actuator was mounted on a reaction frame which was connected to the strong floor as shown in Figure 3.27. The vertical and the actuator are connected through the load cell and the endplate as shown in Figure 3.28.



Figure 3.27: Torque actuator fixed onto the reaction frame



Figure 3.28: Torque actuator, load cell and vertical assembly

The twisting induced to the specimen was deformation controlled (angle control). The sensor used to control the rotational deformation at the torque actuator was a rotary variable differential transformer (RVDT) mounted onto a magnet and held in place by a fixture as shown in Figure 3.29 and Figure 3.30. The RVDT was validated with an independent string potentiometer that was also connected to the torque actuator as shown in Figure 3.30.

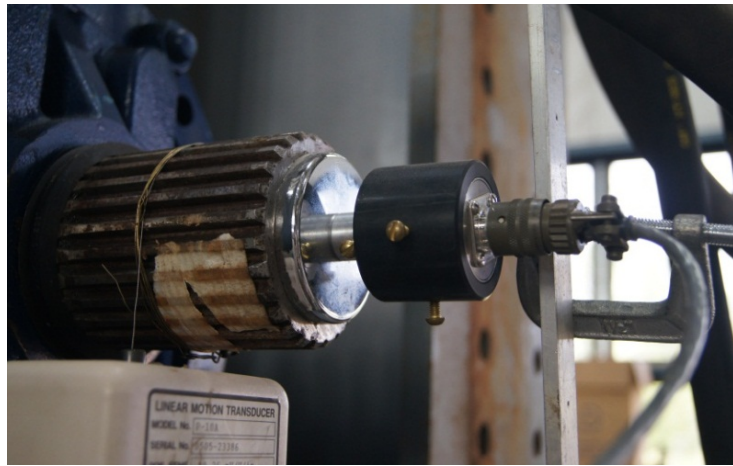


Figure 3.29: RVDT mounted to the torque actuator



Figure 3.30: Rotary variable differential transformer (RVDT) mounted to the torque actuator and connected to the reaction frame

### **3.5 Experimental Results**

#### **3.5.1 Rotational Response of Specimen and Instrument Performance**

Initial tests were completed with the installed test setup. These tests were used to assess the fixity of the vertical to the strong wall, the functionality of the torque actuator, and to adjust instrumentation. Datasets were collected for these tests to get the stress distribution along the vertical and along the gusset plates. With this information, a finite element model (described in Chapter 4.1) was checked and updated to better correlate with the experimental results. With the help of the finite element model, the maximum rotation angle for elastic behavior was determined.

The main purpose of the initial testing was to find the appropriate test frequency and angle change for the fatigue test. Two different angle changes (5 and 9 degree) were tested, and for each angle change, data sets with different frequencies were collected. The different testing frequencies were 0.05, 0.1, 0.5, 1.0, 2.0 and 3.0 Hz. Data were collected at a sampling rate varying from 100 to 400 Hz. With the collected data, the different instruments were evaluated and recalibrated as needed.

After evaluating the instrumentation performance it was found that the strain gages, strain rosettes and the angular rate sensor were not affected by the amplitude of the angle of twist or different loading frequencies. However, the inclinometers (INC0-INC3) were credible only up to a loading frequency of 0.5 Hz. Data from these sensors at higher loading frequencies were not valid.



Test data was collected for several different test runs. Since the data collected at a low rotational frequency (e.g. 0.05 or 0.1 Hz) resulted in data with low noise content and within the operational frequency range of the inclinometers, data presented in this report were collected at a 0.05 Hz rotational frequency, a target rotation of  $\pm 9.0$  degrees, and a sampling rate of 100 Hz.

### 3.5.1.1 Time-History Data

The test run consisted of 5 cycles and the load was induced as a sinusoidal function. The results for the rotation at the actuator (RVDT) are plotted in Figure 3.31.

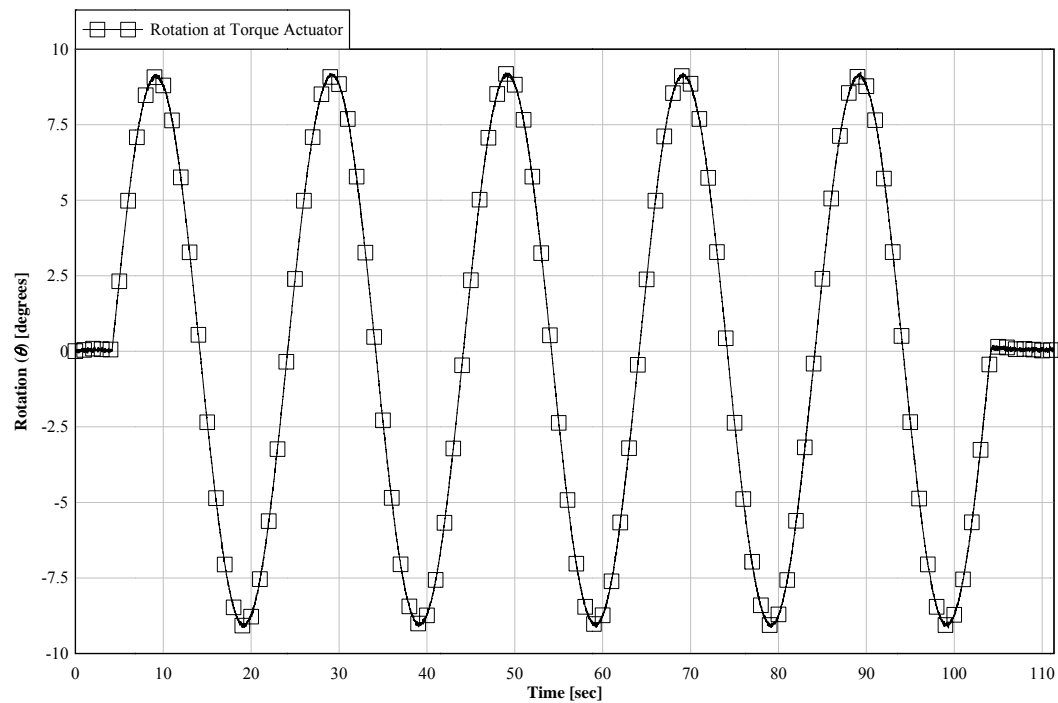


Figure 3.31: Time-history plot of the rotation at the torque actuator (target of  $\pm 9$  degrees)

The resulting torque measured at the torque actuator (load cell) are shown in Figure 3.32

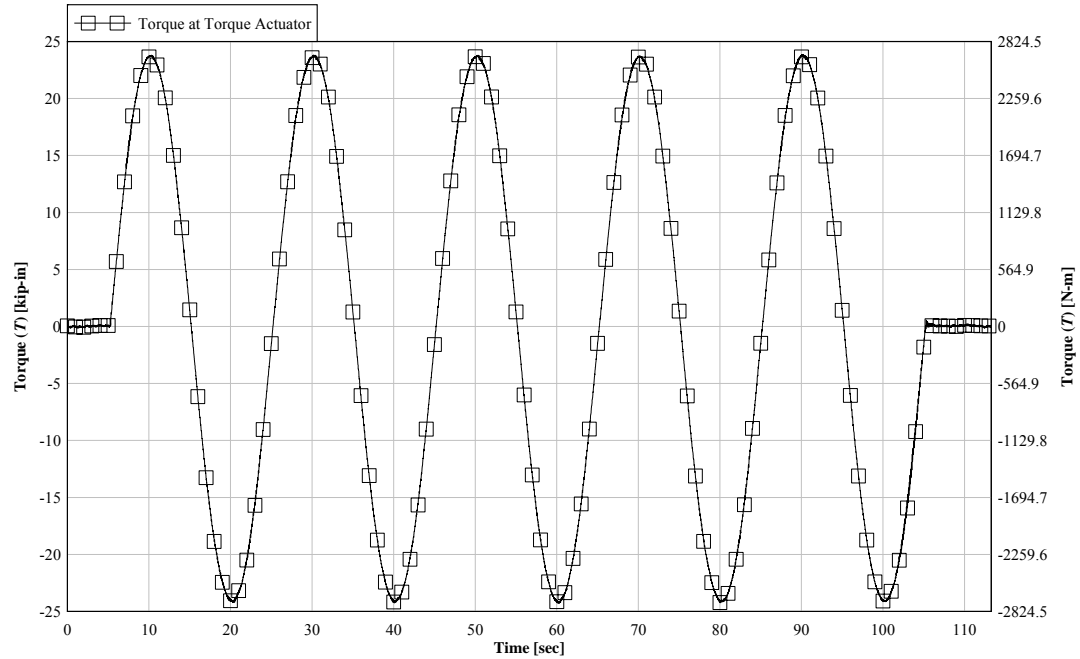


Figure 3.32: Time-history plot of the torque force ( $T$ ) at the torque actuator (target of  $\pm 9.0$  degrees)

The angular rate sensor measured the angle change per second. Therefore, the results of this sensor were integrated over time to obtain rotation values. Since an integration constant occurs when a function is integrated, the trend of the integrated curve was manually removed as shown in Figure 3.33.

Time history results for the different inclinometers along the length of the I-section were plotted in Figure 3.34. The location of these sensors can be found in Figure 3.11.

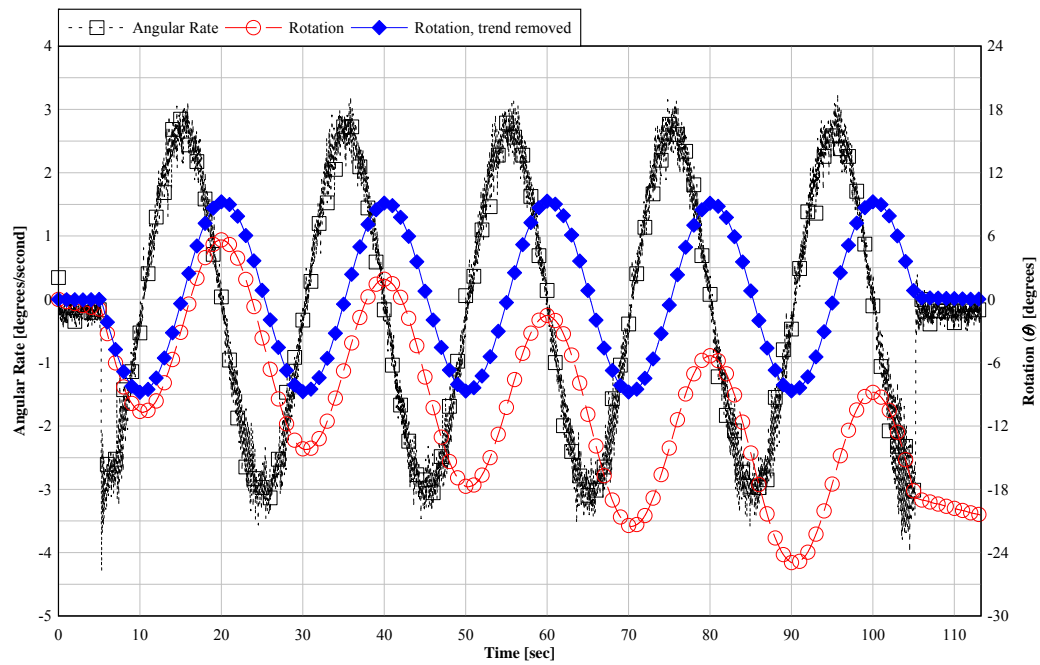


Figure 3.33: Time-history plot of the angular rate sensor (AR1)

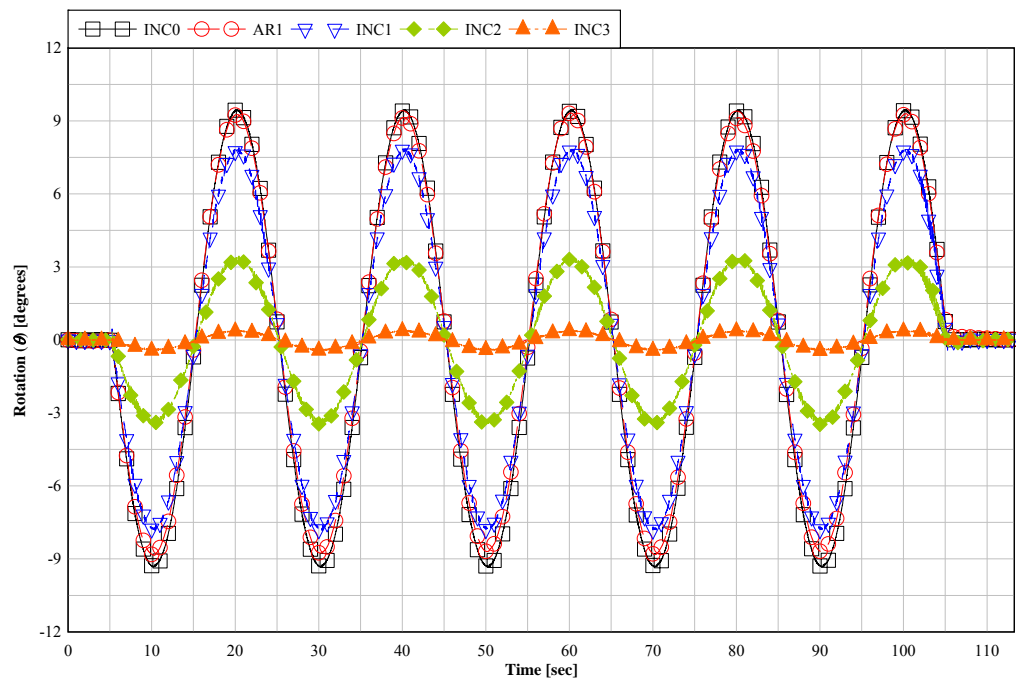


Figure 3.34: Time-history plot of the inclinometers (INC0-3) and angular rate sensor (AR1) along the vertical

The inclinometers used in this study, provided accurate measurements of twist angle up to a testing frequency of 0.5 Hz. For the higher frequencies tested, the results collected from the inclinometer were not credible. However, the angular rate sensor provided accurate results throughout the frequency ranges considered. The two different sensors (INC0 = Inclinometer and AR1=Angular rate sensor) are compared at a testing frequency of 1 Hz and a target angle of twist of  $\pm 9$  degrees in Figure 3.35. As seen here, the inclinometer could not adequately capture the maximum twist angle.

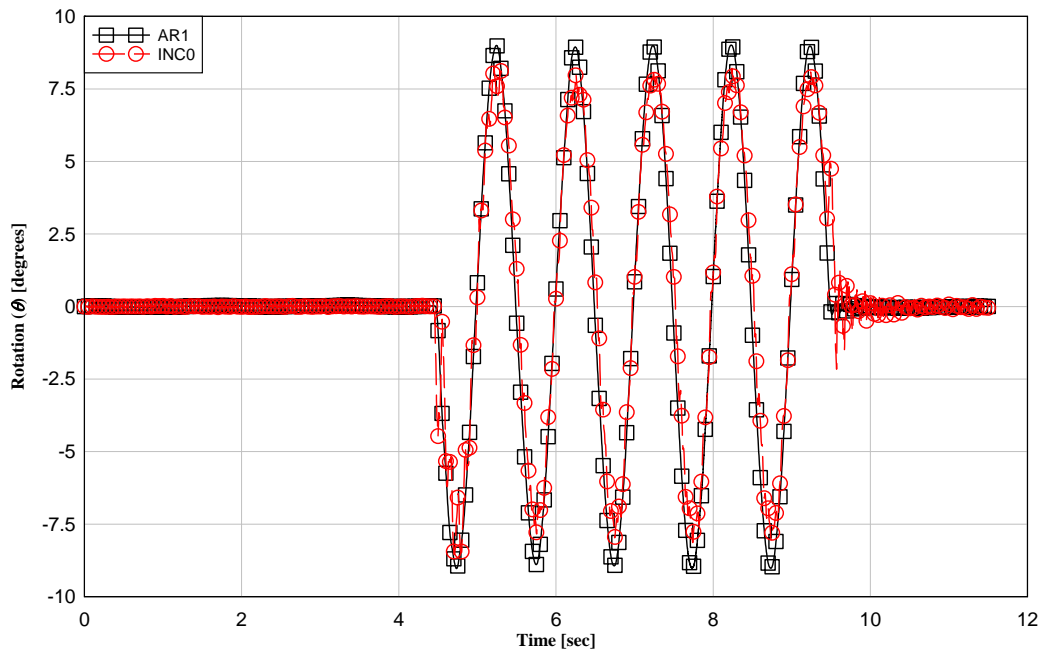


Figure 3.35: Time-history comparison of INC0 (inclinometer) and AR1 (angular rate sensor) at a testing frequency of 1 Hz

Displacement sensors (DSP1-DSP2) were used to assess the fixation of the reaction box to the strong wall. The collected time-history data for DSP1 and DSP2 (control measurements for slip between strong wall and reaction box) showed that there is no noticeable slip between the wall and the setup. The data collected was not separable from the electrical

noise inherent of the data acquisition system. Therefore, zero slip between the strong wall and the reaction box was assumed.

The time history data of DSP 3 and DSP 4 are plotted in Figure 3.36. This data shows a small displacement between the top flange of the I-section and the endplate. This movement indicates that the endplate does not fully restrain the warping deformations of the I-section flanges.

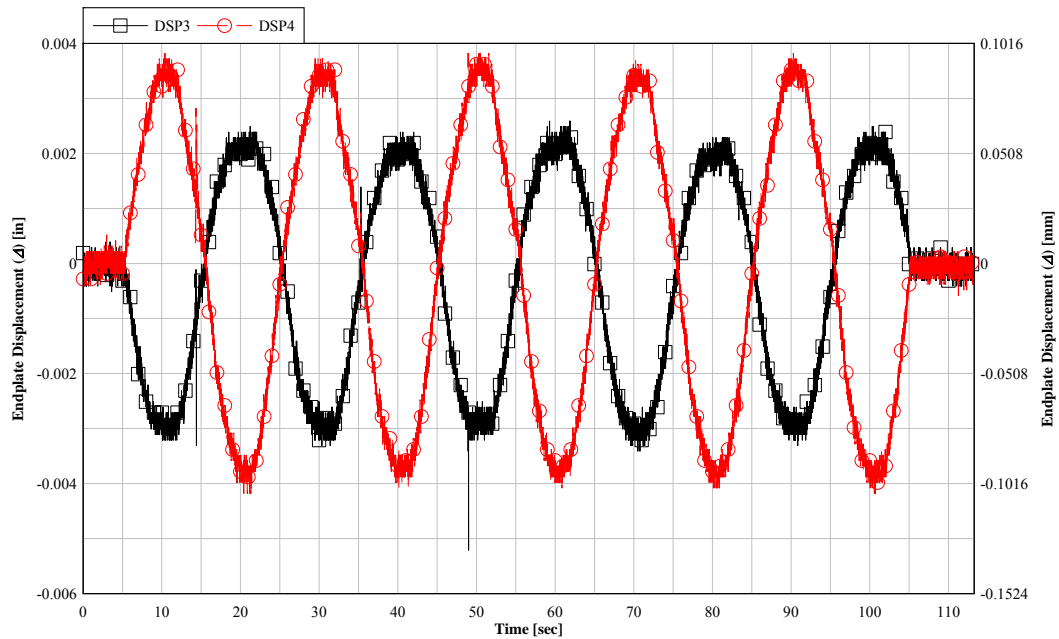


Figure 3.36: Time-history displacement response at sensors DSP3 and 4

Since time-history data for stresses are not a useful way to show results of strain rosettes and strain gages, only example results from each gage type are shown in Figure 3.37 and Figure 3.38. However, the stress results are synthesized for magnitude and distribution along the specimen as will be described subsequently.

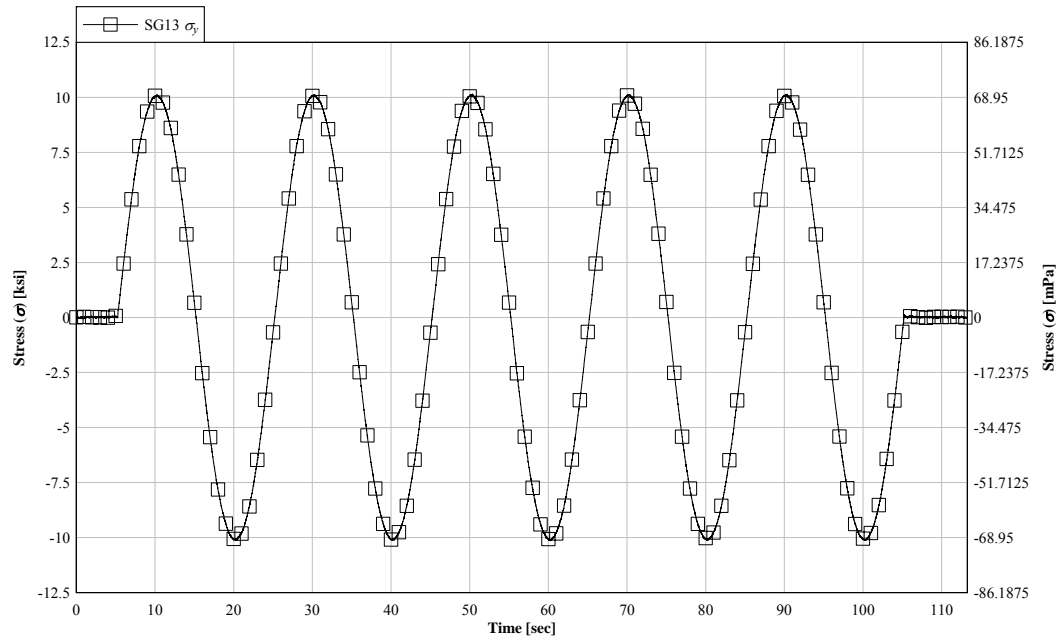


Figure 3.37: Example time-history plot of a strain gage (SG13)

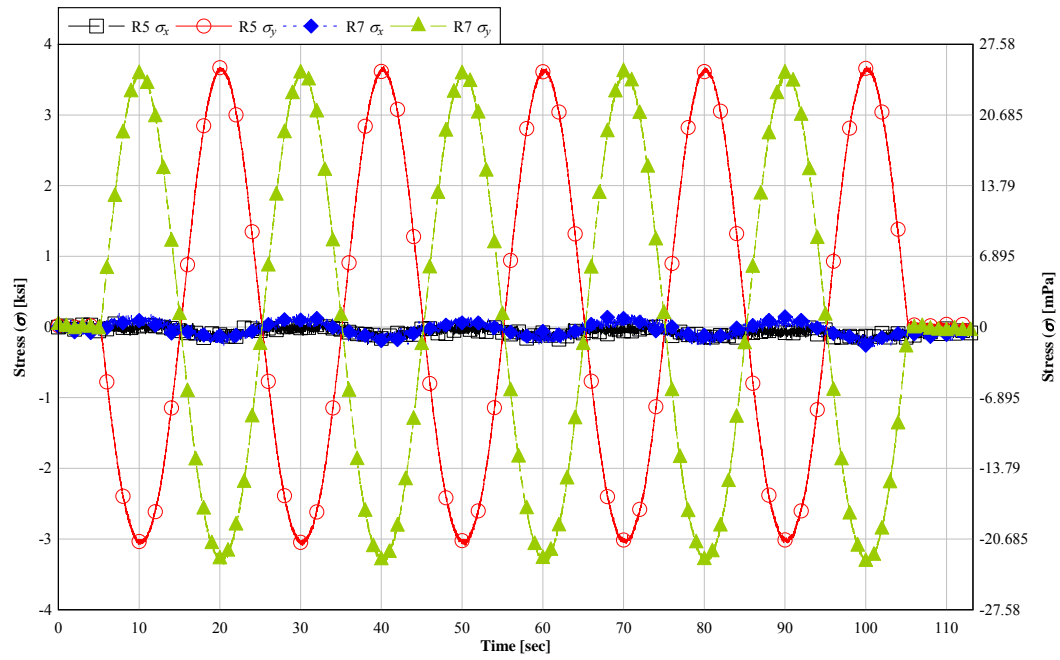


Figure 3.38: Example time-history plot of strain rosettes (R5 and R7)

### 3.5.1.2 Average Peak to Peak Results

All the data collected were initially plotted as time-histories. From these results the average peak-to-peak values were obtained for each of the different sensors. To get these values, the difference between the maximum and the minimum peak was determined and divided by two. This procedure was repeated for each cycle. Therefore, for each sensor, strain gage or strain rosette, five peak values were obtained. From these five values, the overall maximum value and the average of the peak values are listed in Table 3.5, Table 3.6 and Table 3.7.

Table 3.5: Maximum and average peak to peak results for the sensors

<b>Target value: 9 Degrees</b>		
<b>Sensor:</b>	<b>Maximum:</b>	<b>Average:</b>
RVDT	9.38 deg	9.33 deg
AR1	9.05	9.00
INC0	9.20	9.20
INC1	7.87	7.84
INC2	3.46	3.44
INC3	0.42	0.42
Load Cell	2.71 kN-m [24.04 kip-in]	2.71 kN-m [24.02 kip-in]

Using the results of the torque cell and inclinometer 0 (INC0), the torsional stiffness of the specimen was determined to be 16.92 kN-m/rad (149.74 kip-in/rad).

The peak-to-peak maximum and average stress values for the strain rosettes are listed in Table 3.6. The stress directions for Table 3.6 are defined as, x-axis in the west-east direction and the z-axis in the north-south direction as shown in Figure 3.11.

Table 3.6: Maximum and average peak-to-peak results for strain rosettes

<b>Target value: 9 Degrees</b>					
<b>Rosette Gage:</b>	<b>Direction:</b>	<b>Normal Stress (<math>\sigma</math>)</b>		<b>Shear Stress (<math>\tau</math>)</b>	
		<b>Max. Stress (MPa) [ksi]</b>	<b>Avg. Stress (MPa) [ksi]</b>	<b>Max. Stress (MPa) [ksi]</b>	<b>Avg. Stress (MPa) [ksi]</b>
R1	<i>Z</i>	3.15 [0.46]	3.06 [0.44]	-	-
	<i>X</i>	2.04 [0.30]	1.95 [0.28]	23.92 [3.47]	23.84 [3.46]
R2	<i>Z</i>	2.13 [0.31]	2.07 [0.30]	-	-
	<i>X</i>	2.22 [0.32]	2.09 [0.30]	32.59 [4.73]	32.53 [4.72]
R3	<i>Z</i>	2.46 [0.36]	2.44 [0.35]	-	-
	<i>X</i>	2.25 [0.33]	2.12 [0.31]	23.73 [3.44]	23.69 [3.44]
R4	<i>Z</i>	8.69 [1.26]	8.65 [1.25]	-	-
	<i>X</i>	11.27 [1.63]	10.99 [1.59]	32.82 [4.76]	32.72 [4.75]
R5	<i>Z</i>	23.35 [3.39]	23.27 [3.37]	-	-
	<i>X</i>	1.20 [0.17]	1.14 [0.17]	22.42 [3.25]	22.38 [3.25]
R6	<i>Z</i>	1.76 [0.25]	1.72 [0.25]	-	-
	<i>X</i>	2.01 [0.29]	1.96 [0.28]	25.16 [3.65]	25.08 [3.64]



R7	<i>Z</i>	24.11 [3.50]	24.04 [3.49]	-	-
	<i>X</i>	1.64 [0.24]	1.57 [0.23]	22.48 [3.26]	22.44 [3.25]
R8	<i>Z</i>	0.80 [0.12]	0.78 [0.11]	-	-
	<i>X</i>	2.22 [0.32]	2.14 [0.31]	24.80 [3.60]	24.76 [3.59]
R9	<i>Z</i>	42.78 [6.20]	42.72 [6.20]	-	-
	<i>X</i>	35.43 [5.14]	35.27 [5.12]	38.98 [5.65]	38.95 [5.65]
R10	<i>Z</i>	1.67 [0.24]	1.53 [0.22]	-	-
	<i>X</i>	7.55 [1.10]	6.91 [1.00]	15.67 [2.27]	15.63 [2.27]
R11	<i>Z</i>	58.09 [8.43]	57.99 [8.41]	-	-
	<i>X</i>	1.02 [0.15]	0.96 [0.14]	30.52 [4.43]	30.49 [4.42]
R12	<i>Z</i>	0.83 [0.12]	0.82 [0.12]	-	-
	<i>X</i>	0.93 [0.14]	0.84 [0.12]	14.92 [2.16]	14.88 [2.16]
R13	<i>Z</i>	47.52 [6.89]	47.47 [6.88]	-	-
	<i>X</i>	3.03 [0.44]	2.98 [0.43]	25.19 [3.65]	25.10 [3.64]
R14	<i>Z</i>	56.85 [8.25]	56.76 [8.23]	-	-
	<i>X</i>	2.57 [0.37]	2.48 [0.36]	28.57 [4.14]	28.49 [4.13]
R15	<i>Z</i>	48.87 [7.09]	48.83 [7.08]	-	-
	<i>X</i>	2.30 [0.33]	2.23 [0.32]	25.44 [3.69]	25.40 [3.68]

R16	<i>Z</i>	41.10 [5.96]	41.02 [5.95]	-	-
	<i>X</i>	7.30 [1.06]	7.27 [1.05]	17.44 [2.53]	17.38 [2.52]
NR1	<i>Z</i>	72.58 [10.53]	72.50 [10.52]	-	-
	<i>X</i>	21.72 [3.15]	21.67 [3.14]	26.03 [3.78]	26.01 [3.77]
NR2	<i>Z</i>	71.25 [10.33]	71.11 [10.31]	-	-
	<i>X</i>	13.38 [1.94]	13.30 [1.93]	29.62 [4.30]	29.52 [4.28]

The peak-to-peak maximum and average stresses for the uniaxial strain gages are listed in Table 3.7.

Table 3.7: Maximum and average peak-to-peak results for uniaxial strain gages

Target value: 9 Degrees			
Strain Gage:	Direction:	Normal Stress ( $\sigma$ )	
		Max. Stress (MPa) [ksi]	Avg. Stress (MPa) [ksi]
SG1	<i>Z</i>	44.20 [6.41]	44.08 [6.39]
SG2	<i>Z</i>	27.50 [3.99]	27.44 [3.98]
SG3	<i>Z</i>	33.71 [4.89]	33.54 [4.86]
SG4	<i>Z</i>	32.52 [4.72]	32.47 [4.71]
SG5	<i>Z</i>	16.20 [2.35]	16.09 [2.33]
SG6	<i>Z</i>	14.21 [2.06]	14.16 [2.05]

SG7	Z	16.00 [2.32]	15.93 [2.31]
SG8	Z	23.93 [3.47]	23.80 [3.45]
SG9	Z	38.28 [5.55]	38.21 [5.54]
SG10	Z	26.91 [3.90]	26.87 [3.90]
SG11	Z	43.38 [6.29]	43.33 [6.28]
SG12	Z	73.05 [10.60]	72.80 [10.56]
SG13	Z	70.00 [10.15]	69.89 [10.14]
SG14	Z	71.43 [10.36]	71.31 [10.34]
SG15	Z	46.57 [6.75]	46.42 [6.73]
SG16	Z	68.10 [9.88]	68.06 [9.87]
SG17	Z	37.94 [5.50]	37.84 [5.49]
SG18	Z	37.06 [5.38]	37.02 [5.37]

The maximum stress in the specimen was 73.05 MPa (10.60 ksi) and was measured at a uniaxial strain gage location (SG13) located on the vertical near the gusset plate. The maximum shear stress measured was found to be 38.98 MPa (5.65 ksi) and was recorded at strain rosette 9 (R9).

### 3.5.2 Rotation Testing

The rotational behavior of the vertical was characterized along the entire length of the vertical. The instrumentation for this series of tests was modified as explained in Chapter 3.3.4. Eight tests were conducted, all at a loading frequency of 0.05 Hz and with a maximum imposed rotation angle change of  $\pm 9$  degrees. Data were collected at a sample rate of 100 Hz. The data from the rotation tests were reduced by using the peak-to-peak average method as described in Chapter 3.5.1.2. The amplitude of the angle of twist along the length of the member is shown in Figure 3.39.

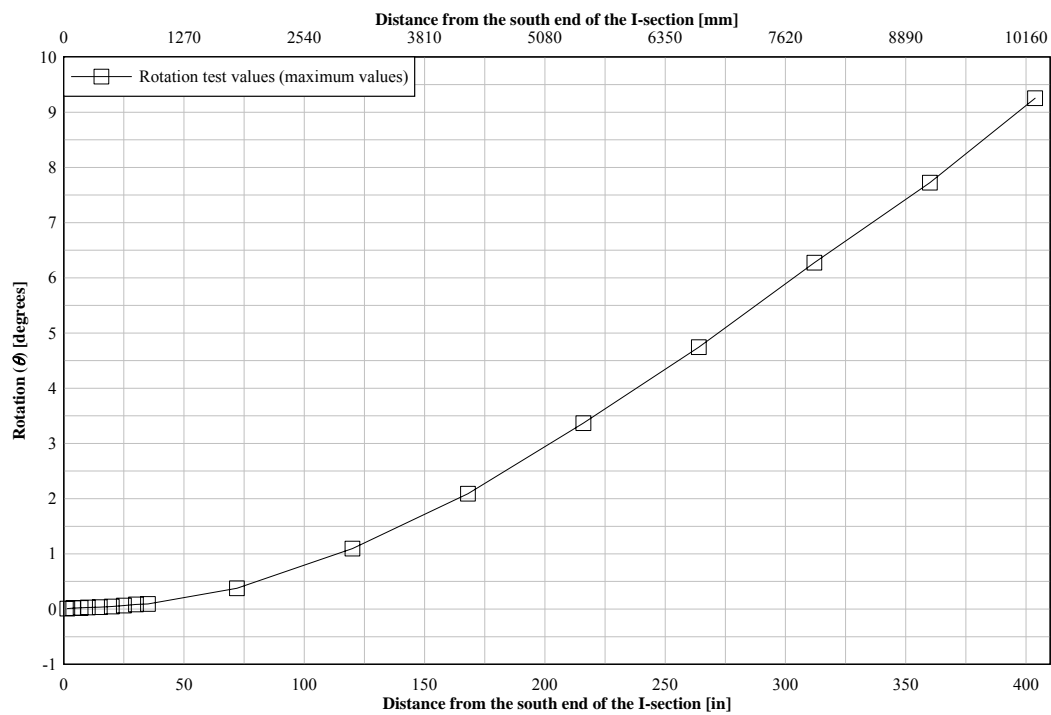


Figure 3.39: Rotation along the span

The rotation becomes zero as the vertical enters the gusset plates. The point of zero rotation was determined from Figure 3.39, when the magnitude of the measured rotation was at the

same magnitude as the inherent electrical noise in the data acquisition system it was no longer possible to distinguish movement. This occurs when the rotation magnitude is 0.05 degrees. Therefore, the point of zero rotation was chosen where the rotational values were less than 0.05 degrees. This condition shifts the point of zero rotation to approximately 508 mm (20 in) from the south end of the I-section as shown in Figure 3.40.

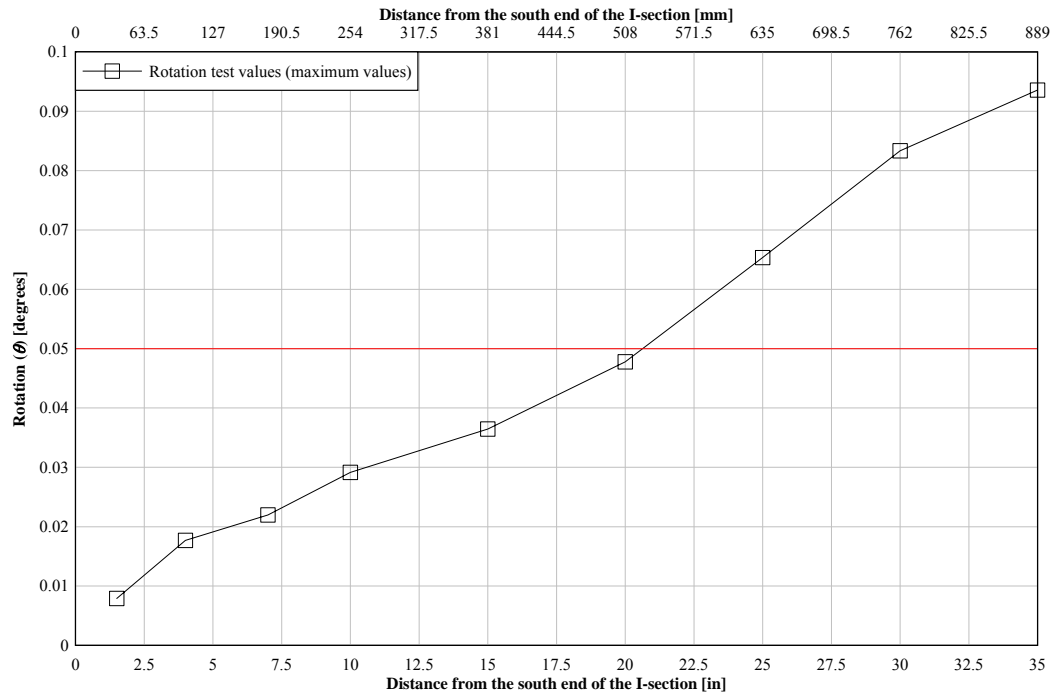


Figure 3.40: Rotation along the span in the region of zero rotation (red line is amplitude of signal noise)

This corresponds to approximately 50% of the connection length (top connection length = 978mm (38.5in)).

The rotation curve in Figure 3.39 was adapted and the new graph is shown in Figure 3.41.

The maximal rotation was determined to be 9.2 degree.

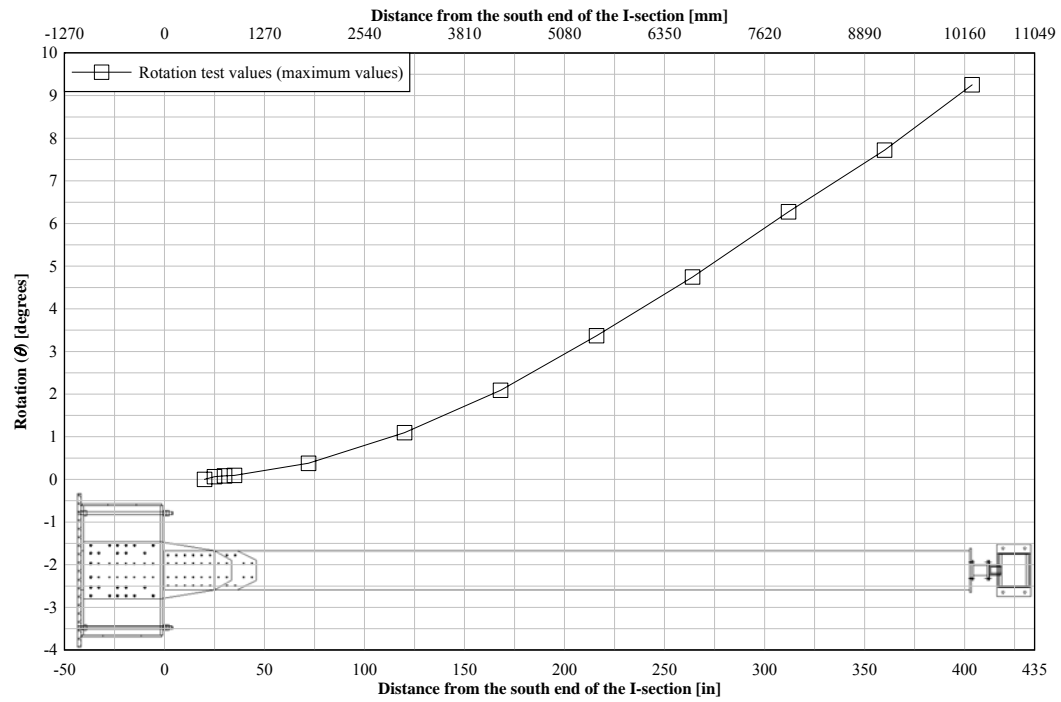


Figure 3.41: Rotation along the span with new defined point of zero rotation

### 3.5.3 Natural Frequency Testing

Several tests were conducted to characterize the natural frequency of the specimen. To characterize the natural frequency, test runs were performed over a range of loading frequencies (3 up to 11 Hz) and with small angles of rotation ( $\pm 0.25$ , 0.5 and 1 degree).

The natural frequency was determined by analyzing the ring down of several test runs. The ring down is defined as end of the test run, where the torque actuator rotation is set to zero and the reaction torque cell measures the torque generated at the end, as shown in

Figure 3.42.

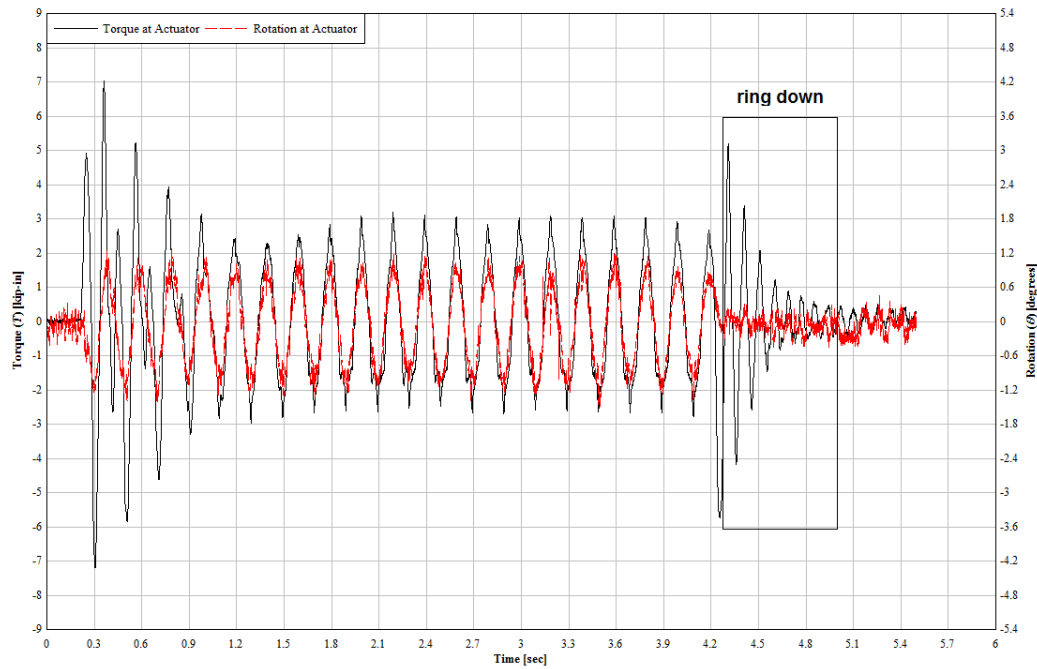


Figure 3.42: Example dynamic test with ring down location identified

The ring down was isolated from the rest of the data and a Fast Fourier Transform (FFT) analysis was conducted to identify the natural frequency. Typical results from the FFT analysis is shown in Figure 3.43.

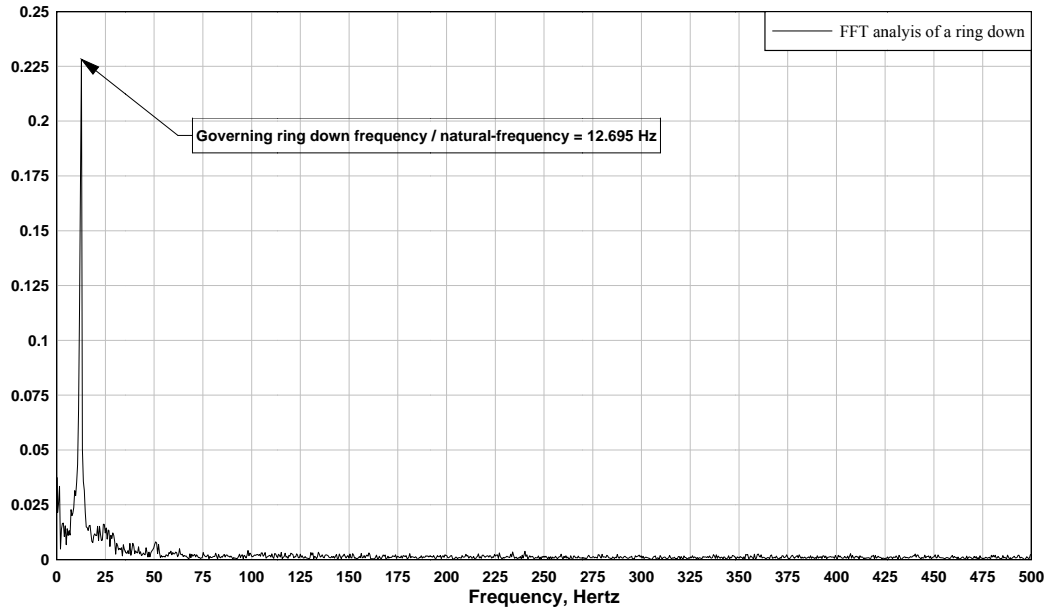


Figure 3.43: Fast Fourier Transform (FFT) for identifying frequency content of ring down

For the experimental setup, the natural frequencies found were between 12.7 and 12.9 Hz.

### 3.5.3.1 Damping

To determine the amount of damping in the test setup the ring down of the natural frequency tests was used. Todesco (1998) gives the equation to calculate the damping from the logarithmic decrement in the ring down as:

$$n\delta = \ln \left( \frac{X_i}{X_{i+n}} \right) \quad [3.1]$$



where  $X_i$  is peak measurement of the ring down and  $X_{i+n}$  is any nonconsecutive peak measurement;  $n$  is taken as an integer. From the ring down tests, the value of damping in the experimental setup was determined to be 2%.

## **4 ANALYSIS METHODS**

Two different analysis methods were used to compare with the observed experimental results. These included finite element methods and available classical analytical expressions for rotation angle, torque, and stresses in members with idealized boundary conditions subject to torsion. The analysis methods are first described and then the results are collectively described.

### **4.1 Finite Element Modeling**

Finite element models (FEMs) were developed as a part of this research project. The software used to develop these models was ABAQUS/Standard Version 6.8-2 (Hibbit, Karlsson & Sorensen, 2002; Abaqus User Manual).

The FEM of the truss vertical deployed general purpose conventional shell elements. These elements use thick shell theory as well as thin shell theory depending on the material thickness defined by the user. Transverse shears are allowed in these elements. To mesh the models, the S4R mesh element was used. This is a 4-node doubly curved general-purpose shell with reduced integration with hourglass control and finite membrane strains. (Hibbit, Karlsson & Sorensen, 2002)

During this research project several different finite element models were developed. An overview of the different models is given in Table 4.1.

Table 4.1: Overview of the different finite element models

<b>Model description:</b>	<b>Analyzing method:</b>	<b>Chapter:</b>
Experimental Vertical	general static / modal dynamic	4.1.1
Existing Bridge Vertical	general static	4.2.1
I-section stiffness with perforations	general static	Appendix F
I-section stiffness without perforations	general static	Appendix F

#### 4.1.1 Experimental Vertical Model Development

##### 4.1.1.1 *Boundary Conditions*

The experimental vertical was modeled with shell elements. All dimensions were kept the same as in the experimental-setup in the structural laboratory. The experimental vertical was modeled including all the relevant cross sectional properties including the perforations. All the section dimensions are listed in Table 4.2 for the experimental vertical including the decrease of the web area due to the perforations. The model of the experimental vertical with perforations is shown in Figure 4.1

Table 4.2: General sectional and overall dimensions of the experimental-setup FEA models

<b>Description:</b>	<b>Variable:</b>	<b>Dimension:</b>
Total length (with endplate)	$L_{setup}$	10255.3 mm / (403 $\frac{3}{4}$ in)
Length of the I-section	$L_{I-section}$	10236.2 mm / (403 in)
Total depth of I-section	$d_{I-section}$	657.2 mm / (25 $\frac{7}{8}$ in)
Flange width	$b_f$	406.4 mm / (16 in)
Flange thickness	$t_f$	12.7 mm / (1/2 in)
Web height	$h$	631.8 mm / (24 $\frac{7}{8}$ in)
Web thickness	$t_w$	7.9 mm / (5/16 in)
Endplate thickness	$t_{endplate}$	19.1 mm / (3/4 in)
Area of one perforation	$A_{perforation}$	150386.8 mm <sup>2</sup> / (233.1 in <sup>2</sup> )
Web area without perforations	$A_{web,tot}$	6467487.1 mm <sup>2</sup> / (10024.6 in <sup>2</sup> )
Web area with perforations	$A_{web,net}$	5264406.4 mm <sup>2</sup> / (8159.8 in <sup>2</sup> )
Decrease of web area	-	18.6 %

#### 4.1.1.2 Parts of FEM Model

To explain the different parts of the FEM, the model has been separated into two regions as shown in Figure 4.1.

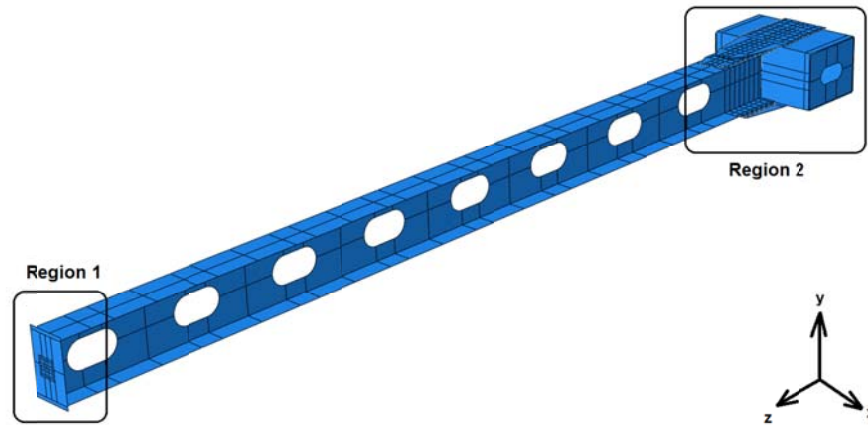


Figure 4.1: Finite element model of the experimental vertical with regions labeled

In Region 1, the load was applied to the endplate of the specimen using a special fictitious loading plate as shown in Figure 4.2. The load was applied as a single concentrated torque to the fictitious loading plate. Since high nodal stresses are induced in the fictitious loading plate, the plate was modeled as rigid. The fictitious loading plate and the endplate of the specimen are connected by rigid connectors which are explained in more detail in Section 0.

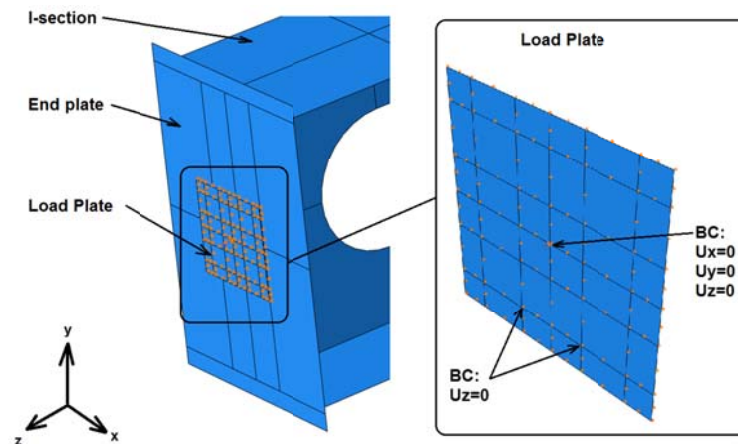


Figure 4.2: Finite element model of the experimental vertical region 1 (load induction zone)

To maintain the geometry of the specimen at the loaded end during the loading process, the center node (Node 40) of the load plate, where the torque was applied, was restrained for translation in any direction ( $U_x = 0$ ,  $U_y = 0$ ,  $U_z = 0$ ). The entire fictitious loading plate was also restrained against displacements into the  $z$  direction ( $U_z = 0$ , over the entire load plate). The rotational degrees of freedom were left unrestrained.

In Region 2 the connection between the vertical and the reaction box can be seen in more detail in Figure 4.3. All parts of the experimental reaction box were modeled. Their steel properties were defined as listed in Table 4.4. The connections between the vertical, the gusset plate, and the reaction box are described in Section 0. The interaction between the gusset plate and the reaction box is described more detail in subsequently in Section 4.1.1.4.

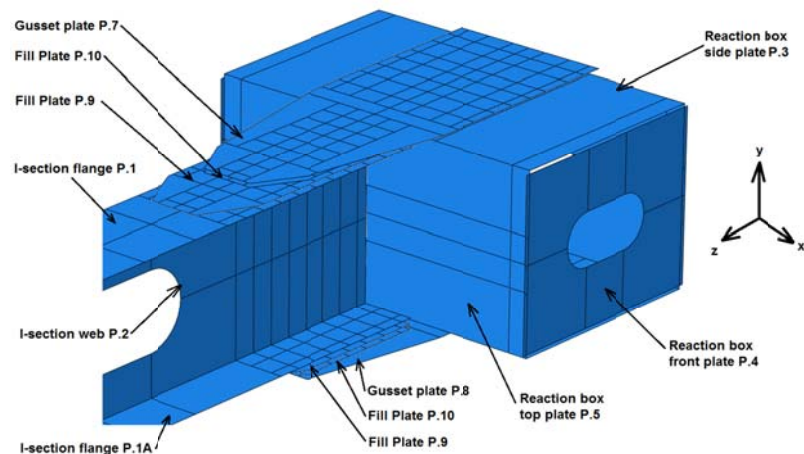


Figure 4.3: Finite element model of the experimental vertical region 2 (gusset plate, reaction box detail)

The connection between the reaction box and the strong wall was modeled with four boundary conditions placed where threaded rods connected the reaction box to the strong wall as shown in Figure 4.4. The translational degrees of freedom were restrained ( $U_x = 0$ ,

$U_y = 0$ ,  $U_z = 0$ ) and the rotational degrees of freedom were unrestrained. To simulate the strong wall pressing against the reaction box, the entire back side of the reaction box was restrained against movement in the  $z$  direction ( $U_z = 0$ ).

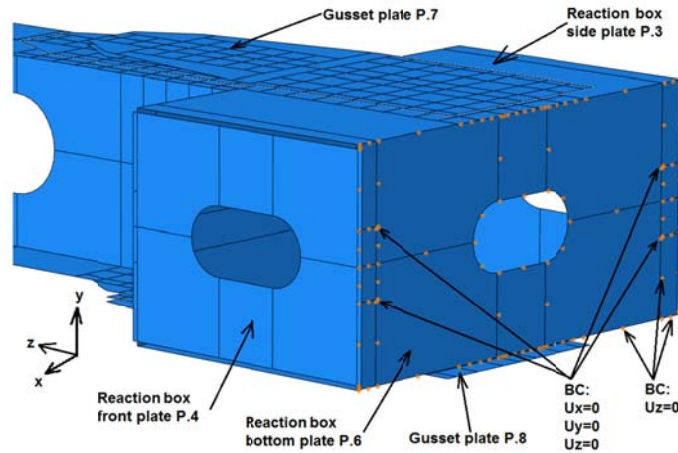


Figure 4.4: Finite element model of the experimental setup region 2 (reaction box, strong wall detail)

#### 4.1.1.3 Connections

The connections were modeled as face-to-face fasteners, defined by ABAQUS. Rigid multi-point constraint (MPC) fasteners were chosen. The displacements were restrained and rotations were left unrestrained. The physical radius for the bolts used was 22.2mm (0.875 in) for the connections between the I-section and the gusset plates as well as for the connection between the reaction box and the gusset plates. For the connection between the load and end plates, a physical radius of 15.9 mm (0.625 in) was chosen.

#### 4.1.1.4 *Interaction between the Gusset Plates and Reaction Box*

For the interaction surfaces between the gusset plates and the reaction box, a normal behavior was chosen. A linear pressure-over-closure with an arbitrary contact stiffness was selected. Since no information about the contact stiffness in the experimental setup was available, the finite element model was run with different stiffness values. The result that best matched the experimental results was selected. A contact stiffness of 87.6 N/mm (0.5 kip/in) produced the best correlation for overall rotation and stress comparisons and this value was used for all the finite element analyses.

#### 4.1.1.5 *Material Definitions*

Two materials were used to build this finite element model, steel and a rigid material. The rigid material was used for parts in the model, where the stress concentrations were high and the results did not affect the present study. The properties for these materials are listed in Table 4.3 and Table 4.4. The steel material properties were determined from the fabrication documents. These documents are attached in Appendix C and are summarized in Table 4.4.



Table 4.3: Material properties and general definitions used in the experimental vertical FEM

<b>Description:</b>	<b>Variable:</b>	<b>Value:</b>
Modulus of elasticity for steel	$E_s$	200000 MPa (29000 ksi)
Poisson's ratio for steel	$\nu_s$	0.3
Material properties for steel	$f_y / f_u$	see Table 4.4
Unit mass density for steel	$\rho_s$	$7.33 \times 10^{-7}$ kip sec <sup>2</sup> /in <sup>4</sup>
Modulus of elasticity for rigid parts	$E_r$	$2.9 \times 10^8$
Poisson's ratio for rigid parts	$\nu_s$	0.3
Material properties for rigid parts	$f_y / f_u$	N/A (elastic behavior)
Unit mass density for rigid parts	$\rho_r$	$7.33 \times 10^{-7}$ kip sec <sup>2</sup> /in <sup>4</sup>
Connection elements	-	rigid MPC fasteners see Chapter 0
Interaction stiffness	$k_i$	87.6 N/mm (0.5 kip/in) see Chapter 4.1.1.4

Table 4.4: Steel material properties for the experimental vertical FEM

Part Name:	Steel State:	Strength: (MPa) [ksi]	Plastic Strain: [in/in]
Reaction box side plates Fabrication drawing: <i>P.3</i> $t = 2$ in	yield ( $f_y$ )	262.35 [38.05]	0
	fracture ( $f_u$ )	482.29 [69.95]	0.33
Reaction box front plates <i>P.4</i> / $t = 3/4$ in End plate <i>P.12</i> / $t = 3/4$ in Fill plates <i>P.9</i> and <i>P.10</i> and <i>P.11</i> / $t = 3/4$ in	yield ( $f_y$ )	275.79 [40.00]	0
	fracture ( $f_u$ )	481.25 [69.80]	0.26
Reaction box top and bottom plates <i>P.5</i> / <i>P.6</i> / $t = 1$ in	yield ( $f_y$ )	293.37 [42.55]	0
	fracture ( $f_u$ )	490.22 [71.10]	0.25
I-section web <i>P.2</i> / $t = 5/16$ in	yield ( $f_y$ )	326.12 [47.30]	0
	fracture ( $f_u$ )	437.82 [63.50]	0.29
I-section flanges <i>P.1</i> and <i>P.1A</i> / $t = 1/2$ in	yield ( $f_y$ )	304.06 [44.10]	0
	fracture ( $f_u$ )	427.47 [62.00]	0.39
Gusset plates <i>P.7</i> and <i>P.8</i> / $t = 3/8$ in	yield ( $f_y$ )	289.58 [42.00]	0
	fracture ( $f_u$ )	489.53 [71.00]	0.295

ABAQUS develops the full stress-strain curves from the properties established in Table 4.4. In the elastic region ( $\sigma_s < f_y$ ) the stress-strain relation is determined with Hook's law and in the plastic region ( $f_y < \sigma_s \leq f_u$ ) as a linear function until the plastic strain is reached. An example is shown in Figure 4.5.

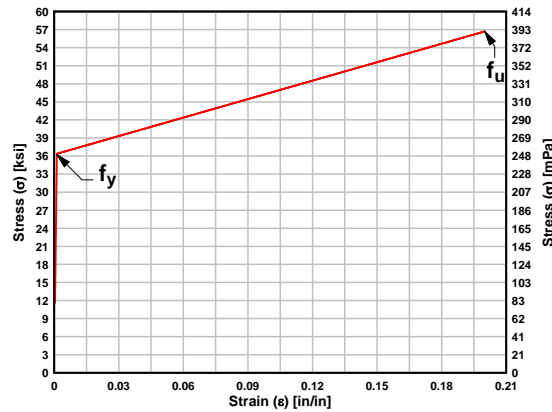


Figure 4.5: Schematic stress-strain diagram of steel

Two different loading cases were analyzed. First, a general static analysis with a torque of 22.6 kN-m (200 kip-in) was applied using force control in the model. From this analysis, the elasto-plastic behavior of the specimen was found.

To characterize the overall behavior of the model, the torque-rotation response was determined as shown in Figure 4.6. From this curve in the elastic region, the predicted torsional stiffness of the specimen was computed to be 17.1 kN-m/rad (151.6 kip-in/rad).

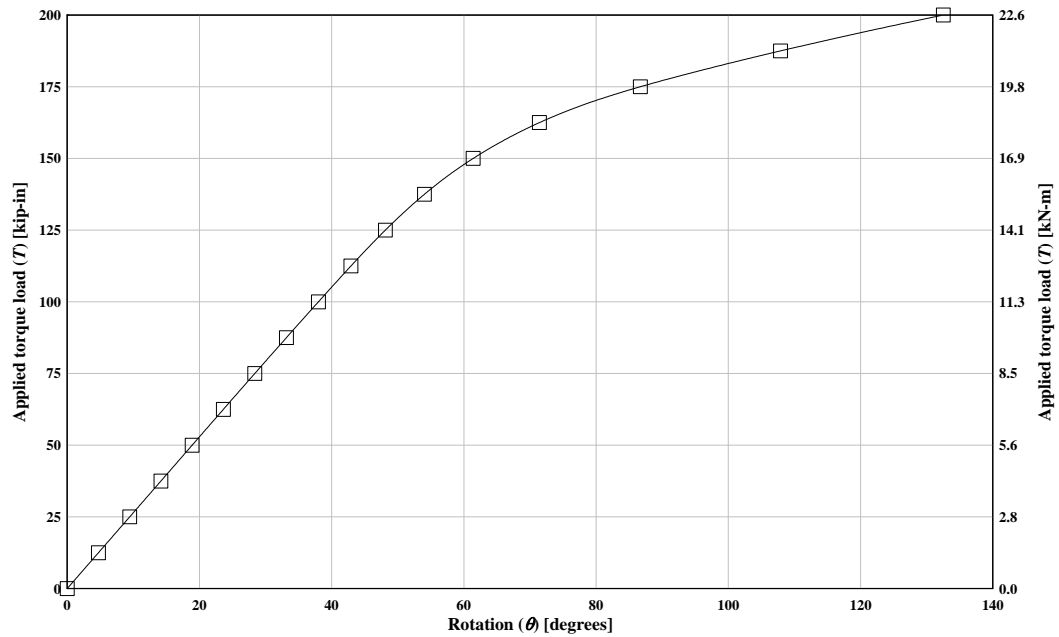


Figure 4.6: FEM rotation angle-torque plot for the experimental setup

To predict the inelastic behavior of the experimental specimen, a general static analysis was performed. A torque of 22.6 kN-m (200 kip-in) was applied to the loading plate. The predicted torque-angle of twist response at the loaded end is shown in Figure 4.6. The final angle of twist was 132.5 degrees.

First yield within the specimen was observed in the top flange of the I-section, where the I-section and the end plate were connected (as illustrated in Figure 4.7). The predicted normal stress – twist angle behavior of the element at the first yield location is shown in Figure 4.8. As seen here, first yield occurred at an applied torque of 5.8 kN-m (51 kip-in) and an angle of twist of 19.3 degree.

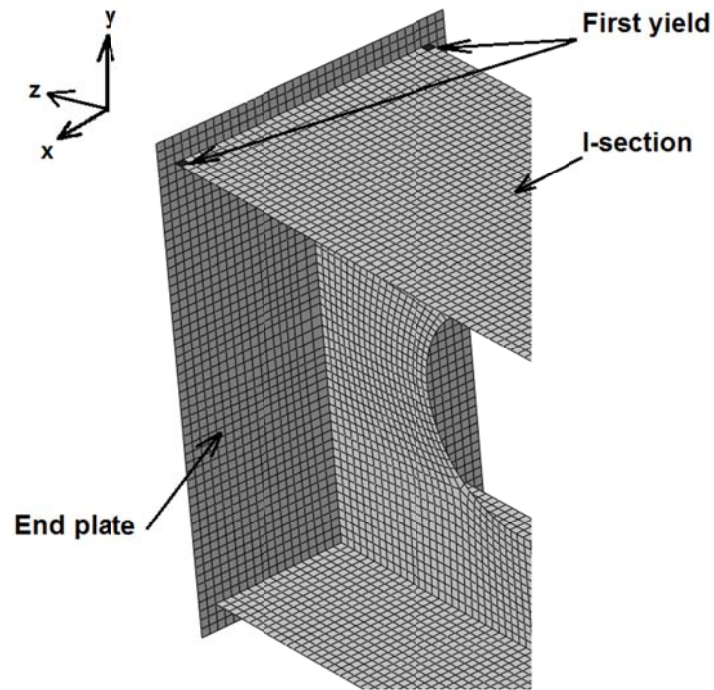


Figure 4.7: Location of first yield in the experimental setup FEM

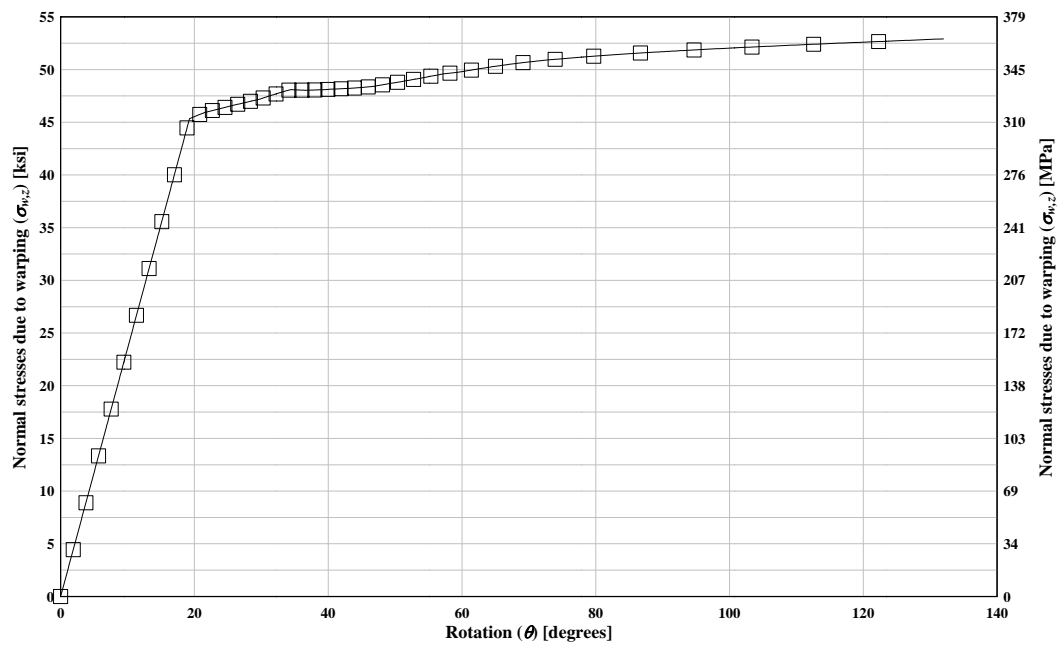


Figure 4.8: FEM predicted normal stress-rotation response at nodal region located near endplate of specimen

Since the point of first yield is in the load induction zone, which has disturbed stresses due to the induction of the torque as required to conduct the experiment, and in which the experimental setup differs from the existing truss bridge vertical (as described in Chapter 3.2.2 and will be discussed further in Section 4.3.2), the second location which showed yielding was also considered. This point was located in the top flange of the I-section close to the gusset plate connection with the chord, as shown in Figure 4.9.

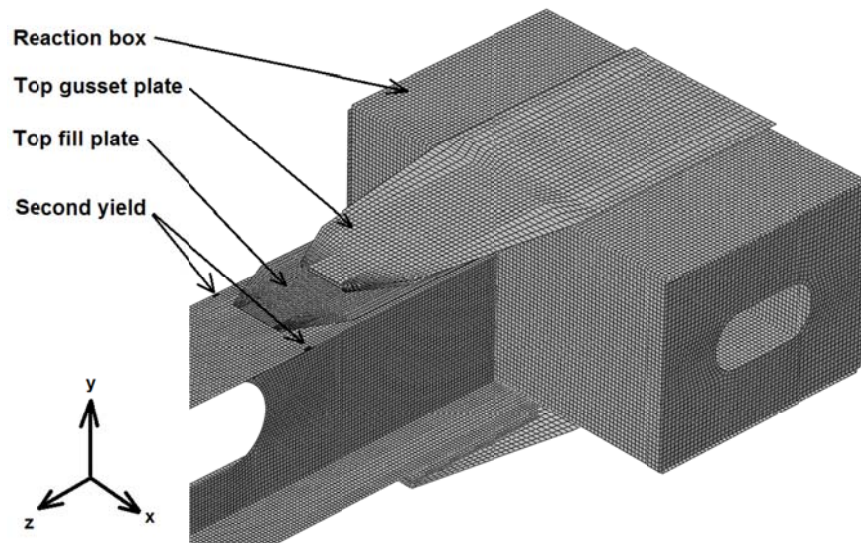


Figure 4.9: Location of second yield in the experimental setup FEM

The predicted normal stress – twist angle behavior at the next location which indicated yielding for the finite element model of the experimental setup is shown in Figure 4.10. Yielding initiated at an angle of twist of 39.2 degrees with a torque of 11.6 kN-m (103.0 kip-in).

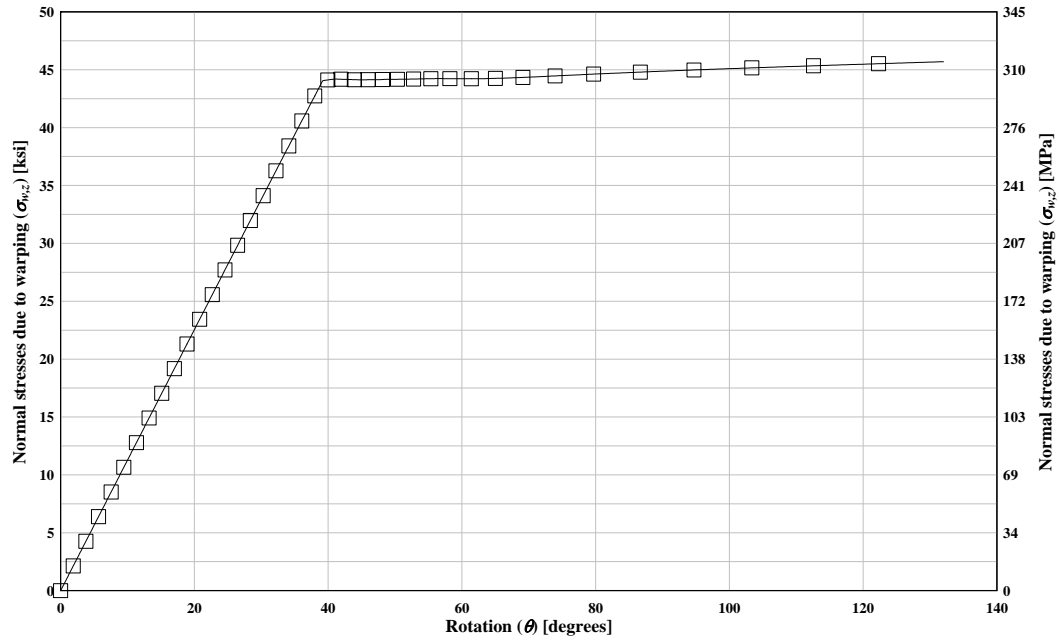


Figure 4.10: FEM predicted normal stress-rotation response at nodal region located near gusset plate of specimen (see Fig. 4.9)

Subsequent finite element analyses were conducted using this model to compare with the experimental results and available AISC design guidelines. The FEM analysis conducted was a dynamic analysis using the load history data from the experimental test results as the input forcing function to the model. The test data were for +/- 9.0 degree angle change with a loading frequency of 0.05 Hz. The FE predicted responses were compared at the local and global levels including twist angle and stress distribution for the specimen. In addition, the FEM predicted and experimentally measured natural frequencies were compared. All results are compared after presentation of the AISC analytical methods, which are presented in the next section.

#### 4.1.2 Analytical Expressions

##### 4.1.2.1 *AISC Steel Design Guide Series 9*

As described in Chapter 2.2, Seaburg and Carter developed analytical methods to calculate rotations and stresses for a given torque. These methods were published as part of the American Institute of Steel Construction (AISC) Steel Design Guide Series 9; as Torsional Analysis of Structural Steel Members. In this section, the boundary conditions representative of the laboratory setup are used which is best represented as fix at one end and free at the other.

##### 4.1.2.2 *Boundary Condition: One End Fixed (AISC Steel Design Guide Series 9, Case 9)*

To calculate the rotations and stresses of the vertical in the structures lab, boundary condition Case 9 was chosen. In this case, the steel member is completely fixed on one end, and free to translate or rotate on the other side as shown in Figure 4.11. The value for  $\alpha$  was chosen as 1.0, since the load is applied at the free end of the beam.

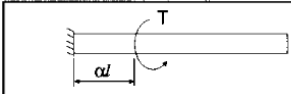
	Torsional End Restraints		Concentrated torque at $\alpha = 1.0$ on member with fixed and free ends
	Left End	Right End	
	Fixed $\theta = \theta' = 0$	Free $\theta'' = 0$	

Figure 4.11: Boundary conditions and definitions for Case 9 with an  $\alpha$  of 1.0  
(Steel Design Guide Series 9, 2003)

The solution for the differential equation for rotation, given in Chapter 2.2 (Eqn. [2.20]), is given by Seaburg and Carter. Since in this case, the distance  $z$  is always smaller or equal to  $\alpha * L$ , the following equation for rotation ( $\theta$ ) with a given torque ( $T$ ) must be used:



$$\theta = \frac{Ta}{GJ} \left[ \left( \sinh \frac{\alpha l}{a} - \tanh \frac{l}{a} * \cosh \frac{\alpha l}{a} + \tanh \frac{l}{a} \right) \left( \cosh \frac{z}{a} - 1.0 \right) - \sinh \frac{z}{a} + \frac{z}{a} \right] \quad [4.1]$$

where  $G$  is the shear modulus of elasticity of steel,  $J$  is the torsional constant (given in Eqn. [2.11] or [2.12]),  $a$  is defined in Eqn. [2.6] (in this equation however  $a$  was defined as  $\alpha$ ),  $l$  is defined as the total length of the steel member,  $z$  is the location of interest measured from the fixed end and  $\alpha l$  is the location of the load measured from the fixed end.

As mentioned in Chapter 2.2, the first, second and third derivative of Eqn. [4.1] are used to calculate the stresses due to torsion in an I-section. These derivatives are shown below.

First derivative of  $\theta$  with respect to  $z$ :

$$\theta' = \frac{aT}{GJ} \left[ \frac{1 - \cosh \frac{z}{a} + \sinh \frac{z}{a} \left( \sinh \frac{\alpha l}{a} + \tanh \frac{l}{a} - \cosh \frac{\alpha l}{a} \tanh \frac{l}{a} \right)}{a} \right] \quad [4.2]$$

Second derivative of  $\theta$  with respect to  $z$ :

$$\theta'' = \frac{aT}{GJ} \left( \frac{\cosh \frac{z}{a} \left( \sinh \frac{\alpha l}{a} + \tanh \frac{l}{a} - \cosh \frac{\alpha l}{a} \tanh \frac{l}{a} \right) - \sinh \frac{z}{a}}{a^2} \right) \quad [4.3]$$

Third derivative of  $\theta$  with respect to  $z$ :

$$\theta''' = \frac{aT}{GJ} \left( \frac{\sinh \frac{z}{a} \left( \sinh \frac{\alpha l}{a} + \tanh \frac{l}{a} - \cosh \frac{\alpha l}{a} \tanh \frac{l}{a} \right) - \cosh \frac{z}{a}}{a^3} \right) \quad [4.4]$$

The design graphs developed by Seaburg and Carter for this boundary condition are shown in Appendix E.

Using the results given by these derivatives, the stresses in an I-section were calculated with equation [2.15], [2.16], and [2.19]. To calculate the rotation, torque and stresses along the length of the vertical in the test-setup, a Microsoft Excel spreadsheet was developed and automated with Microsoft Visual Basic code.

In the calculations, the length of the vertical was defined from the end plate (loaded end) to the point of zero rotation within the gusset plate as described in Chapter 3.5.2. This resulted in an equivalent member length of 9747.25 mm (383.75 in). Since the point of zero rotation was determined to be 508mm (20 in) away from the south end of the vertical, the calculated values from the modified equation [4.1] needed to be shifted to the new point of zero rotation. This shifting was performed for all analytical results and is illustrated in Figure 4.12. These shifted results, will be used in the subsequent discussion comparing the analytical results with the finite element model and the experiment.

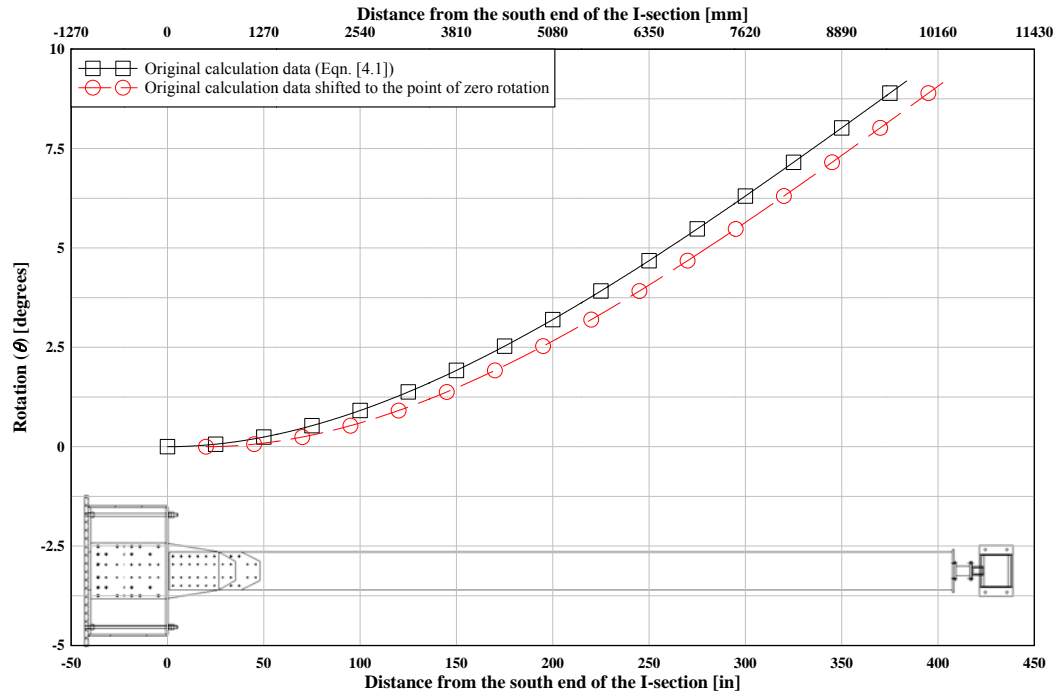


Figure 4.12: Rotation along the I-section, calculated from equation [4.1]

#### 4.1.3 Comparison of FEM and Analytical Methods with Experimental Results

##### 4.1.3.1 *Natural Frequency of Experimental Vertical*

The first five natural frequencies of the experimental specimen predicted with the finite element model were determined and are reported in Table 4.5. The mode shapes for these results are listed in Appendix D.

Table 4.5: Finite element predicted model frequencies of the experimental setup

<b>Mode:</b>	<b>Description:</b>	<b>Value: [Hz]</b>
1	Weak axis bending	12.6
2	First torsional	14.1
3	Distortional (warping of the cross section)	27.0
4	Strong axis bending	27.3
5	Second torsional	28.7

The natural frequencies for the experimental setup were also calculated with the equations described in Chapter 2.1.2. For the experimental setup, a fixed-simply supported boundary condition was assumed (Eqn. [2.3]). The first torsional frequency ( $\omega_{torsion}$ ) was 12.7 Hz.

This corresponds closely to the FEM results for the first torsional mode. The experimentally measured first torsional mode was 12.7 to 12.9 Hz and was well captured by both the FEM and analytical expressions. The close match indicates that the specimen is well represented as a fixed-free ended member. The different torsional natural frequency results of the experimental vertical are summarized in Table 4.6.

Table 4.6: Natural frequency comparison for the experimental vertical

<b>Description:</b>	<b>Chapter:</b>	<b>Eqn. / Table:</b>	<b>Value: [Hz]</b>
Approximate analytical method (Carr)	2.1.2	[2.3]	12.7
Finite element model	4.1.3.1	Table 4.5	12.6
Experimental result	3.5.1	-	12.7 – 12.9

#### 4.1.3.2 *Torsional Stiffness of Experimental Vertical*

From the applied torque and measured twist angle at the loaded end, the overall torsional stiffness of the experimental specimen was found to be 16.9 kN-m/rad (149.7 kip-in/rad) as described previously. These results were compared with the analytically predicted stiffness and those from the FEM.

Using a rearrangement of equation [4.1] the torque was computed for the prescribed 9.0 degree angle of twist. The 9.0 degree angle of twist input value was selected because this corresponds with the experimental results described previously. Using the torque-twist results at the end of member, the analytically predicted torsional stiffness of the experimental vertical was calculated and determined to be 15.8 kN-m/rad (140.0 kip-in/rad).

Using the FEM results in the elastic range for the overall torque-twist response at the loaded end of the member, shown previously in Fig. 4.6, the predicted torsional stiffness of the specimen was computed as 17.1 kN-m/rad (151.6 kip-in/rad).

The different results for the torsional stiffness of the experimental vertical are summarized and listed in Table 4.7. As seen here, the experimental results fall within the range of the analytical and FEM predictions. The torsional stiffness obtained from the analytical method differs from the experimental torsional stiffness by 6.5 %, and from the finite element model by 1.2 %. Both methods could reasonably predict the overall member torsional stiffness.

Table 4.7: Torsional stiffness comparison for the experimental vertical

<b>Description:</b>	<b>Chapter:</b>	<b>Torsional Stiffness:</b>	
		[kN-m/rad]	[kip-in/rad]
Analytical method	4.1.3.2	15.8	140.0
Finite element model	4.1.3.2	17.1	151.6
Experimental result	3.5.1.2	16.9	149.7

#### 4.1.3.3 *Magnitude and Distribution of Angle of Twist for Experimental Vertical*

The FEM predicted maximum angle of twist was 9.2 degrees and corresponded well with the experimentally measured value. Twist angles and stress distributions in the FEM of the specimen were determined at the peak twist angle.

The angle of twist along the span of the I-section of the experimental vertical was calculated using the rearranged equation [4.1]. The experimental results, the calculated values, and the finite element results for the angle of twist at the centerline of the I-section were compared and are shown in Figure 4.13.

The finite element model as well as equation [4.1] reasonably predicted the magnitude and distribution of the angle of twist in the experimental vertical. Deviation between the experimental data and equation [4.1] was largest in the region near the mid-length of the experimental vertical. The FEM predicted angle of twist corresponded closely to the experimental results along the entire length of the vertical.

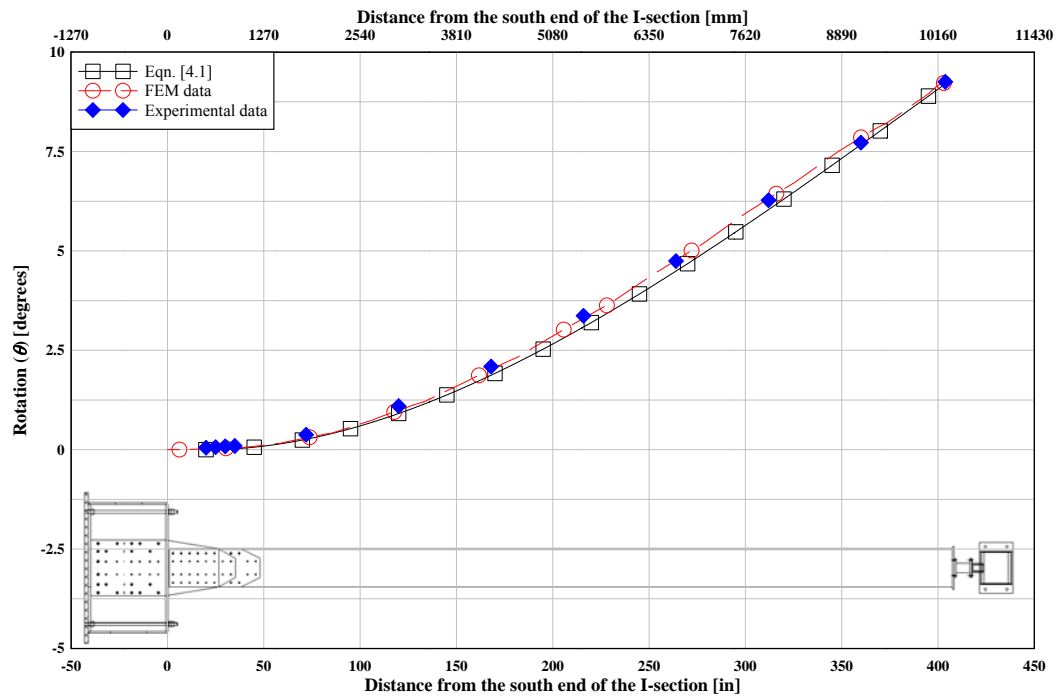


Figure 4.13: Comparison of the experimentally measured and analytical predicted angle of twist

#### 4.1.3.4 Angle of twist Comparison for Time History Data

The time history comparison of the experimental data and the finite element results is shown in Figure 4.14. The time-history behavior of the finite element model is very similar to the experimental vertical behavior. The maximum difference between experimental data and the finite element model over all five cycles was determined to be 1.2 %.

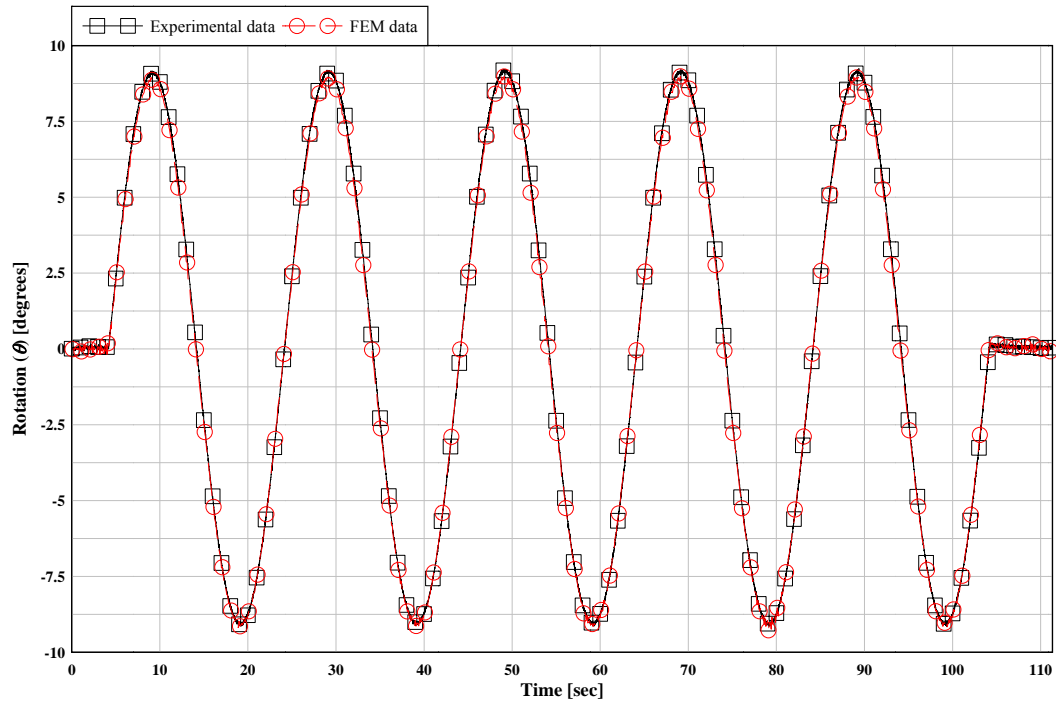


Figure 4.14: Comparison of the experimental and FEM predicted time-history of angle of twist at the loaded end of the member

#### 4.1.3.5 Stresses along Experimental Vertical

Four regions were selected, where stresses from the finite element model were determined and later compared to the experimental data and to the analytical results. The selected regions of interest are shown in Figure 4.15. The first and second regions are located at the flange tips of the I-section along the entire span, as shown in Figure 4.15. The first region is placed at the tip of the top flange and the second region is located at the tip of the bottom flange. Since a symmetrical behavior in the I-section was assumed, only the flange tips of one side (west side) of the I-section were selected. Within these regions, the maximum normal stresses were monitored.



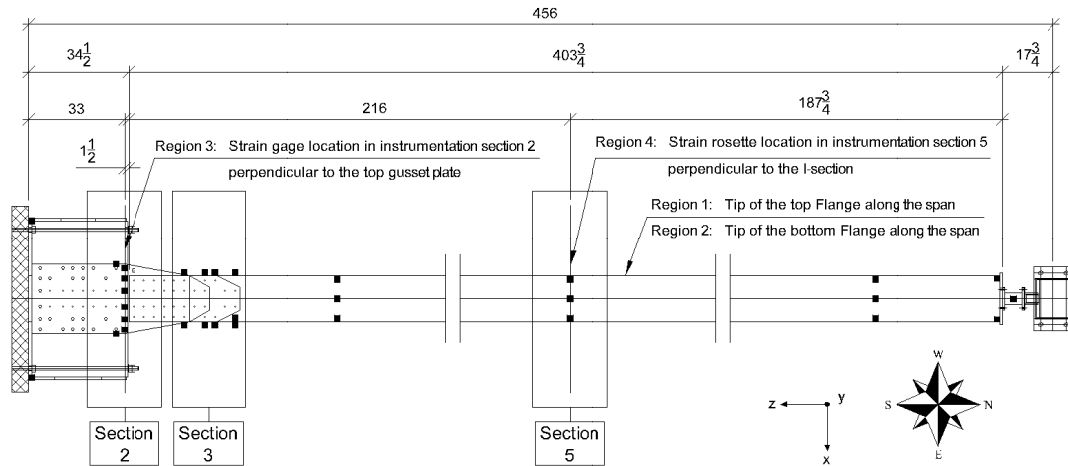


Figure 4.15: Regions of interest in the experimental setup FEM

#### 4.1.3.6 Normal Stress along the Length of Experimental Vertical

Using the torque results calculated in the modified equation [4.1] and [2.19] the calculated normal stresses due to warping at the flange tips of the I-section are shown in Figure 4.16. The maximum normal stress due to warping at the tip of the flanges was determined to be 73.1 mPa (10.6 ksi) at 508mm (20 in) away from the south end of the I-section.

Since all strain rosettes in the top flange were placed at approximately 25.4 mm (1 in) away from the tip of the flange, as described in Chapter 3.3.1, the measured average peak to peak results, listed in Table 3.6, were linearly increased and plotted together with the finite element results and the analytical results in Figure 4.16.

Figure 4.16 shows peak normal stresses due to warping at two locations. The stress concentration located at 10255.3 mm (403.75 in) is a result of the end plate being fixed to the I-section for the load induction. Since this plate is not part of the existing bridge vertical (as described in Chapter 3.2.2), the stress concentrations at this location were not

considered in detail. The second stress maximum is located at 957.6 mm (37.7 in) away from the south end of the I-section in the top flange. This corresponds to the midpoint between the start of the top fill plate and the first row of bolts in the top flange and is located in the instrumentation as section 3 called out in Figure 3.11. From the finite element model, the maximum stress in the top flange tips of the I-section was found to be 69.6 MPa (10.1 ksi) at the peak twist angle of 9.2 degrees. The location of the top flange stress maximum is at the same location that was predicted to show the onset of yielding as the torque increases as the second yield point in the I-section (438 mm (36.5in) away from the south end) and was shown in Figure 4.9. The maximum stress location in the bottom flange was located in the same region. Since the bottom flange gusset plate was shorter, the stresses in the bottom flange were smaller and closer to the end of the I-section. The maximum stress in the bottom flange was determined to be 66.2 MPa (9.6 ksi).

Both the finite element model and the analytical equation [4.1] reasonably predicted the normal stresses in the flange tip of the I-section. The maximum stress found with the analytical equation [2.19], was 73.1 MPa (10.6 ksi). The finite element model predicted a maximum normal stress of 69.6 MPa (10.1 ksi) in the region of the gusset plate. The maximum stress in the region of the gusset plate, determined from the experimental results, was 73.1 MPa (10.6 ksi) as listed in Chapter 3.5.1.2. The maximum stress location differs slightly between the analytical calculation (508mm (20 in) away from the south end of the vertical) due to the analytical expressions ignoring the influence of the length of the gusset plate overlapping the member and the experimental data (438 mm (36.5in) away from the south end of the vertical).

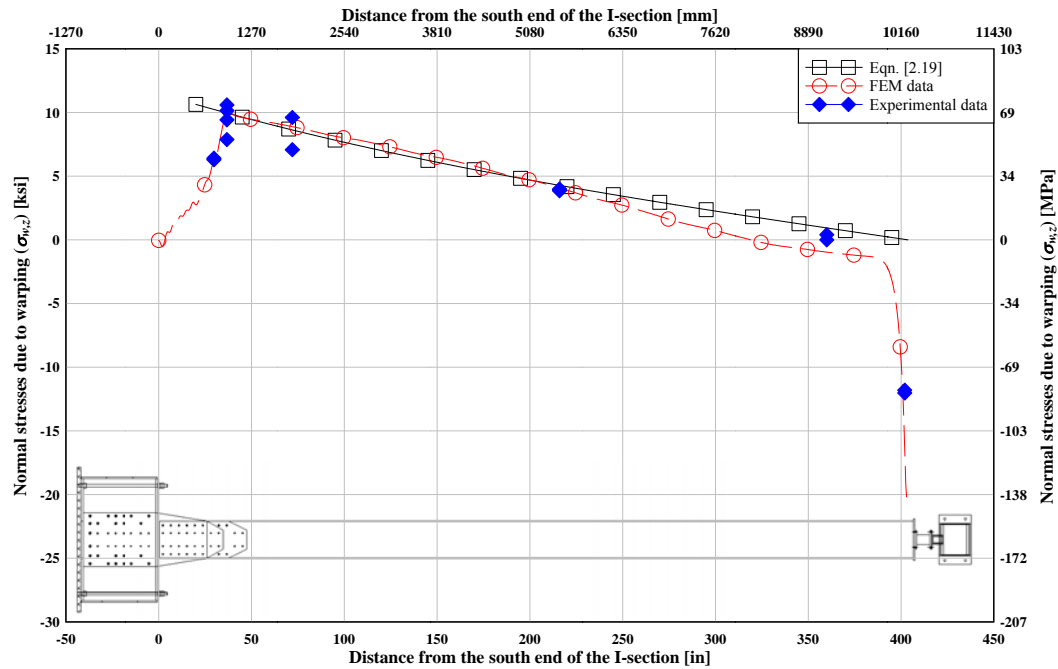


Figure 4.16: Comparison of the experimentally measured and predicted normal stresses at the tips of the flange

#### 4.1.3.7 Normal Stress for the Top Gusset Plate of Experimental Vertical

The third region of interest as shown in Figure 4.15 was selected in the top gusset plate in the instrumentation section 2. The region corresponds to the location where the gusset plate is located over the edge of the reaction box.

The normal stresses due to warping in the top gusset plate were determined by calculating the moment in the top flange of the I-section using the maximum normal stresses due to warping in the I-section, as described in Chapter 4.1.3.6. From the maximum stresses, the corresponding moment was calculated using a modified equation [2.8]. The in-flange moment was calculated as 25.6 kN-m (226.1 kip-in). A uniform load transformation from the I-section into the gusset plate (through the connecting bolts) was assumed. With this

assumption, the normal stresses due to warping in the gusset plate were calculated using equation [2.8]. The maximum normal stress in the top gusset plate was determined to be 43.3 MPa (6.3 ksi). The resulting stress distribution in the top gusset plate is shown in Figure 4.17.

The maximum stress location in the top gusset plate corresponds with the edge bolt axis, located at 38.1 mm (1.5 in) from the edge of the plate (shown in Figure 4.17). The maximum normal stress in the top gusset plate was found to be 40 MPa (5.8 ksi).

The finite element model as well as the analytical method reasonably predicted the normal stresses in the gusset plate due to warping.

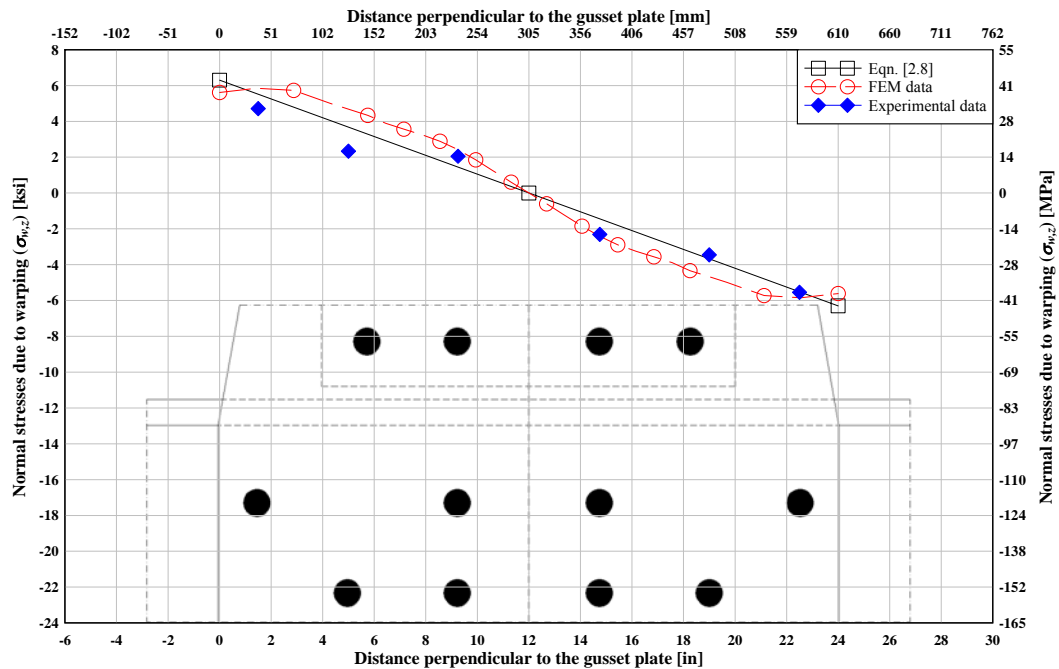


Figure 4.17: Comparison of the experimentally measured and predicted normal stresses in the top gusset plate

#### 4.1.3.8 *Normal Stress in the Top Flange of the I-Section of Experimental Vertical*

The fourth region for the stress comparison was chosen to be in the middle of the I-section (instrumentation section 5) as shown in Figure 4.15. Since there are no stress disturbing influences (like bolts or end plates) close to this section, the section was chosen to represent the uniform behavior of the I-section.

The maximum normal stress in the flange tips at this location was determined from Chapter 4.1.3.6 and was found to be 26.2 MPa (3.8 ksi). The stress distribution due to warping in the flange was taken to be linear, as shown in Figure 2.4, with the peak values at the tips of the flanges. The normal stresses due to warping in the top flange of the I-section in the experimental vertical were collected and compared in Figure 4.18.

Since the maximum normal stress of the section corresponds with the tip of the I-section flange, the maximum normal stresses due to warping along the span of the I-section can be seen in Figure 4.16.

Figure 4.18 shows that the finite element model reasonably predicted the experimental results. The calculated values for this graph are taken from the stress calculation along the span (shown in Figure 4.16) and distributed linearly over the top flange.

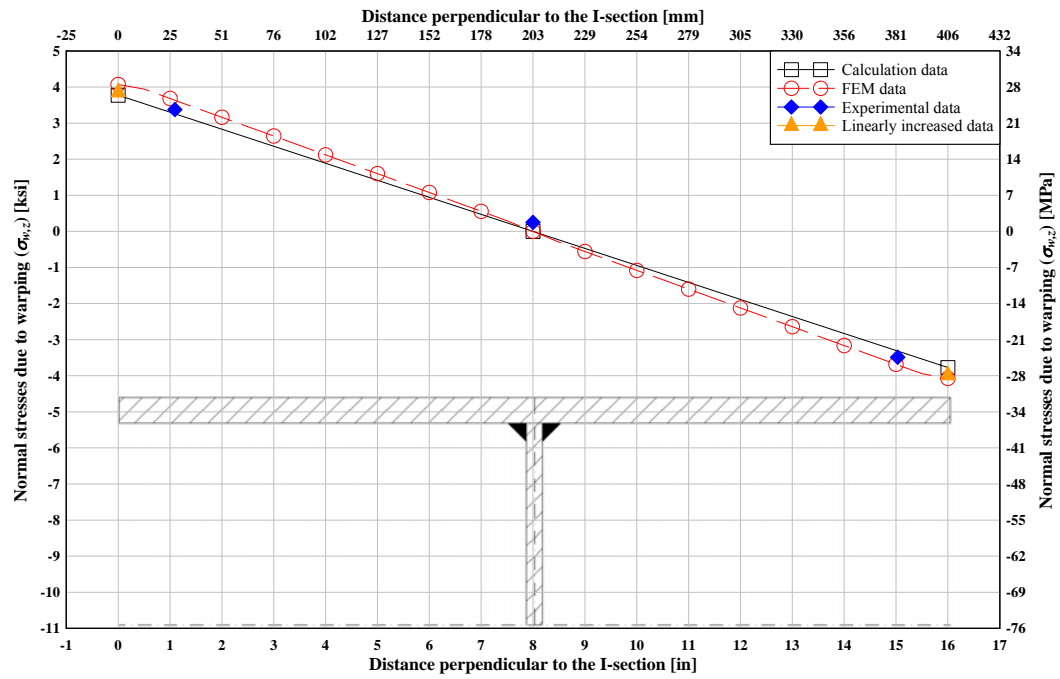


Figure 4.18: Comparison of the experimentally measured and analytical predicted normal stresses in the top flange of the I-section

## 4.2 Prediction of Behavior of Existing Bridge Vertical (L13-M13)

### 4.2.1 Existing Bridge Vertical (L13-M13) FEM Development

The existing bridge vertical does not have the fictitious boundary condition (end plate at the location of the torque actuator) at mid-height that was necessary to conduct the experimental tests. To investigate the response of the in-situ bridge vertical, a FEM of the existing bridge vertical member L13-M13 was modeled. The model was constructed similarly to that previously described for the experimental specimen using shell elements. The bridge member is shown in Fig. 4.21. The length of the existing vertical used in the model was 19 m (62.747 ft) and corresponds to the actual member length. Since the boundary conditions of the existing vertical at location M13 (as shown in Figure 4.19) cannot be modeled easily, the same reaction box as used for location L13 was used on both ends of the vertical as shown in Figure 4.20. The connections and interactions in this model were unchanged from the finite element model of the experimental vertical. The web perforations in the I-section were again included.

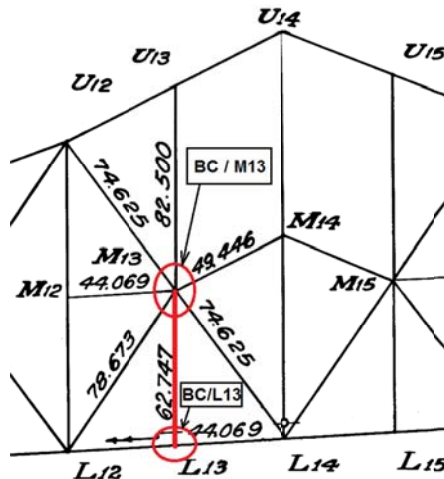


Figure 4.19: Boundary condition and system length of the existing vertical

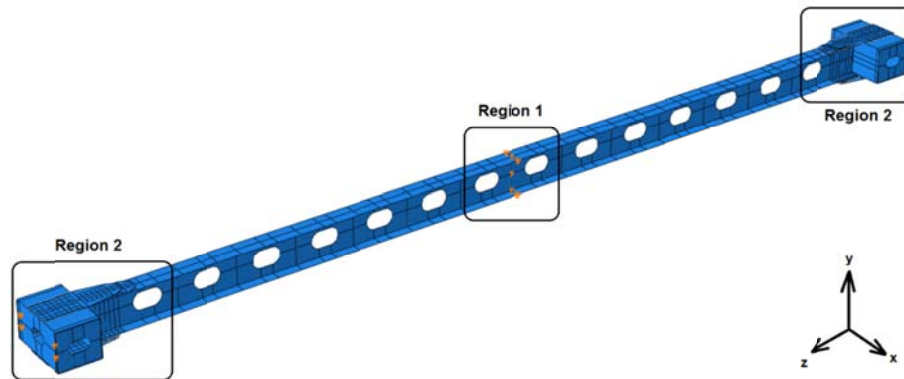


Figure 4.20: Finite element model of the existing bridge vertical with regions labeled

The angle of twist at the center of the vertical was achieved by displacing the edge and center points of the cross-section as illustrated in Fig. 4.23. The X and Y coordinates corresponding to a 10 degree angle change are listed in Table 4.8.

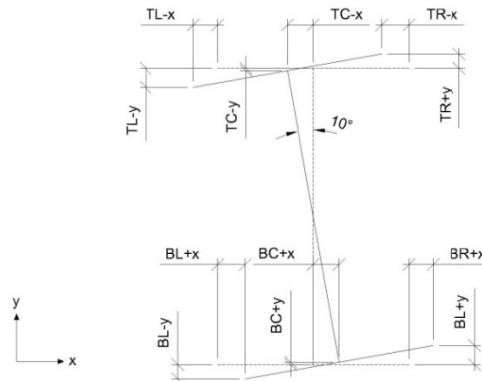


Figure 4.21: Coordinate system and direction of rotation of the existing bridge vertical



Table 4.8: Displacement coordinates for a 10 degree angle change

<b>Location:</b>	<b>X-Axis displacement: (mm) / [in]</b>	<b>Y-Axis displacement: (mm) / [in]</b>	<b>Z-Axis displacement: (mm) / [in]</b>
Top left ( <i>TL</i> )	-51.771 / [-2.038]	-40.085 / [-1.578]	0
Top center ( <i>TC</i> )	-54.858 / [-2.160]	-4.799 / [-0.189]	0
Top right ( <i>TR</i> )	-57.945 / [-2.281]	30.486 / [1.200]	0
Bottom left ( <i>BL</i> )	57.945 / [2.281]	-30.486 / [-1.200]	0
Bottom center ( <i>BC</i> )	54.858 / [2.160]	4.799 / [0.189]	0
Bottom right ( <i>BR</i> )	51.771 / [2.038]	40.085 / [1.578]	0
Center center ( <i>CC</i> )	0	0	0

The locations of the modified displacement boundary conditions in the finite element model are shown in Figure 4.22. High stress concentrations were found at the modified displacement boundary conditions. Since it was not possible to use a rigid region in the load induction zone and yielding of the steel was undesired, this analysis was run with elastic steel behavior and corresponds to the expected range of behavior in the field.

Region 2 for the existing vertical model is the same as for the experimental vertical, and were previously shown in detail in Figure 4.3 and Figure 4.4.

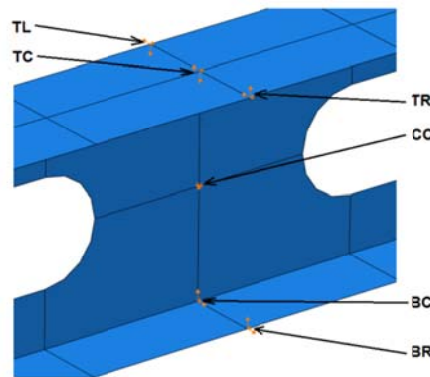


Figure 4.22: Finite element model of the existing vertical in region 1 (load induction zone)

#### 4.2.1.1 *Material Definitions for Model of Existing Bridge Vertical*

The materials used and general definitions for this model are shown in Table 4.9.

Table 4.9: Material properties and general definitions used in the existing vertical models

<b>Description:</b>	<b>Variable:</b>	<b>Value:</b>
Modulus of elasticity for steel	$E_s$	200000 MPa (29000 ksi)
Poisson's ratio for steel	$\nu_s$	0.3
Material properties for steel	$f_y / f_u$	N/A (elastic behavior)
Unit mass density for steel	$\rho_s$	$7.33 \times 10^{-7}$ kip sec <sup>2</sup> /in <sup>4</sup>
Modulus of elasticity for rigid parts	$E_r$	N/A
Poisson's ratio for rigid parts	$\nu_s$	N/A
Material properties for rigid parts	$f_y / f_u$	N/A (elastic behavior)
Unit mass density for rigid parts	$\rho_r$	N/A
Connection elements	-	rigid MPC fasteners see Chapter 0
Interaction stiffness	$k_i$	87.6 N/mm (0.5 kip/in) see Chapter 4.1.1.4

General section properties and overall dimensions are shown in Table 4.10.

Table 4.10: General sectional and overall dimensions of the existing vertical FEA model

<b>Description:</b>	<b>Variable:</b>	<b>Dimension:</b>
Total length (with reaction box)	$L_{setup}$	19989.8 mm / (787 in)
System length	$L_{system}$	19126.2 mm / (753 in)
Length of the I-section	$L_{I-section}$	18237.2 mm / (718 in)
Total depth of I-section	$d_{I-section}$	657.2 mm / (25 7/8 in)
Flange width	$b_f$	406.4 mm / (16 in)
Flange thickness	$t_f$	12.7 mm / (1/2 in)
Web height	$h$	631.8 mm / (24 7/8 in)
Web thickness	$t_w$	7.9 mm / (5/16 in)
Area of one perforation	$A_{perforation}$	150386.8 mm <sup>2</sup> / (233.1 in <sup>2</sup> )
Web area without perforations	$A_{web,tot}$	11522718.9 mm <sup>2</sup> / (17860.25 in <sup>2</sup> )
Web area with perforations	$A_{web,net}$	9417327.8 mm <sup>2</sup> / (14596.9 in <sup>2</sup> )
Decrease of web area	-	18.3 %

#### 4.2.2 Analytical Expressions for the Existing Bridge Vertical

The existing bridge vertical in the field was assumed to have fixed boundary conditions on both ends. Therefore, Case 6 from the AISC Steel Design Guide Series 9 was chosen as shown in Figure 4.23. The value for  $\alpha$  was chosen to be 0.5, since symmetrical behavior over the bridge vertical can be assumed. Since a symmetrical behavior of the bridge vertical can be assumed, only the equation for the values of  $z$  between 0 and  $al$  ( $0.5l$ ) was considered. The equation for the other side of the vertical can be found in Appendix E.

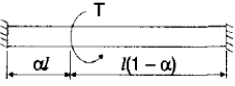
	Torsional End Restraints		Concentrated torque at $\alpha = 0.5$ on member with fixed ends
	Left End	Right End	
	Fixed $\theta = \theta' = 0$	Fixed $\theta = \theta' = 0$	

Figure 4.23: Boundary conditions and definitions for Case 6 with an  $\alpha$  of 0.5  
(Steel Design Guide Series 9, 2003)

The solution for the differential equation for fixed-fixed boundary condition, for  $0 \leq z \leq \alpha l$  is given as:

$$\theta = \frac{Ta}{(H+1)GJ} \left\{ \left[ H * \left( \frac{1}{\sinh \frac{l}{a}} + \sinh \frac{\alpha l}{a} - \frac{\cosh \frac{\alpha l}{a}}{\tanh \frac{l}{a}} \right) + \left( \sinh \frac{\alpha l}{a} - \frac{\cosh \frac{\alpha l}{a}}{\tanh \frac{l}{a}} + \frac{1}{\tanh \frac{l}{a}} \right) \right] * \left[ \cosh \frac{z}{a} - 1.0 \right] - \sinh \frac{z}{a} + \frac{z}{a} \right\} \quad [4.5]$$

where  $H$  is a constant and is defined as:

$$H = \frac{\left[ \frac{\left( 1.0 - \cosh \frac{\alpha l}{a} \right)}{\tanh \frac{l}{a}} + \frac{\left( \cosh \frac{\alpha l}{a} - 1.0 \right)}{\sinh \frac{l}{a}} + \sinh \frac{\alpha l}{a} - \frac{\alpha l}{a} \right]}{\left[ \frac{\left( \cosh \frac{l}{a} + \cosh \frac{\alpha l}{a} * \cosh \frac{l}{a} - \cosh \frac{\alpha l}{a} - 1.0 \right)}{\sinh \frac{l}{a}} + \frac{l}{a} (\alpha - 1.0) - \sinh \frac{\alpha l}{a} \right]} \quad [4.6]$$

First derivative of  $\theta$  with respect to  $z$ :

$$\theta' = \frac{aT}{G(1+H)J} \left[ \frac{1 - \cosh \frac{z}{a}}{a} + \frac{\left( \coth \frac{l}{a} - \cosh \frac{\alpha l}{a} \coth \frac{l}{a} + \sinh \frac{\alpha l}{a} + H \left( -\cosh \frac{\alpha l}{a} \coth \frac{l}{a} + \operatorname{csch} \frac{l}{a} + \sinh \frac{\alpha l}{a} \right) \right) \sinh \frac{z}{a}}{a} \right] \quad [4.7]$$

Second derivative of  $\theta$  with respect to  $z$ :

$$\theta'' = \frac{aT}{G(1+H)J} \left\{ \frac{\cosh \frac{z}{a} \left[ \coth \frac{l}{a} - \cosh \frac{\alpha l}{a} \coth \frac{l}{a} + \sinh \frac{\alpha l}{a} + H \left( -\cosh \frac{\alpha l}{a} \coth \frac{l}{a} + \operatorname{csch} \frac{l}{a} + \sinh \frac{\alpha l}{a} \right) \right]}{a^2} - \frac{\sinh \frac{z}{a}}{a^2} \right\} \quad [4.8]$$

Third derivative of  $\theta$  with respect to  $z$ :

$$\theta''' = \frac{aT}{(1+H)GJ} \left\{ \frac{\left[ \coth \frac{l}{a} - \cosh \frac{\alpha l}{a} \coth \frac{l}{a} + \sinh \frac{\alpha l}{a} + H \left( -\cosh \frac{\alpha l}{a} \coth \frac{l}{a} + \operatorname{csch} \frac{l}{a} + \sinh \frac{\alpha l}{a} \right) \right] \sinh \frac{z}{a}}{a^3} - \frac{\cosh \frac{z}{a}}{a^3} \right\} \quad [4.9]$$

The design graphs for this case can be found in Appendix E.

Using the different derivatives of the rotation, the stresses due to torsion can be calculated.

The above expressions were used to predict the stresses and twisting deformations in the existing bridge vertical and are compared with the FEM results below.

#### 4.2.3 Comparison of FEM and Analytical Methods for Existing Bridge Vertical

The results are for an angle of twist of 9 degrees with remains in the elastic range for the FEM and allows application of the analytical expressions. This also allows some comparisons between the laboratory results and the more likely in-situ vertical response.

##### 4.2.3.1 *Natural Frequency of Existing Bridge Vertical*

The first five predicted natural frequencies of the existing bridge vertical finite element model were determined. The values are listed in Table 4.11 and their mode shapes are shown in Appendix D.

Table 4.11: Finite element model frequencies of the existing bridge vertical

<b>Mode:</b>	<b>Description:</b>	<b>Value: [Hz]</b>
1	Strong axis bending	4.7
2	Weak axis bending	5.5
3	First torsional	6.5
4	Second strong axis bending	8.0
5	Second torsional	12.8

The natural frequencies for the existing bridge vertical were calculated with the equations described in Chapter 2.1. For the existing vertical, a fixed-fixed boundary condition was chosen (Eqn. [2.2]) and a first torsional frequency ( $\omega_{torsion}$ ) of 6.0 Hz was determined and is slightly less than that predicted with the FEM. This may be due to the rigid end connection assumption used in the analytical formulations. The torsional natural-frequencies for the existing vertical were summarized in Table 4.12.

Since there was no experimental data available for the existing vertical, the analytical result and the finite element result were compared to the torsional natural frequency determined by Higgins and Turan 2009. The finite element results are reasonably close to the ones obtained by Higgins and Turan differing only by 3.1 %. The results obtained by the approximation of Carr are further off, differing by 7.7 %.

Table 4.12: Natural frequency comparison for the existing vertical

<b>Description:</b>	<b>Chapter:</b>	<b>Eqn. / Table:</b>	<b>Value: [Hz]</b>
Approximate analytical method (Carr)	2.1.2	[2.2]	6.0
Finite element model	4.2.3.1	Table 4.11	6.5
Higgins and Turan 2009 (U13-L13 after revision in 1997)			6.7

#### 4.2.3.2 *Torsional Stiffness of Existing Bridge Vertical*

Using a rearranged equation [4.5], a member length of 17221.2 mm (678 in) and an angle of twist of 9 degrees, the analytical torsional stiffness of the existing vertical was calculated and determined to be 125.19 kN-m/rad (1108.00 kip-in/rad).

The FEM results for the existing bridge vertical are reported with respect to the angle of twist at mid-length. The predicted elastic torsional stiffness of the existing bridge was determined to be 152.7 kN-m/rad (1351.43 kip-in/rad).

The torsional stiffnesses of the existing vertical are summarized in Table 4.13. The torsional stiffness determined from the finite element model is 22 % greater than the one obtained from the analytical method. This large difference could be a result from the load induction into the finite element model as described in Chapter 4.2.1. Since the load was induced as displacements in the  $x$  and  $y$  direction, the total force might have been increased above that which would be uniformly applied over the cross-section.

Table 4.13: Torsional stiffness comparison for the experimental vertical

Description:	Chapter:	Torsional Stiffness:	
		[kN-m/rad]	[kip-in/rad]
Analytical method	4.2.3.2	125.19	1108.60
Finite element model	4.2.3.2	152.7	1351.43



#### 4.2.3.3 Angle of Twist of Existing Bridge Vertical

The angle of twist along the span of the I-section of the existing vertical was calculated using a rearrangement of equation [4.5]. The angle of twist along the length of the existing vertical, calculated from the analytical expression and determined with the finite element model, are shown in Figure 4.24.

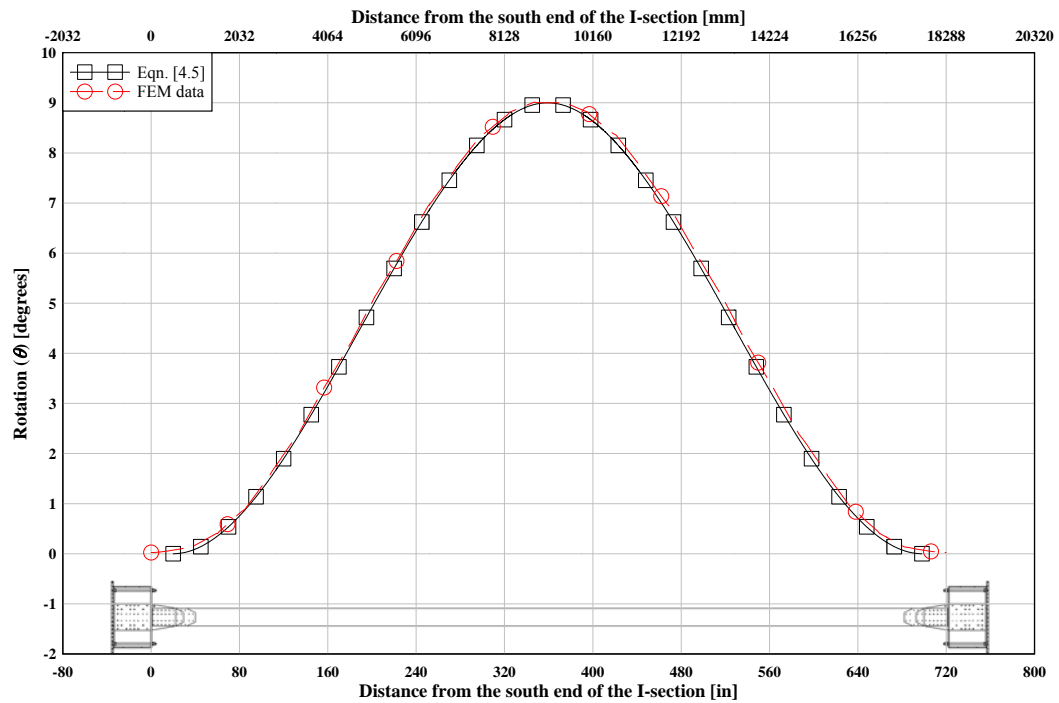


Figure 4.24: Comparison of the analytically predicted angle of twists for the existing bridge vertical

The results for the analytical and the finite element angle of twist for the existing vertical correspond well. The maximum error was below 5%.

#### 4.2.3.4 Normal Stresses along the Length of Existing Bridge Vertical

The normal stresses due to warping in the flange tips of the top and the bottom flange along the length of the existing vertical finite element model are shown in Figure 4.25.

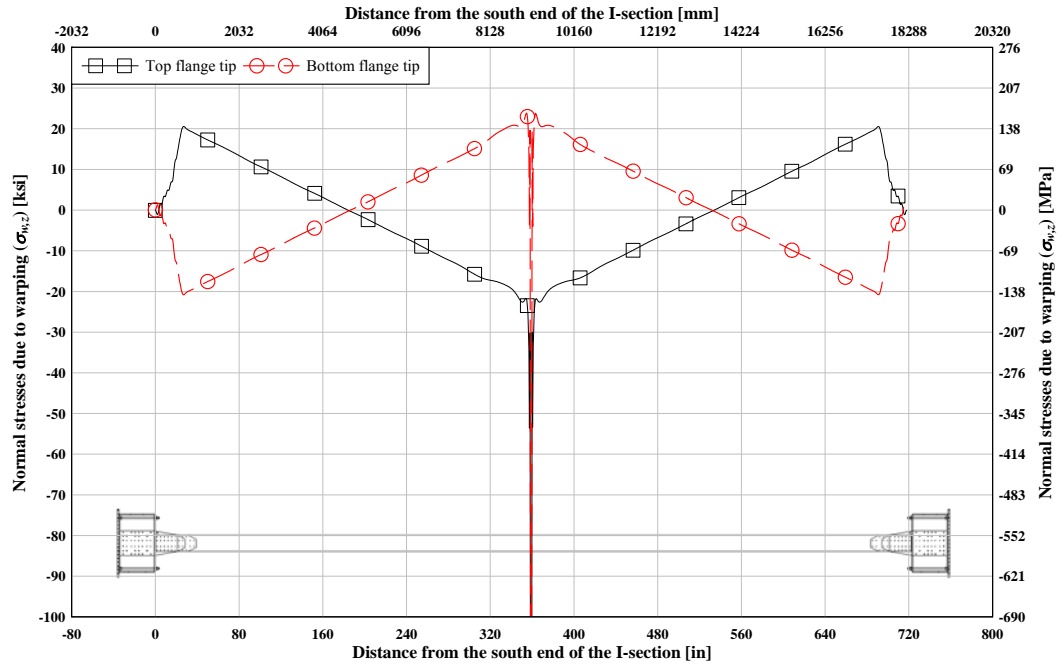


Figure 4.25: FEM normal stresses ( $\sigma_{w,z}$ ) at the flange tips along the span length (z-axis stresses) for the existing bridge vertical

Figure 4.25 shows a stress peak at the center location of the I-section. These stress peaks are a result from the load induction method chosen for this finite element model as described in Section 4.2.1. Only six single nodes in the cross-section of the I-section at the center of the existing vertical were used (as shown in Figure 4.21 and Figure 4.22) to induce the angle of twist of 9 degrees. Therefore, stress concentrations at these six locations were expected. Since these concentrations are an artifact of the selected modeling approach and are nonexistent in the existing bridge vertical, the stress peaks in Figure 4.25 were removed and the resulting graph for the top flange tip is shown and compared to the analytical expression results in Figure 4.26. For the top flange, the stress maximum closer to the ends was determined to be 145.5 MPa (21.1 ksi) and the maximum at the center of the vertical was determined to be 160.7 MPa (23.3 ksi). The stress peaks at the end of the I-

section are in the same location as described for the experimental setup in Chapter 4.1.3.6. The location of the stress concentration in the top flange was shown in Figure 4.9. It should be noted that since the results of the finite element model data for the normal stresses due to warping were modified, to remove stress concentrations, the peak stresses at the center location of the I-section may differ from the results shown in Figure 4.26.

Normal stresses in the flange tips were also calculated using equation [2.19]. The maximum normal stress found in the region of the gusset plate for the analytical data was 148.9 MPa (21.6 ksi) and 146.9 MPa (21.3 ksi) for the center of the vertical.

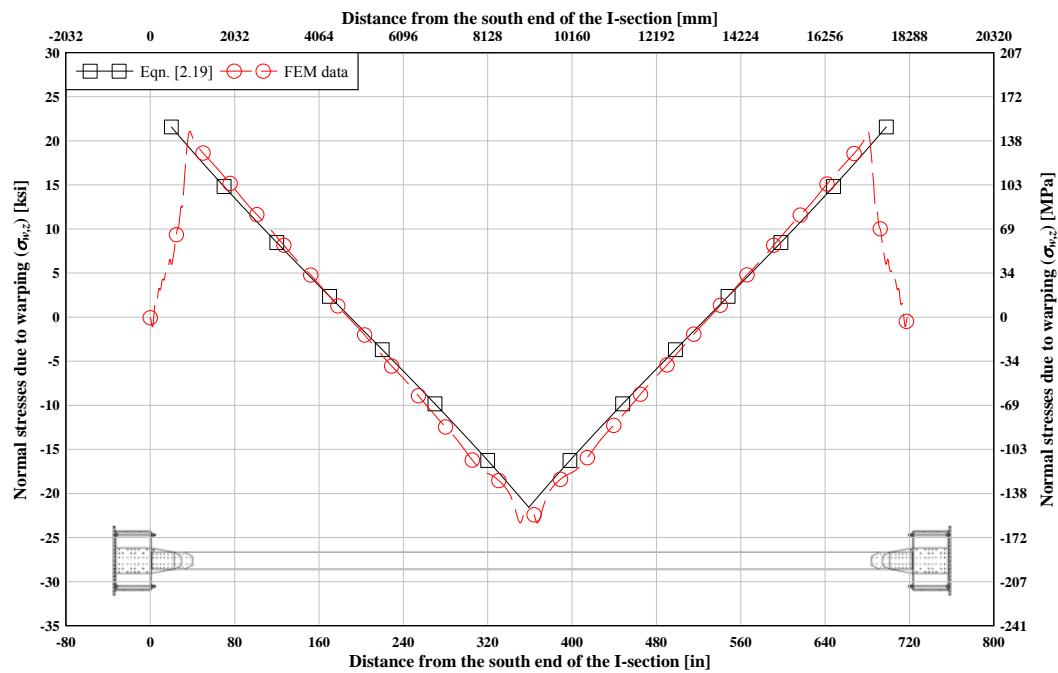


Figure 4.26: Comparison of the analytically predicted normal stresses at the tips of the top flange for the existing bridge vertical

The maximum normal stresses in the tips of the flanges due to warping in the existing vertical were determined to be 148.9 MPa (21.6 ksi) and were located 508 mm (20 in)

away from the end of the vertical, at the same location as the point of zero rotation. The stresses located at the mid-length of the vertical were determined to be in the same range (146.9 MPa (21.3 ksi)) once the high localized stresses at load introduction were filtered out. The reported FEM values obtained at the center span should be carefully regarded since the results in this region were manipulated as described previously.

#### 4.2.3.5 *Normal Stress in the Top Gusset Plate of Existing Bridge Vertical*

To determine the stresses in the top gusset plate of the I-section, the method described in Chapter 4.1.3.7 was used (with equation [2.8]). The resulting in-flange moment was determined to be 52.1 kN-m (460.8 kip-in). Using this moment, the normal stresses in the top gusset plate were determined to be 88.3 MPa (12.8 ksi). The normal stress distribution due to warping in the top gusset plate is shown and compared to the FEM results in Figure 4.27.

The finite element data for the normal stresses due to warping in the gusset plate are offset from the center location of the gusset plate (which should be zero for pure warping), by about 6.2 MPa (0.9 ksi). The maximum normal stress due to warping in the gusset plate was 99.3 MPa (14.4 ksi).

Figure 4.27 shows that the analytical results for the normal stresses are close to the finite element model stresses at the edges of the gusset plate. However, the simple calculation described in Chapter 2.2 and 4.1.3.7 was not able to predict the slightly larger peak stresses found in the finite element results. The maximum stress predicted by the analytical

calculation was 88.3 MPa (12.8 ksi); and the one determined from the finite element model was 99.3 MPa (14.4 ksi), this is a difference of 12.5%.

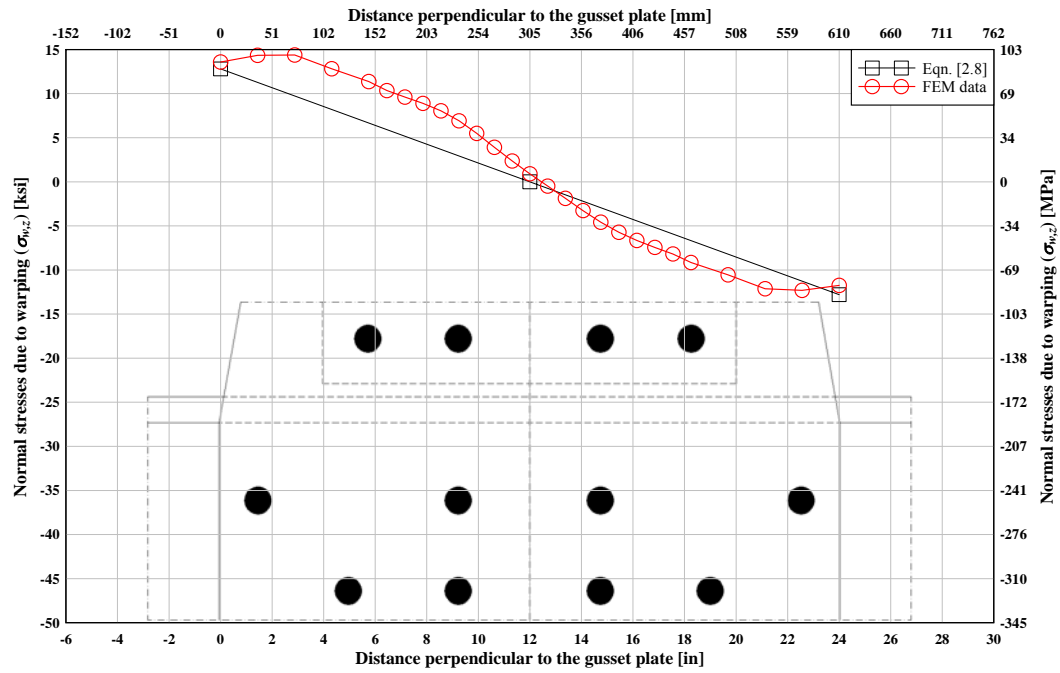


Figure 4.27: Comparison of the analytically predicted normal stresses in the top gusset plate for the existing bridge vertical

### 4.3 Further Evaluation of Comparative Results

#### 4.3.1 Boundary Condition: Both Ends Fixed, Uniformly Distributed Torque (AISC Steel Design Guide Series 9, Case 7)

Based on findings comparing the analytical results and the laboratory results described previously, it was determined that Case 7 from the AISC Steel Design Guide Series 9 would better and more conservatively predict the in-situ wind induced response of the bridge verticals. Case 7 has fixed-fixed boundary conditions and a uniformly distributed torque ( $t$ ) along the span length, as shown in Figure 4.28.

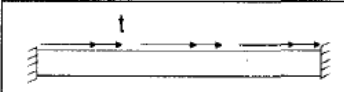
	Torsional End Restraints		Uniformly distributed torque on member with fixed ends
	Left End	Right End	
	Fixed $\theta = \theta' = 0$	Fixed $\theta = \theta' = 0$	

Figure 4.28: Boundary conditions and definitions for Case 7  
(Steel Design Guide Series 9, 2003)

To determine the angle of twist from the uniformly distributed torque, the following equation is used:

$$\theta = \frac{tla}{2GJ} \left[ \left( \frac{1 + \cosh \frac{l}{a}}{\sinh \frac{l}{a}} \right) \left( \cosh \frac{z}{a} - 1.0 \right) + \frac{z}{a} \left( 1 - \frac{z}{l} \right) - \sinh \frac{z}{a} \right] \quad [4.10]$$

The angle of twist and the normal stress due to warping have been calculated, based on the rotation equation [4.10] and equation [2.19], respectively. The results are shown in Figure 4.29.

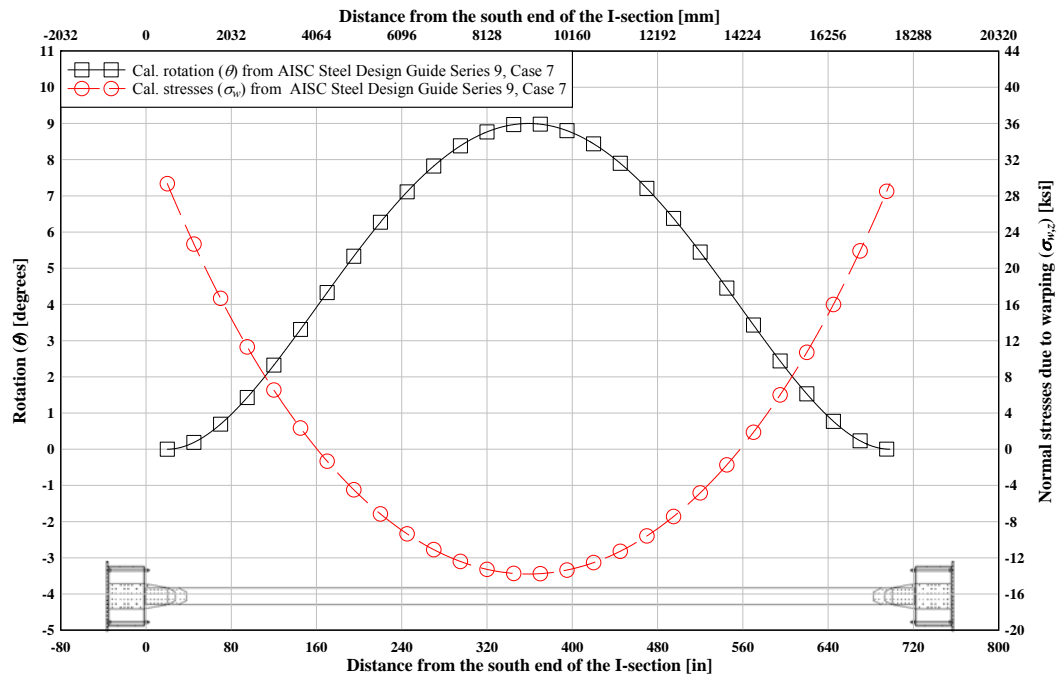


Figure 4.29: Calculated rotation and normal stress along the I-section for the existing vertical with AISC Steel Design Guide Series, Case 7 (uniform torque along length)

The maximum normal stresses due to warping were determined to be 202.4 Mpa (29.35 ksi) and are located at the ends of the vertical at the gusset plates.

Unfortunately, no finite element results or experimental results were available to compare with the results determined in Figure 4.29. Applying uniform torque along the length of the member would produce stress concentrations that were observed for the concentrated torque seen previously. However, considering the close correlation between the AISC design guide and previous FEM and experimental results, the predicted stress magnitudes and distributions are credible.

### 4.3.2 Comparison of Experimental and Analytical Results

All the results are shown in Figure 4.30. In this figure, the experimental results are shown as solid diamond symbols. The figure contains the above reported FEM results (circular symbols) for the laboratory specimen, existing bridge vertical with concentrated torque at mid-length, and existing bridge vertical with uniformly distributed torque along the length. The figure also contains the AISC design guide results (square symbols) for the laboratory specimen, existing bridge vertical with concentrated torque at mid-length, and existing bridge vertical with uniformly distributed torque along the length

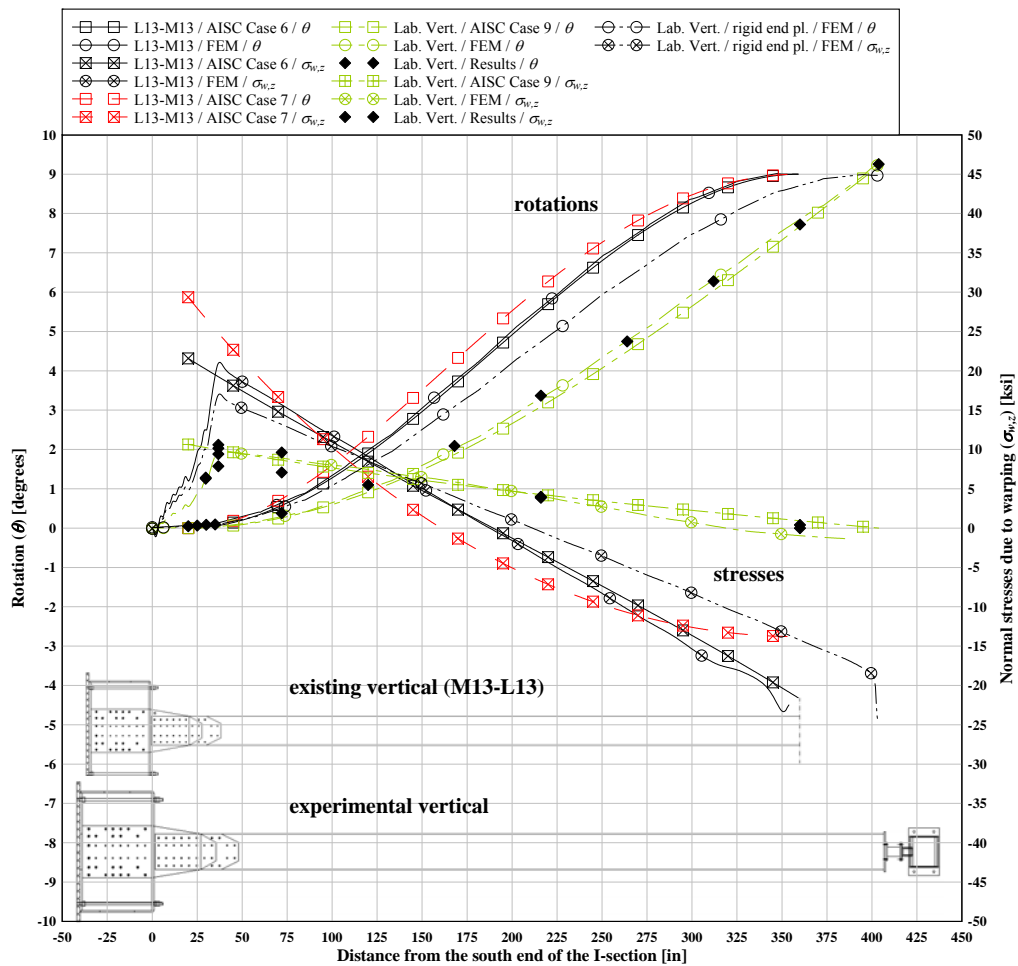


Figure 4.30: Summary of experimental and analytical (FEM and calculated) results



As the end plate in the experimental vertical is not fully rigid (as measured experimentally, as discussed in section 3.5.1), an additional finite element model (shown as “rigid end pl.” in Figure 4.30) was created to see what would happen if a more rigid end plate in the experimental vertical finite element model were used and how it might change the angle of twist and stress distribution. As seen in Fig. 4.30, using a more rigid end plate (approximately 16 in. thick) produced results between the experimental vertical finite element model and the existing bridge vertical.

From Figure 4.30, it can be seen that using the AISC Steel Design Guide Series 9, Case 7 resulted in the highest warping stresses in the existing bridge vertical (202.4 Mpa (29.35 ksi)), and is therefore the most conservative approach to predicting the stress magnitude in the vertical at the gusset plate location.

## 5 Fatigue Life Development

Higgins and Turan (2009) listed different verticals of the Astoria-Megler Bridge that were considered for possible wind induced vibrations. These verticals are listed in Table 5.1.

Locations of these verticals can be found in bridge diagrams in Appendix A.

Table 5.1: Bridge verticals considered for wind excited response  
(edited from Higgins and Turan, 2009)

Vertical:		Torsional Frequency: [Hz]	Member Length for Fatigue Calculations: (mm) / [in]
U9-L9		6.002	25,833 / [1,017]
U12-L12		4.857	19,042 / [750]
U19-L19		5.992	25,860 / [1,018]
U27-L27	Before 1986	8.088	19,785 / [779]
	After 1986	7.528	19,785 / [779]
U28-L28	Simplified	5.122	19,839/ [781]
	Whole Frame	7.692	19,839/ [781]
U13-L13	U13-M13 (Before 1997)	4.154	25,146 / [990]
	U13-M13 (After 1997)	9.459	25,146 / [990]
	M13-L13 (Before 1997)	6.733	19,125 / [753]
	M13-L13 (After 1997)	6.733	19,125 / [753]

### 5.1 Fatigue Life Calculation

To estimate the fatigue life of an existing bridge vertical, equation [2.21] given in Chapter 2.3 was re-arranged to determine the number of cycles that can be applied for a given stress range and fatigue detail. The re-arranged equation is given as:

$$F_{SR} = \left( \frac{C_f}{N} \right)^{0.333} \Rightarrow N = \frac{C_f}{F_{SR}^{\frac{1}{0.333}}} \quad [5.1]$$

The fatigue life of the vertical can be predicted by using equation [5.1], since the stress range of a specific angle of twist can be determined from analytical calculations (in this case, from AISC Steel Design Guide Series 9, Case 7, as described in Chapter 4.3).

To calculate the fatigue life for the existing bridge verticals, an average value for the location of zero rotation in the member was assumed to be the full connection length 1016 mm (40 in) from the work point of the gusset plate. This conservatively results in a shorter length member which produces higher warping stresses for a given angle of twist at mid-length. The connection end distance was twice subtracted from the length of the verticals listed in Table 5.1 to account for the gusset plate chord connections above and below the verticals. This resulting member length was then used in stress range calculations. The stress range was calculated at the tip of the flanges of the I-section.

To predict the total fatigue life of the bridge vertical, a one-hour long duration of vibration, occurring at the vertical member's torsional natural frequency, were assumed. The

predicted fatigue life, based on different analytically predicted rotational angle ranges for bridge vertical L13-M13 (after 1997), are shown in Table 5.2.

Table 5.2: Fatigue life prediction, for the L13-M13 (after 1997) bridge vertical

<b>Rotational Angle Range: (<math>\theta</math>) [deg] (Angle of Twist)</b>	<b>Stress Range: (<math>F_{SR}</math>) (MPa) [ksi]</b>	<b>Life Cycle : (<math>N</math>) Category C</b>	<b>Life Cycle: (<math>N</math>) Category B</b>	<b>One-Hour Event Count:</b>	
				<b>Cat C:</b>	<b>Cat B:</b>
2 (+/- 1°)	44.8 [6.5]	$\infty$	$\infty$	$\infty$	$\infty$
4 (+/- 2°)	89.6 [13.0]	1,991,032	$\infty$	82	$\infty$
6 (+/- 3°)	134.4 [19.5]	589,217	1,606,957	24	66
8 (+/- 4°)	179.2 [26.0]	248,361	677,349	10	28
10 (+/- 5°)	223.9 [32.5]	127,076	346,571	5	14
12 (+/- 6°)	268.7 [39.0]	73,499	200,452	3	8
14 (+/- 7°)	313.5 [45.5]	46,264	126,174	2	5
16 (+/- 8°)	358.3 [52.0]	30,981	84,493	1	3
18 (+/- 9°)	403.1 [58.5]	21,751	59,321	1	2
20 (+/- 10°)	447.9 [65.0]	15,851	43,231	1	2

The AISC Steel Manual defines the threshold fatigue stress range ( $F_{TH}$ ) for Category C as 69 MPa (10 ksi) and for Category B as 110 MPa (16 ksi), as described in Chapter 2.3 and

shown in Figure 2.7. Therefore, the fatigue life for both fatigue categories with a given angle of twist range of 2 degrees ( $\pm 1$  degree) or less is expected to be infinite. If Category B is the assumed stress category, then long life is expected up to an angle of twist range of 4 degrees ( $\pm 2$  degrees).

## 5.2 Fatigue Life Prediction

To predict the fatigue life of the bridge verticals likely to be most influenced by torsional vibrations, it was assumed that three one-hour events occur each year. Therefore, the one-hour event count for each vertical was divided by three and the results for the critical verticals for fatigue Category C are shown in Figure 5.1.

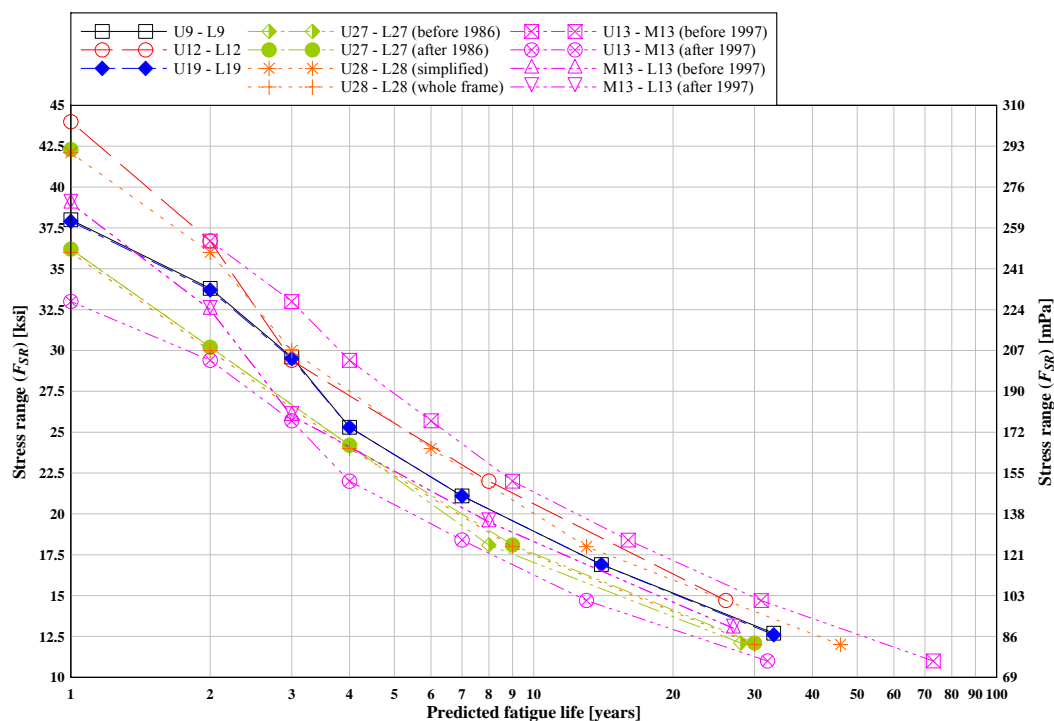


Figure 5.1: Fatigue life prediction for critical bridge verticals (Category C)

The predicted fatigue life for the verticals in Table 5.1 for fatigue Category B are shown in Figure 5.2. As seen in these figures, if the twist angles are sufficient, some verticals may be approaching the end of their fatigue lives or even exceeded their anticipated fatigue lives.

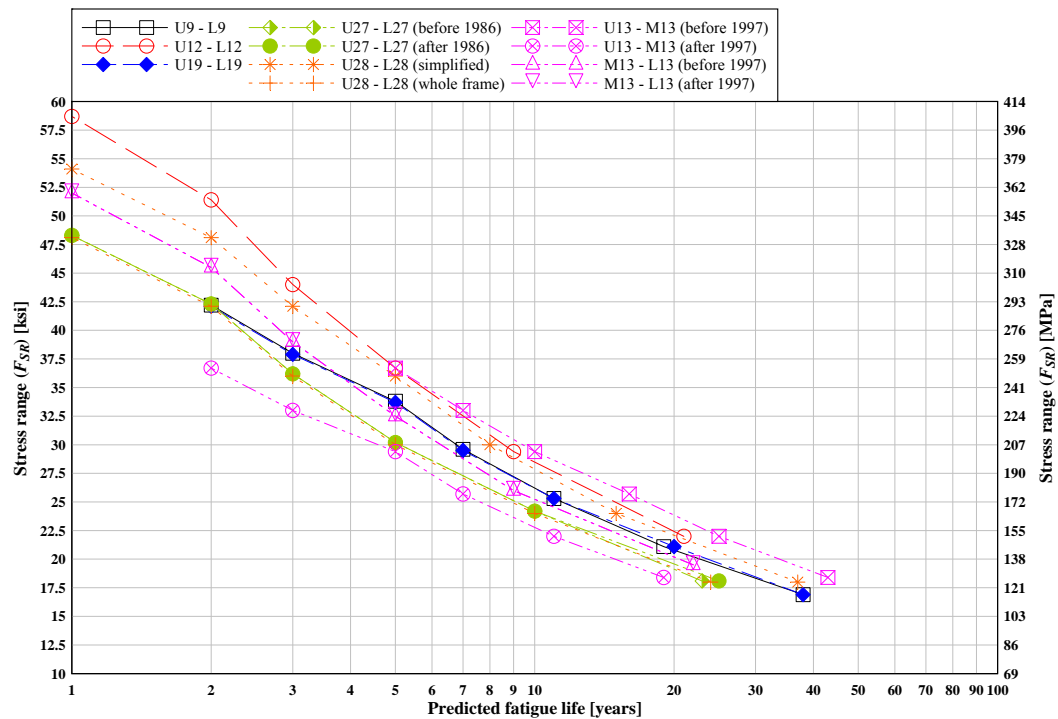


Figure 5.2: Fatigue life prediction for critical bridge verticals (Category B)

## 6 Summary and Conclusions

Vortex shedding for some long truss verticals produced wind-induced torsional vibration in an important steel truss bridge. These vibrations can create large numbers of repeated stress cycles for which the members and connections were not designed. To assess the impact of this behavior on the service life of the bridge members, an experimental and analytical investigation was undertaken. A full-scale representation of a truss vertical that exhibited such induced torsional response was fabricated and tested. Experimental data were collected to characterize the rotational behavior and the stress distribution along the vertical. The experimental data were compared with existing analytical methods and predictions from finite element models. The expected fatigue lives of the existing bridge verticals were predicted based on assumed storm duration and recurrence.

Based on the experimental and analytical results, the following conclusions are presented:

- The experimental specimen was representative of a member with fixed end at the gusset plate and free end (warping unrestrained) at the location of the applied torque.
- The end plate used in the experimental program for the load induction induced undesired stress concentrations in this region which do not occur in the actual bridge members. The high localized stress would likely be the location for crack initiation for the test specimen, which would not occur in-situ.
- The FEM reasonably predicted the warping stresses in the experimental vertical along the length as well as within the disturbed regions: at the end plate as well as within the gusset plate connection.

- The experimentally measured location of the maximum fatigue stress range occurred in the vertical member as it entered the gusset plate connection (measured at the first row of fasteners). The finite element model, as well as the calculations using the AISC Steel Design Guide Series 9 also predicted the location for a possible fatigue crack initiation in the bridge vertical at the first bolt line connection to the gusset plate. This corresponds to similar locations identified for other bridges (Commodore Barry Bridge, Delaware, USA and Dongping Bridge, China) in previous research papers.
- Experimentally measured and FEM predicted stresses in the gusset plate connection were smaller than those in the vertical and would not likely control the fatigue life.
- The experimental results including twist angle, stress distribution, and stress magnitude were well captured by both the finite element model and the analytical equations.
- Calculations using the AISC Steel Design Guide Series 9, Torsional Analysis of Structural Steel Members, showed good correlation with the experimental results for the angle of twist and warping stress magnitude in the vertical. However, to perform these calculations, the point of zero rotation in the existing bridge vertical is required.
- The location of zero rotation was identified experimentally at approximately half the length of the gusset plate connection where it overlaps the vertical member.
- The existing bridge verticals are best modeled as rigid-rigid end connections with uniformly distributed torque along the member length. The member length is conservatively estimated as the end of gusset plate to end of gusset plate (or fill



plate, whichever are longer). This produces the highest warping stress at the ends of the member for a given twist angle at mid-length for use in fatigue life estimation.

- It was determined that fatigue in the existing bridge vertical (L13-M13) is unlikely, as long as the angle of twist of the vertical is below 2 degrees range of motion (+/- 1 degree).
- For the assumed storm duration and recurrence, if the angle of twist induced in-situ is sufficient, some of the bridge verticals may be approaching the end of their expected fatigue lives.

The following recommendations are given:

- To locate possible fatigue cracks in the Astoria-Megler Bridge, bridge inspectors should concentrate their efforts on to the first row of bolts in the vertical and inspect the gusset plates above the chord line. The mid-height elevation of the vertical is another location that shows relatively high twisting induced stress ranges and should be included for the longer bridge verticals.
- To use the AISC Steel Design Guide Series 9, the location of zero rotation in the vertical must be defined. This research project suggests that the distance between the end of the vertical and the point of zero rotation is taken as half the distance between the end of the vertical and the end of the gusset plate or the fill plate, whichever is longer. It is conservative to use the shortest member length and this can be taken from the end of the gusset plate at the bottom of the member to the end of the gusset plate on the top of the member.

## **6.1 Further Research**

The primary interest of this research project was to design and conduct torsional tests for an oscillating vertical of the Astoria-Megler Bridge. To conduct fatigue tests of the vertical would require a different load induction system which eliminates the stress concentration at the end plate detail connecting the member to the torque actuator. It would be desirable to conduct a fatigue test to verify that cracking would initiate in the vertical at the gusset plate connection. However, a number of replicate specimens would be required to satisfactorily categorize the fatigue performance.

The results from this research project may be used to develop retrofit strategies for the existing bridge verticals. The following alternative solutions could be analyzed:

- Sloshing dampers
- Tuned mass dampers
- Adding torsional stiffness to the I-section (closing the open cross section)
- Disturbing the wind flow around the cross section

## BIBLIOGRAPHY

- AISC (2008) Steel Construction Manual, 13<sup>th</sup> Edition, Fourth Printing, *American Institute of Steel Construction*, Chicago, Illinois.
- Boresi, A. P., Sidebottom, M. O. (1985) *Advanced Mechanics of Materials*, Fourth Edition, John Wiley & Sons Inc., 260-266.
- Carr, J. B. (1969) The Torsional Vibration of Uniform Thin-Walled Beams of Open Section. *The Aeronautical Journal of the Royal Aeronautical Society*, 73, 672-674.
- Chen, Z. Q., Liu, M. G., Hua, X. G., Mou, T. M., et al. (2012) Flutter, Galloping and Vortex-Induced Vibrations of H-Section Hangers. *Journal of Bridge Engineering*, May / June, 2012, 500-508.
- Higgins C., Turan T., (2009) *Analysis of Astoria-Megler Bridge #7949 to Guide Instrumentation and Monitoring of Wind Induced Vibrations*. Salem, Oregon: Oregon Department of Transportation.
- Hibbit, Karlsson& Sorenson, Inc. (2002) ABAQUS/Standard (Version 6.3-8) [Computer Software].
- HydeSoft Computing, LCC (2001) DPlot, Graph Software for Scientists & Engineers (Version 2.3.1.8) [Computer software].
- Maher, F. J., Wittig, L. E. (1980) Aerodynamic Response of Long H-Sections. *Journal of the Structural Division*, ST1, 183-198.
- Microsoft Corporation (2006) Microsoft Excel 2010 [Computer software].
- Nakamura, Y. (1996) Vortex Shedding from Bluff Bodies and a Universal Strouhal Number. *Journal of Fluids and Structures*, 10, 159-171

Scanlan, R. H. (1976) Modern Approaches to Solution of the Wind Problem of Long Span Bridges, *Engineering Journal / American Institute of Steel Construction*, Chicago, Illinois.

Steel Design Guide Series 9 (2003), Torsional Analysis of Structural Steel Member, Second Printing, *American Institute of Steel Construction*, Chicago, Illinois.

Tedesco, J. W, McDougal, W. G., Ross, C. A. (1998) *Structural Dynamics Theory and Applications*, First Edition, Addison Wesley Longman Inc., 86-87.

#### **INTERNET SOURCES**

- [1] Official Oregon State website, Department of Transportation,  
[http://www.oregon.gov/ODOT/HWY/GEOENVIRONMENTAL/historic\\_bridges\\_coastal1.shtml](http://www.oregon.gov/ODOT/HWY/GEOENVIRONMENTAL/historic_bridges_coastal1.shtml) (accessed March 14, 2011)
- [2] Department of applied mechanics website, Indian Institute of Technology, Madras  
<http://apm.iitm.ac.in/fmlab/research.html> (accessed May 30, 2012)

## **APPENDICES**

**APPENDIX A – SELECTED ORIGINAL BRIDGE DRAWINGS**

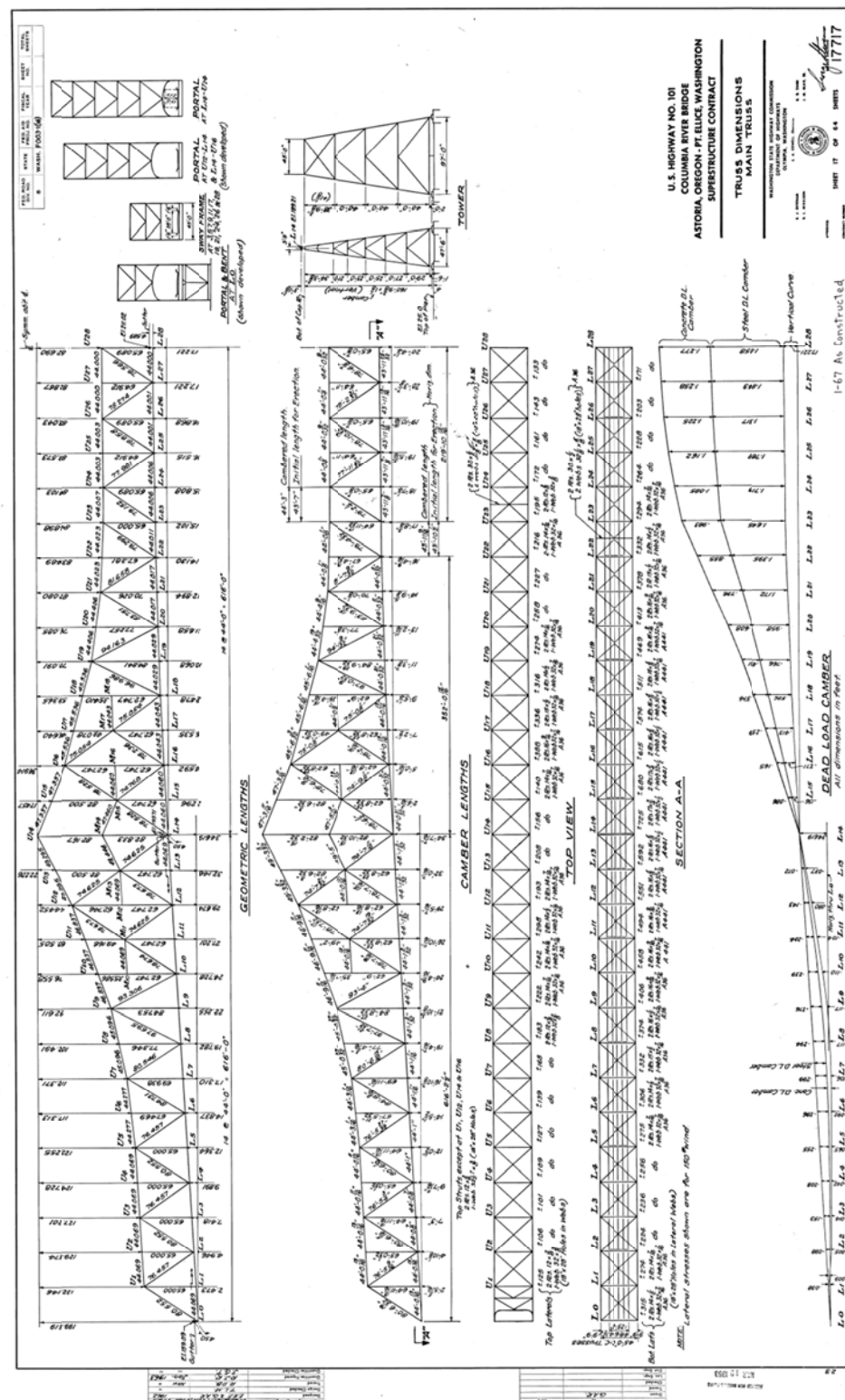


Figure A.1 : Truss dimensions main trusses

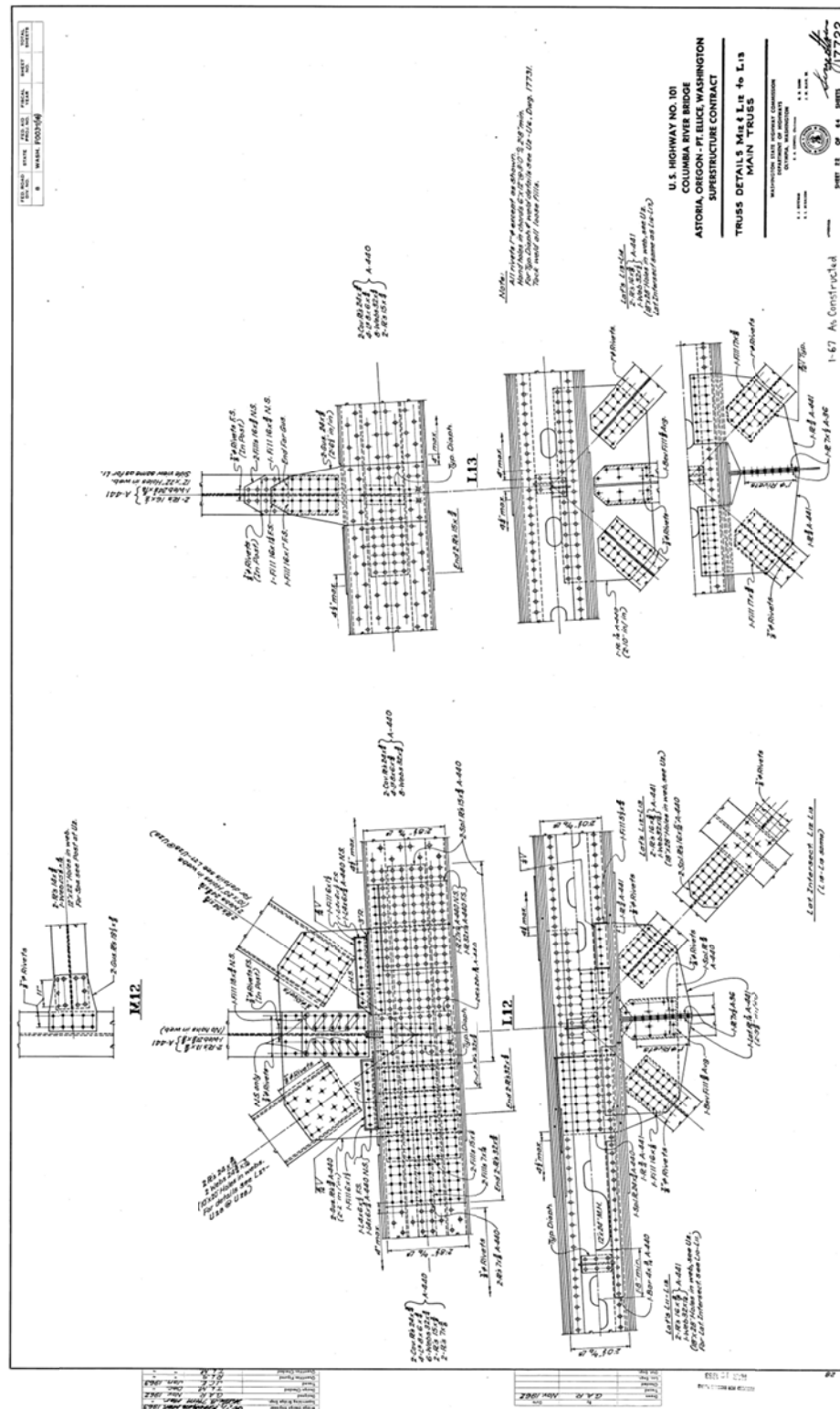


Figure A.2 : Truss detail L13



**APPENDIX B – FABRICATION DRAWINGS FOR THE  
EXPERIMENTAL SETUP**

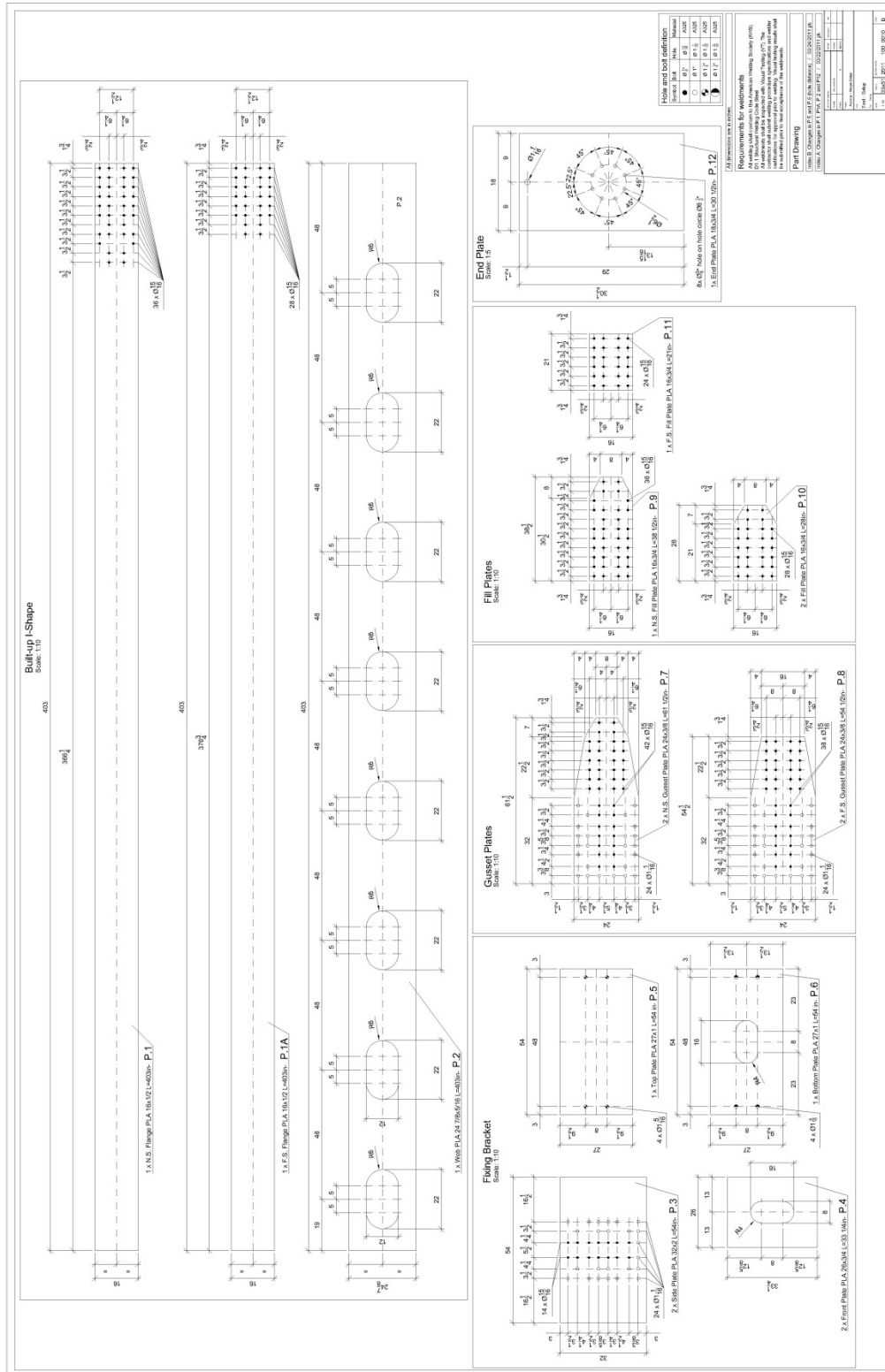


Figure B.1 : New fabrication drawing, parts

Figure B.2 : New fabrication drawing, assembly

**APPENDIX C – SELECTED FABRICATION DOCUMENTS**

**The Lynch Company**4706 SE 18th Ave  
Portland, OR 97202**Daily Report of Structural Steel**

Project: Test Setup  
 Address: 4706 SE 18th Ave Portland, OR 97202 TLC Job #: 35000  
 TLC Representative: Hitch Nicksen 09041614 was on site this date 5/10/11 to perform  
 (inspector name and Cert No.)

Special Inspection for ☐ permit ☐ DFS#(s) \_\_\_\_\_ jurisdiction \_\_\_\_\_

In some cases more than one box may be checked for a given item.

**SCOPE OF INSPECTION**

Location of steel inspection [to include grid lines, elevations (floors) and drawing details]:

2. Inspection was "IBC" ☐ Continuous ☒ Periodic  
 3. Work performed ☐ in the field ☒ at fab shop  
 Shop name: The Lynch Company  
 4. If shop inspection do they have fabrication and QC procedures ☒ Yes ☐ No ☐ N/A

Performed VT inspection on 3 test setup as per Design # 2011-100-0011 Rev B and AWS D16.2010. All welds visually acceptable

**INSPECTION**

Yes No N/A

1. Reviewed previous inspection reports?			<input checked="" type="checkbox"/>
2. Verified steel materials are in compliance by reviewing random samples of the mill test reports, steel ID markings or other documentation.	<input checked="" type="checkbox"/>		
3. Verified weld filler materials conform.	<input checked="" type="checkbox"/>		
4. Checked steel members to see they were fabricated and erected in accordance with the workmanship and tolerances required.	<input checked="" type="checkbox"/>		
5. Checked welded studs and structural connections were installed as required.		<input checked="" type="checkbox"/>	
6. Verified high strength bolts and fasteners conform.	<input checked="" type="checkbox"/>		
7. Verified the quality of welds produced by welders, welding operators, and tackers conform.	<input checked="" type="checkbox"/>		
8. Verified steel frame joint details for bracing, stiffening, member locations, and application of joint details at each connection are in compliance by random sampling.		<input checked="" type="checkbox"/>	

**REPORT SUMMARY**

1. Work inspected was: ☒ Completed ☐ In progress  
 2. Completed work inspected ☒ was ☐ was not in compliance with.  
☒ Approved plans and specifications ☐ shop drawings  
☐ RFI ☐ Design change ☐ Submittal ☐ N/A  
 Document #(s) 2011-100-0011 Rev B

**WELDER INFORMATION**

Welders Name: Mike Whitlow, Jeremy Woods  
 Certification #: C-2491, C-2716

Yes No N/A

1. Verified the contractor's Welding Procedure Specifications are in conformance with AWS requirements.	<input checked="" type="checkbox"/>		
2. Verified essential variables outlined in the Welding Procedure Specification were employed during execution of the work.	<input checked="" type="checkbox"/>		
3. Verified the weldability of reinforcing steel other than ASTM A706.			<input checked="" type="checkbox"/>

3. Noncompliance item(s) were noted this date. Details on following page(s). ☐ Yes ☐ No ☒ N/A  
 4. Noncompliance item(s) were reinspected with this date, details details on following page(s). ☐ Yes ☐ No ☐ N/A  
☐ Conform ☐ Remain in progress

Report(s) findings were discussed and left with

Dick Johnson  
 of The Lynch Company

Inspector Signature: [Signature]  
☐ See additional report page(s) ☐ Distribute attachments

Figure C.1 : Fabrication report for the laboratory vertical



**The Lynch Company**

The Lynch Company, Inc.  
4706 SE 18th Avenue  
Portland OR 97202  
T: (503) 236-3825  
F: (503) 238-4550  
www.thelynchco.com

### D1.1 Welding Procedure Specification (WPS)

Prequalified: Yes

Qualified by Testing: No

WPS No.: SMW407-1F/C

Welding Process: FCAW

Revision: 1

Date: 11/02/2003

Type: Semi-Automatic

Supporting PQR No.(s): B-U2a-GF

Joint Design: 11 V-Groove with Backing

Joint Detail

Backing: Yes

Range:

Backing Material (TYPE): ASTM A-36

Ro: 3/16 to 9/16 T: 1/8 to  
Unlimited Theta: 40  
Deg to 65 Deg.

Notes: Reference Fig. 4.30 Welder Qualification Limitations and  
And Joint Design in Accordance with (ANSI / AWS D1.1 Latest  
Edition) Fig 3.3 and 3.4. \*Consult manufacturer's recommendations  
for ranges.

Joint Design used		Position	
Root opening: 3/16 to 9/16 Root face dimension: 0.0		Position of Groove: F, V, OH Fillet: All	
Groove Angle: 40 Deg to 65 Deg Radius(J-U): N/A		Vertical Progression: Up	
Back Gouging: No Method: NA			
Base Metals:		Electrical Characteristics:	
Material Specification: ASTM A-36 to ASTM A-36		Transfer Mode (GMAW): Spray	
Type or Grade: N/A-N/A		Current: DCEP	
Thickness: Groove 1/8 to Unlimited Fillet: 1/8 to Unlimited		Other: None	
Diameter (Pipe): = to or >24		Tungsten Electrode (GTAW)	
		Size: N/A	
		Type: N/A	
Filler Metals		Technique	
AWS Specification: A5.20		Stringer or Weave Bead: Either	
AWS Classification: E71T-1		Multi pass or single pass per side: Multi-pass	
Shielding		Number of Electrodes: Single	
Flux: N/A		Electrode Spacing	
Gas: Ar, Co2		Longitudinal: N/A	
Composition: 75% Ar, 25% Co2		Lateral: N/A	
Flow Rate: 30-50 CFM		Angle: N/A	
Gas Cup Size: 1/2 I.D. Minimum		Contact Tube to work Distance: 3/4 + or - 1/4	
Electrode: N/A		Peening: No Peening	
Flux Class: N/A		Interpass Cleaning: Mechanical Only	

Figure C.2 : Welding specifications for the laboratory vertical



**The Lynch Company**

The Lynch Company, Inc.  
4706 SE 18th Avenue  
Portland OR 97202  
T: (503) 236-3825  
F: (503) 238-4550  
www.thelynchco.com

---

**Preheat**

Preheat Temp Min: 70 Deg F.

Interpass Temp Min: 70 Deg F.

---

**Postweld Heat Treatment**

Temp: N/A

Time: N/A

---

**Welding Procedure**

Pass or Weld Layer(s)	Process	Filler Metals		Current		Volts	Travel
		Class	Diam	Type & Polarity	Amps or wire feed Speed		
All	FCAW	E71T-1	.045	DCEP	150-290 Amps	25-30	Varies

Figure C.3 : Welding specifications for the laboratory vertical (continued)

WELDER CERTIFICATION

Cert. No: C-2491  
 Welder: MICHAEL WHITLOW  
 SS#: ---  
 City of Portland Expiration Date: 09/17/2011

---

Welder Signature *Michael Whitlow* Date \_\_\_\_\_  
 CFI Authorized Signature \_\_\_\_\_ 08/30/2010

Carlson Testing, Inc.  
 Tigard, Oregon (503) 684-3460  
 See Reverse Side for Qualification Data

Qual. Spec: ASME SEC. IX  
 Process: GTAW Position: 1G  
 Weld Desc: VEE-GROOVE  
 Material: SAF2507  
 Filler: SFA5.9 2507/P100 Thickness: 1/2" PLATE  
 Remarks:

Qual. Spec: AWS D1.1-06  
 Process: GMAW Position: 1G  
 Weld Desc: VEE-GROOVE  
 Material: A-36  
 Filler: ER70S-6 Thickness: 1/8" TO 3/4"  
 Remarks: BACKING REQUIRED, SHEET STEEL TRAINING CERT

Qual. Spec: AWS D1.1-06  
 Process: FCAW Position: 3G  
 Weld Desc: VEE-GROOVE  
 Material: A-36  
 Filler: E71T-1 Thickness: 1/8" TO UNLIMITED  
 Remarks: BACKING REQUIRED, SHEET STEEL TRAINING CERT

WELDERS RECORD OF EMPLOYMENT

January-March  
 FIRM: \_\_\_\_\_  
 SUPERVISOR: \_\_\_\_\_ PHONE: \_\_\_\_\_

April-June  
 FIRM: \_\_\_\_\_  
 SUPERVISOR: \_\_\_\_\_ PHONE: \_\_\_\_\_

July-September  
 FIRM: \_\_\_\_\_  
 SUPERVISOR: \_\_\_\_\_ PHONE: \_\_\_\_\_

October-December  
 FIRM: \_\_\_\_\_  
 SUPERVISOR: \_\_\_\_\_ PHONE: \_\_\_\_\_

Figure C.4 : Welding certifications



WELDER CERTIFICATION

Cert. No: C-2716  
 Welder: JEREMY WOODS  
 SS#: 3691  
 City of Portland Expiration Date: 08/12/2011

---

Welder Signature [Signature] Date 08/17/2010  
 CTT Authorized Signature \_\_\_\_\_

Carlson Testing, Inc.  
 Tigard, Oregon (503) 684-3460  
 See Reverse Side for Qualification Data

Qual. Spec: AWS D1.3-08  
 Process: SMAW Position: 1G  
 Weld Desc: ARC SPOT  
 Material: A-653 TO A-36  
 Filler: E6022 Thickness: 20 GA. ONLY  
 Remarks:

Qual. Spec: AWS D1.6-07  
 Process: GMAW Position: 1G  
 Weld Desc: VEE-GROOVE  
 Material: 304 SS  
 Filler: 308LSI Thickness: 1/16" TO 3/4"  
 Remarks: BACKING REQUIRED

Qual. Spec: D1.1-08  
 Process: FCAM Position: 3G  
 Weld Desc: VEE-GROOVE  
 Material: A-36  
 Filler: E71T-1 Thickness: 1/8" TO 3/4"  
 Remarks: BACKING REQUIRED

#### WELDERS RECORD OF EMPLOYMENT

January-March

FIRM: \_\_\_\_\_

SUPERVISOR: \_\_\_\_\_

PHONE: \_\_\_\_\_

April-June

FIRM: \_\_\_\_\_

SUPERVISOR: \_\_\_\_\_

PHONE: \_\_\_\_\_

July-September

FIRM: \_\_\_\_\_

SUPERVISOR: \_\_\_\_\_

PHONE: \_\_\_\_\_

October-December

FIRM: \_\_\_\_\_

SUPERVISOR: \_\_\_\_\_

PHONE: \_\_\_\_\_

Figure C.5 : Welding certifications (continued)



## MATERIAL CERTIFICATION

**SOLD TO:**

UNITED WELDING SUPPLY  
2313 N.E. MLK JR., BLVD.  
PORTLAND OR 97212

DATE 23-Feb-11  
P.O. NUMBER  
TYPE Actual

**PRODUCT NAME** Pinnacle Alloys

**LOT/HEAT**

MF0120K8 PREMIER 712 .045 X SP. AWS A5.20

**Chemical Analysis**

C	Cr	Ni	Mo	Mn	Si	Cu	P	S	N
0.06	0.04	0.03	0.01	1.39	0.55	0.01	0.012	0.005	0.000
Sn	Al	Cb+Ta	Ti	V	Co	W	B	Fe	Other
----	----	0	0	0.03	-----	----	----	----	----

**Mechanical Properties**
**Ferrite**
**Note:**

Tensile Strength	89 (KSI)	Schaeffler	N/A
Yield Strength	81 (KSI)	DeLong	N/A
Elongation(2"),	27.0%	WRC- 1988	N/A
Charpy V-Notch	69 FT LB @ -20F		

E71T-  
1C/1M,9C/9M,12C/12M

Figure C.6 : Material certifications Steel 1

**ArcelorMittal Burns Harbor Plate**

QUALITY ASSURANCE  
REPORT OF TEST AND ANALYSES

SHIPMENT NO. 803-05966		DATE SHIPPED 04-05-11		CAR OR VEHICLE NO. TPPX 082057		PAGE 1	
S FARWEST STEEL CORP PO BOX 889 EUGENE OR 97440				S FARWEST STEEL CORP SIDING 4148 EUGENE OR			

N O T E	SERIAL NUMBER	PAT NO.	HEAT NUMBER	NO. PCS	SIZE AND QUANTITY				YIELD POINT	TENSILE STRENGTH	ELONG.	RED.
					THICKNESS	WIDTH OR DIA.	LENGTH	WEIGHT				
					INCHES	INCHES	INCHES	POUNDS	PSI	PSI	IN	%
QUALITY STEEL MELTED & MANUFACTURED IN THE U. S. A.												
PLATES - ASTM A 36-08												
MFST - MFST MILL SERIAL# LIFT MAX 12 TON UNLDG												
OH-MAGNET LOAD MAX 185000 #												
CO# 101-8234 GH 877-0465												
					821S11500	6	1 1/2	96	240	58806	47800	71400 2 28
										41100	69300 2 31	
	(M55)MFST REF#:ITEM 01				822S34600	1	1 1/2	96	240	9801	42500	73400 2 31
	(M55)MFST REF#:ITEM 01											
PLATES - ASTM A 36-08												
MFST - MFST MILL SERIAL# LIFT MAX 12 TON UNLDG												
OH-MAGNET LOAD MAX 185000 #												
CO# 101-8234 GH 877-0465A												
					811S11490	3	2	96	240	39204	38700	70100 2 33
										37400	69800 2 33	
	(M55)MFST REF#:ITEM 02											
					813S67650	4	2	96	240	52272	39700	71300 2 33
										42000	72100 2 33	
	(M55)MFST REF#:ITEM 02											

Q-QUENCH TEMPERATURE				T-TEMPERATURE				N-NORMALIZE TEMPERATURE			
----------------------	--	--	--	---------------	--	--	--	-------------------------	--	--	--


SERIAL NUMBER	PAT NO.	HEAT NUMBER	HARD BHN	REND	THICKNESS INCHES	TYPE	SIZE	DIR	TEST TEMP F	CHARPY IMPACT								
										ENERGY FT LBS			SHEAR(%)			LAT. EXP MILS		
										1	2	3	1	2	3	1	2	3

HEAT NUMBER	CHEMICAL ANALYSIS																MOQUAD GRAIN SIZE
	C	Mn	P	S	Si	Cu	Ni	Cr	Mo	V	Ti	Al	B	Co	N	Sn	
821S11500	.16	1.07	.012	.007	.202	.021	.01	.03	.006	.001	.002	.034	.0002	.002	.004	.003	
822S34600	.17	1.07	.009	.005	.197	.025	.04	.05	.024	.001	.002	.031	.0002	.002	.005	.005	
811S11490	.17	1.06	.013	.005	.200	.028	.01	.04	.006	.001	.002	.034	.0002	.002	.004	.006	
813S67650	.16	1.14	.015	.005	.205	.017	.01	.03	.005	.001	.002	.035	.0002	.002	.005	.004	

I certify that the above results are a true and correct copy of actual results contained in records maintained by ArcelorMittal Burns Harbor and are in full compliance with the requirements of the specification cited above. This test report cannot be altered and must be transmitted intact with any subsequent third party test reports, if required.

BHP.LTRPT.TIF SUPV. QUALITY ASSURANCE D. W. ELWOOD PER WNK

Figure C.7 : Material testing certifications Steel 1



**EVRAZ**  
Evraz Oregon Steel 1403 N. Evergreen Blvd., Portland, Oregon 97203

**REPORT OF CHEMICAL/PHYSICAL TESTS**

CERTIFICATE NO. 1150925  
DATE Apr 15, 2011  
PAGE 1

ISO 9001  
REGISTERED  
U.S. PLATE MARKING

**FARWEST STEEL CORPORATION**  
PO BOX 889  
EUGENE, OR 97440  
USA

CUSTOMER ORDER NO. 101-8295  
JOB/REQ. NO.

HEAT NO. NW0854  
SLAB PSX 100  
YIELD 472  
TENSILE 635 25  
PSX 100 8 2  
% PA 453 615 32

DESCRIPTION  
3 PCS 15315 LBS  
3 PCS 15315 LBS  
1 PC 5105 LBS  
7 PCS 35735 LBS TOTALS

HEAT NO. NW0863  
SLAB PSX 100  
YIELD 473  
TENSILE 635 29  
PSX 100 8 2  
% PA 450 610 32  
443 610 32


SHIPPING NO. 1150925  
DATE 04/15/2011

CARRIER  
FARWEST (OWN)

CAPTRUCK NO. 160

THIS MATERIAL HAS BEEN MANUFACTURED, TESTED AND FOUND TO MEET THE SPECIFICATIONS AND PURCHASE ORDER REQUIREMENTS  
CARBON STRUCTURAL QUALITY PLATE ASTM A36-08/ASME SA36 2007/09 ADD. ABS GRADE A.

WE HEREBY CERTIFY THAT THE MATERIAL DESCRIBED HEREIN HAS BEEN MANUFACTURED TO THE APPLICABLE SPECIFICATION AND TESTED IN ACCORDANCE WITH THE REQUIREMENTS OF THE AMERICAN BUREAU OF SHIPPING RULES WITH SATISFACTORY RESULTS.  
1 0.3125 X 120.000ME X 480.000



**CHEMICAL ANALYSIS**

HEAT NO.	C	Mn	P	S	Si	Cu	Ni	V	Cr	Mo	Ti	B	N	Ca	CE	W
NW0854	08	1.09	.011	.011	.27	.02	.05	.009	.005	.037	.02	.00				
NW0863	09	1.06	.008	.009	.29	.02	.05	.003	.005	.035	.03	.00				
NW0866	08	1.07	.009	.009	.28	.02	.05	.002	.005	.037	.03	.00				

HEATS INDICATED WITH (+) WERE MELTED & MANUFACTURED IN THE USA. HEATS INDICATED WITH (\*) WERE ROLLED IN THE USA.

..... END OF REPORT .....

I certify the above to be correct as contained in the records of EVRAZ INC. NA By Chitwale  
Technical Support Coordinator

Figure C.8 : Material testing certifications Steel 1 (continued)


 <b>EVRAZ</b> Evraz Oregon Steel 14400 N. Rivergate Blvd., Portland, Oregon 97203		<b>REPORT OF CHEMICAL/PHYSICAL TESTS</b>													
<b>ISO 9001</b> REGISTERED TO US PATENT & TRADEMARK OFFICE		<b>S O L D</b> TO		<b>EVRAZ INC. NA</b> Evraz Oregon Steel 14400 N. Rivergate Blvd., Portland, Oregon 97203		<b>FARVEST STEEL CORPORATION</b> PO BOX 889 EUGENE, OR 97440 USA		<b>FARVEST STEEL CORPORATION</b> PO BOX 889 EUGENE, OR 97440		<b>CERTIFICATE NO.</b> 1153787	<b>DATE</b> Apr 28, 2011	<b>PAGE</b> 1			
<b>ISO 9001</b> REGISTERED TO US PATENT & TRADEMARK OFFICE				<b>FARVEST STEEL CORPORATION</b> PO BOX 889 EUGENE, OR 97440 USA				<b>FARVEST STEEL CORPORATION</b> PO BOX 889 EUGENE, OR 97440		<b>MILL ORDER NO.</b> 243142	<b>DATE</b> 04/28/2011	<b>PAGE</b> 1			
<b>ISO 9001</b> REGISTERED TO US PATENT & TRADEMARK OFFICE				<b>FARVEST STEEL CORPORATION</b> PO BOX 889 EUGENE, OR 97440 USA				<b>FARVEST STEEL CORPORATION</b> PO BOX 889 EUGENE, OR 97440		<b>CUSTOMER ORDER NO.</b> 101-8608	<b>DATE</b> 04/28/2011	<b>PAGE</b> 1			
<b>ISO 9001</b> REGISTERED TO US PATENT & TRADEMARK OFFICE				<b>FARVEST STEEL CORPORATION</b> PO BOX 889 EUGENE, OR 97440 USA				<b>FARVEST STEEL CORPORATION</b> PO BOX 889 EUGENE, OR 97440		<b>JOB/REQ. NO.</b> 207	<b>DATE</b> 04/28/2011	<b>PAGE</b> 1			
<b>ISO 9001</b> REGISTERED TO US PATENT & TRADEMARK OFFICE				<b>FARVEST STEEL CORPORATION</b> PO BOX 889 EUGENE, OR 97440 USA				<b>FARVEST STEEL CORPORATION</b> PO BOX 889 EUGENE, OR 97440		<b>SHIPPING NO.</b> 1153787	<b>DATE</b> 04/28/2011	<b>PAGE</b> 1			
<b>ISO 9001</b> REGISTERED TO US PATENT & TRADEMARK OFFICE				<b>FARVEST STEEL CORPORATION</b> PO BOX 889 EUGENE, OR 97440 USA				<b>FARVEST STEEL CORPORATION</b> PO BOX 889 EUGENE, OR 97440		<b>CARRIER</b> FARWEST (OWN)	<b>DATE</b> 04/28/2011	<b>PAGE</b> 1			
<b>ISO 9001</b> REGISTERED TO US PATENT & TRADEMARK OFFICE				<b>FARVEST STEEL CORPORATION</b> PO BOX 889 EUGENE, OR 97440 USA				<b>FARVEST STEEL CORPORATION</b> PO BOX 889 EUGENE, OR 97440		<b>CAR/TRUCK NO.</b> 207	<b>DATE</b> 04/28/2011	<b>PAGE</b> 1			
<b>PHYSICAL PROPERTIES</b>															
ITEM	DESCRIPTION	HEAT NO.	SLAB	YIELD PSI X 100	TENSILE PSI X 100	% ELONG 8" 2"	% RA	HARDNESS BRIN TEST	IMPACTS						
WE HEREBY CERTIFY THAT THE MATERIAL DESCRIBED HEREIN HAS BEEN MANUFACTURED TO THE APPLICABLE SPECIFICATION AND TESTED IN ACCORDANCE WITH THE REQUIREMENTS OF THE AMERICAN BUREAU OF SHIPPING RULES WITH SATISFACTORY RESULTS.															
1	0.3125 X 96.000NE X 480.000														
	1 PC 4084 LBS	NW0846		418	600 29										
				451	615 34										
	5 PCS 20420 LBS	NW0847		442	600 34										
				472	625 34										
2	0.5000 X 96.000NE X 480.000														
	1 PC 6534 LBS	NW0852		441	620 39										
<b>CHEMICAL ANALYSIS</b>															
HEAT NO.	C	Mn	P	S	Si	Cu	Ni	V	Ch	Mo	Ti	B	N	Ca	CE
NW0846	.08	1.07	.012	.011	.23	.01	.05	.004	.005	.039	.03	.00			
NW0847	.08	1.12	.013	.011	.26	.01	.05	.007	.005	.039	.03	.00			
NW0852	.07	1.07	.010	.009	.28	.02	.05	.004	.005	.038	.02	.00			
HEATS INDICATED WITH (+) WERE MELTED & MANUFACTURED IN THE USA. HEATS INDICATED WITH (+) WERE ROLLED IN THE USA.															
Signature: <i>[Handwritten Signature]</i>															

Figure C.9 : Material testing certifications Steel 1 (continued)

REPORT OF CHEMICAL/PHYSICAL TESTS						CERTIFICATE NO.	DATE	PAGE
						1153787	Apr 28, 2011	2
						MILL ORDER NO.	DATE	
						243142		
						CUSTOMER ORDER NO.		
						101-8608		
						JOB REQ. NO.		
						SHIPPING NO.	DATE	
						1153787	04/28/2011	
						CARRIER	FARWEST (OWN)	
						CART/TRUCK NO.	207	
<b>PHYSICAL PROPERTIES</b>								
HEAT NO.	C	Mn	P	S	Si	Cu	Ni	V
CHEMICAL ANALYSIS								
TENSILE % ELONG HARDNESS BEND IMPACTS YIELD TENSILE PSI X 100 8" 2" % FA BHIN TEST								
WE HEREBY CERTIFY THAT THE MATERIAL DESCRIBED HEREIN HAS BEEN MANUFACTURED TO THE APPLICABLE SPECIFICATION AND TESTED IN ACCORDANCE WITH THE REQUIREMENTS OF THE AMERICAN BUREAU OF SHIPPING RULES WITH SATISFACTORY RESULTS.								
7 PCS 31038 LBS TOTALS								
THIS MATERIAL HAS BEEN MANUFACTURED, TESTED AND FOUND TO MEET THE SPECIFICATIONS AND PURCHASE ORDER REQUIREMENTS CARBON STRUCTURAL QUALITY PLATE ASTM A36-08/ASME SA36 2007/09 ADD. ASS GRADE A.								
FARWEST STEEL CORPORATION PO BOX 889 EUGENE, OR 97440 USA								
FARWEST STEEL CORPORATION PO BOX 889 EUGENE, OR 97440								
ISO 9001 REGISTERED U.S. PATENT PENDING								
EVRAZ INC. NA Evraz Oregon Steel 14400 N. Rivergate Blvd., Portland, Oregon 97203								
END OF REPORT								
CE								

Figure C.10 : Material testing certifications Steel 1 (continued)

02/22/2011 TUE 5:33 FAX --- Imaging

002/004

HB3860 CT2164

**ThyssenKrupp Steel USA**1 ThyssenKrupp Drive  
Calvert, AL 36513**Mill Certificate**

CUSTOMER ORIGINAL

Order Number 923	Certificate Number 1100314980	Delivery Item 80008511-20	Ship Date 01/13/2011	Page Number 1 of 1
<b>Contact - Customer Service Company</b> ThyssenKrupp Steel USA PO Box 456 CALVERT AL 36513 USA		Customer Number: 10822  <b>Customer Sold-to:</b> ThyssenKrupp Steel Services Trading 13338 Orden Dr SANTA FE SPRINGS CA 90670 USA	PO: 1736574  <b>Customer Ship-to:</b> ThyssenKrupp Steel Services Trading UP teamtrack 735 Yard #9 local train YST-09 STOCKTON CA 95206 USA	
<b>Product/Description/Specification</b>  Hot Roll Black SS GRADE 36 [250] TYPE 2 / 0.3640 " X 60.0000 "			<b>Customer Part Number</b>  Material Testing Standard ASTM A1018	

<b>Heat Number</b>	014324	<b>Pieces</b>		<b>Net Weight</b>	Gross Weight
<b>Coil Number</b>	1100314980	01		24.296 TON	24.296 TON

**Chemistry**

C	Si	Mn	S	AL	B	Cr
0.191 %	0.012 %	0.790 %	0.0070 %	0.035 %	0.0002 %	0.034 %
Cu	Mo	N	Nb	Ni	Ti	V
0.019 %	0.005 %	0.0047 %	0.001 %	0.020 %	0.001 %	0.001 %
Sn	As	H				
0.002 %	0.002 %	3.600 %				

**Tensile Test**

<b>Tensile Strength</b>	<b>Lower Yield Strength</b>	<b>Total Elongation</b>
71 ksi	42 ksi	29.5 %

"ThyssenKrupp Steel USA, LLC certify that the material herein described has been manufactured, sampled, tested and inspected in accordance with the contract requirements and is fully in compliance"

Figure C.11 : Material certifications Steel 2

**NUCOR**  
P.O. Box 279  
Winton, NC 27796  
(252) 356-3700

**PLATE MILL**

**Mill Test Report**  
Page 3

**NUCOR**  
It's our Nature.

Issuing Date : 03/23/2011  
Vehicle No : PTXX 137237  
Specification : 1,000" x 96,000" x 480,000"  
ASTM A36-06/ABS Grade A/ASME SA36-03a/ASTM A709 Grade 36-10

Lead No. : 288882  
Sold To : CHAPEL STEEL CO  
P.O. Box 1008  
FAIRF 215-793-8415  
SPRINGHOUSE, PA 19477

Our Order No. : 897853  
Ship To : CHAPEL STEEL CO  
c/o GREEN TRANSFER SPURS 215503  
RAIL DESTINATION: EAST ST. JOHN,  
OR  
EAST ST. JOHN'S, OR 97283

Part No. : 242276

Doc No. : 242276

Heat No : 1502162

Plate Serial No : 1502162-03

Chemical Analysis

Heat No	C	Mn	P	S	Si	Cu	Ni	Cr	Mo	Al	V	Nb	TI	N	Ca	B	Sn	CEQ	PCM
1502162	0.18	0.85	0.011	0.000	0.19	0.25	0.08	0.07	0.02	0.027	0.004	0.001	0.002	0.0013	0.0002	0.011	0.38	0.24	

Mechanical Properties

Plate Serial No	Place	Tensile	Yield	Elongation	Reduction of Area	Charpy	Temp
1502162-03	3	13,600	43,500	23.8	26.9	23.8	Min
							Avg

Marking :

Charpy Impacts

Dir.	1	2	3	Avg	Temp
Charpy	23.8	26.9			

Manufactured in fully killed five grain practice by Electric Arc Furnace. Welding or weld repair was not performed on this material. We hereby certify that the contents of this report are accurate and correct. All test results and operations performed by the material manufacturer are in compliance with the applicable specifications, including customer specifications.

Yield by U.S.E.L. method unless otherwise specified. Ceq = C(Mn/16) + (Cr+Mo+V/5) + (Cu+Ni/15)  
Form = 0.0001(Mn/20) + 0.0001(Cu/20) + 0.0001(Mo/10) + 0.0001(Ni/10) + 0.0001(V/10) + 0.0001

Inspected 8/24/11 by 1470brec

04/03/2011 10:05:33 AM

Figure C.12 : Material testing certifications Steel 2



POR-000000-060

PART NO.

Align



# Mill Test Report

Page 1

P.O. Box 279  
Winston, NC 27946  
(252) 356-3700

Issuing Date : 03/23/2011  
Vehicle No : PTX 137237  
Specification : 0.7500" x 96.000" x 480.000"  
ASTM A36-08/ABS Grade A/ASME SA36-03/ASTM A709 Grade 36-10

Load No. : 288682

Sold To : CHAPEL STEEL CO  
P.O. Box 1000  
FAX# 216-793-9415  
SPRINGHOUSE, PA 19477

Our Order No. : 895972

Ship To : CHAPEL STEEL CO  
c/o GREEN TRANSFER, SPUR# 215503  
RAIL DESTINATION: EAST ST. JOHN,  
OR  
EAST ST. JOHN'S, OR 97283

Cust. Order No. : POR-3074

Marking :

Heat No	C	Mn	P	S	Si	Cu	Ni	Cr	Mo	Albnd	V	Nb	Ti	N	Ca	B	Sn	CEQ	PCM
1502161	0.16	0.84	0.010	0.001	0.14	0.25	0.08	0.08	0.02	0.028	0.005	0.001	0.001	0.0013	0.0002	0.012	0.36	0.23	
Plate Serial No	Tensile Test										Charpy Impacts								
	Pieces	Tons	Dir.	Yield	Tensile	Elongation % in 2"	Elongation % in 8"	Dir.	1	2	3	shear	shear	shear	Ave.	CS	Size	Temp	Ave.
1502161-07	5	24.50	T	41,200	70,400	26.6	25.4												
				39,800	68,200														

Manufactured to fully killed fine grain practice by Electric Arc furnace. Welding or weld repair was not performed on this material. Mercury has not been used in the direct manufacturing of this material. Produced as continuous cast discrete slabs as rolled, unless otherwise noted in Specification.  
Yield by 0.002 inch offset method unless otherwise specified. Ceq = C+Mn/6+(Cr+Mo)/5+(Cu+Ni)/15  
Form = CH2009-1(W209)(C409)(V409)(S409) (ASTM A36-08/ABS Grade A/ASME SA36-03/ASTM A709 Grade 36-10)  
Form = CH2009-1(W209)(C409)(V409)(S409) (ASTM A36-08/ABS Grade A/ASME SA36-03/ASTM A709 Grade 36-10)  
DIN 50940 3.1 (EN 10204 3.1B) (2006) compliant. For ABS grades only. Quality Assurance certificate CH-MMPQA-448

We hereby certify that the contents of this report are accurate and correct. All test results and operating procedures used by the material manufacturer are in compliance with the applicable specifications, including customer specifications.

T. A. Dignato  
T. A. Dignato, Metallurgist

04/08/2011 10:53:33 AM

Doc No. 242274 Indexed 8 April 10 147nbhroc

Figure C.13 : Material testing certifications Steel 2 (continued)

fax server 5/2/2011 4:11:59 PM PAGE 1/001 Fax Server

Certification provided by PFC, To: VANCOUVER BOLT Order: 198408

**Jinn Her Enterprise Co., Ltd.**  
 No. 197, GIMALLI ST, KANGSHAN, 320 KACHSHUNG, TAINAN P.R.C.  
 TEL: +886 (07) 622 8801 FAX: +886 (07) 622 7555 +886 (07) 622 7553

**CERTIFICATE OF INSPECTION**

1/1

CUSTOMER NAME : PORTEOUS FASTENER CO.  
 CUSTOMER'S ADDRESS : 1040 WATSON CENTER RD.  
 CARSON, CA. 90745  
 U.S.A.  
 ORDER NUMBER : 10082501  
 PART NUMBER : 00152-3440-024  
 DESCRIPTION : ASTM A325 STRUCTURE BOLT TY. 1, I.D MARK "A325" & "JH"  
 SIZE : 7/8-9X4 NC  
 FINISH : H.T. HOT DIP GAL  
 QUANTITY : 715.0  
 BOLT MFR. : JINN HER ENTERPRISE CO., LTD.  
 NUT MFR. :  
 WASHER MFR. :  
 REPORT NO : JH10121601004  
 REPORT DATE : 2010/12/28  
 BOLT LOT NO : B926514G 1  
 BOLT MATERIAL : 10H35  
 BOLT HEAT NO : 2B11  
 NUT LOT NO :  
 NUT MATERIAL :  
 NUT HEAT NO :  
 WASHER LOT NO :  
 WASHER MATERIAL :  
 WASHER HEAT NO :  
 ASSEMBLY LOT NO :  
 BOLT MFR. DATE : 2009/10/26  
 NUT MFR. DATE :  
 WASHER MFR. DATE :

BOLT DIMENSIONAL INSPECTION			INSPECTION : 2010/01/22			SAMPLING STANDARD : ASTM B18.18.2M		
CHARACTERISTIC	TEST METHOD	STANDARD	UNIT	TEST VALUE	SAMPLE	ACC	REJ	
WIDTH ACROSS CORNERS	JIS B1071	40.37-42.16	mm	40.60-40.86	8	8	0	
WIDTH ACROSS FLATS	JIS B1071	35.41-36.52	mm	35.64-35.74	8	8	0	
HEIGHT	JIS B1071	13.49-14.30	mm	13.96-14.11	8	8	0	
BODY DIA.	JIS B1071	21.64-22.73	mm	22.16-22.23	8	8	0	
BODY LENGTH	JIS B1071	MIN 56.39	mm	57.49-58.09	8	8	0	
GRIP LENGTH	JIS B1071	MAX 63.50	mm	60.91-61.59	8	8	0	
LENGTH	JIS B1071	96.78-101.60	mm	99.17-99.72	8	8	0	
THREAD	ASME B1.3M	NONE	N/A	PASS	8	8	0	

BOLT MECHANICAL INSPECTION			INSPECTION : 2009/10/30			SAMPLING STANDARD : ASTM F1470		
CHARACTERISTIC	TEST METHOD	STANDARD	UNIT	TEST VALUE	SAMPLE	ACC	REJ	
CORE HARDNESS	ASTM A325	25.0-34.0	HRC	30-31	4	4	0	
TENSILE STRENGTH	ASTM A325	MIN 120.0	ksi	141-142	3	3	0	
PROOF LOAD	ASTM A325	MIN 85.0	ksi	PASS	3	3	0	

BOLT FINISH INSPECTION			INSPECTION : 2010/01/22			SAMPLING STANDARD : ASTM F1470		
CHARACTERISTIC	TEST METHOD	STANDARD	UNIT	TEST VALUE	SAMPLE	ACC	REJ	
THICKNESS OF COATING	ASTM F2329	MIN 51.0	um	57-60	15	15	0	
ADHESION TEST	ASTM F2329	NONE	N/A	PASS	3	3	0	

BOLT APPEARANCE INSPECTION			INSPECTION : 2010/01/22			SAMPLING STANDARD : ASTM F1470		
CHARACTERISTIC	TEST METHOD	STANDARD	UNIT	TEST VALUE	SAMPLE	ACC	REJ	
PRESENCE FINISH	ASTM F2329	NONE	N/A	PASS	15	15	0	

BOLT APPEARANCE INSPECTION			INSPECTION : 2010/01/22			SAMPLING STANDARD : ASME B18.18.2M		
CHARACTERISTIC	TEST METHOD	STANDARD	UNIT	TEST VALUE	SAMPLE	ACC	REJ	
GENERAL WORKMANSHIP	VISION	NONE	N/A	PASS	8	8	0	

CHEMICAL ANALYSIS %  
 HEAT NO C-x100 MN-x100 P-x1000 S-x1000 SI-x100 CU-x100 NI-x100 CR-x100 MO-x100 AL-x1000 B-x10000 V-x100  
 2B11 35 76 13 5 20 22 13

\* Heads of steel, having the elements listed in section 5.4 of ASTM A325, intentionally added, were not used to produce the bolts.



#### BOLT MARKING

- Remark : 1. Lab is accredited according to ISO/IEC 17025 requirements. This certificate is valid with signature of Yi-Sung Chen.  
 2. This test certificate is responsible for designated samples only. This test certificate only relates to the items listed and tested, it's not allowed to be partially used.  
 3. The above composition is quoted from original mill certs which is not in the scope of Lab Accreditation.  
 4. This test certificate is in accordance with EN 10204 type 3.1.  
 5. Unless specified by the customer, the latest version of the testing specs was used.  
 6. Quality System conforms to ISO 9001 requirements and certified by TLV.

*Yi-Sung Chen*

Figure C.14 : Certificate of inspection for the bolts

Fax Server

2/14/2011 6:21:11 AM PAGE 1/001 Fax Server

Certification provided by PFC, To: VANCOUVER BOLT Order:196465


**Jinn Her** Enterprise Co., Ltd.

 NO. 197, SHIN-LI ST, KANGSHAN, 320 KAOHSIUNG, TAIWAN R.O.C.  
 TEL: +886 (07) 622 9801 FAX: +886 (07) 622 9755 +886 (07) 621 1063

**CERTIFICATE OF INSPECTION**

1/1

CUSTOMER NAME : PORTEOUS FASTENER CO.  
 CUSTOMER'S ADDRESS : 1040 WATSON CENTER RD.  
 CARSON, CA. 90745  
 U. S. A.  
 ORDER NUMBER : 19082013  
 PART NUMBER : 00152-3430-024  
 DESCRIPTION : ASTM A325 STRUCTURE BOLT TY. 1, I.D. MARK "A325" & "JH"  
 SIZE : 7/8-9X3 NC  
 FINISH : H.T. HOT DIP GAL.  
 QUANTITY : 1530.0  
 BOLT MFR. : JINN HER ENTERPRISE CO., LTD.  
 NUT MFR. :  
 WASHER MFR. :

REPORT NO. : JH09112503010  
 REPORT DATE : 2009/12/15  
 BOLT LOT NO. : BBA1286G 1  
 BOLT MATERIAL : 10B53  
 BOLT HEAT NO : 2B107  
 NUT LOT NO :  
 NUT MATERIAL :  
 NUT HEAT NO :  
 WASHER LOT NO :  
 WASHER MATERIAL :  
 WASHER HEAT NO :  
 ASSEMBLY LOT NO :  
 BOLT MFR. DATE : 2009/10/28  
 NUT MFR. DATE :  
 WASHER MFR. DATE :

BOLT DIMENSIONAL INSPECTION				INSPECTION : 2009/11/09			
SPECIFICATION : ASME B18.2M-2006				SAMPLING STANDARD : ASME B18.2M-1987			
CHARACTERISTIC	TEST METHOD	STANDARD	UNIT	TEST VALUE	SAMPLE	ACC	REJ
WIDTH ACROSS CORNERS	JIS B1071:1985	40.37-42.16	mm	40.82-41.00	4	4	0
WIDTH ACROSS FLATS	JIS B1071:1985	35.41-36.52	mm	35.74-35.90	4	4	0
HEIGHT	JIS B1071:1985	13.49-14.30	mm	13.87-13.89	4	4	0
BODY DIA.	JIS B1071:1985	21.64-22.73	mm	22.14-22.17	4	4	0
BODY LENGTH	JIS B1071:1985	MIN 30.99	mm	32.46-32.77	4	4	0
GRIP LENGTH	JIS B1071:1985	MAX 38.10	mm	35.15-35.58	4	4	0
LENGTH	JIS B1071:1985	71.38-76.20	mm	74.11-74.45	4	4	0
THREAD	ASME B1.3M-1992	NONE	N/A	PASS	4	4	0
BOLT MECHANICAL INSPECTION				INSPECTION : 2009/10/01			
SPECIFICATION : ASTM A325-07a				SAMPLING STANDARD : ASTM F1470-02			
CHARACTERISTIC	TEST METHOD	STANDARD	UNIT	TEST VALUE	SAMPLE	ACC	REJ
CORE HARDNESS	ASTM A325-07a	25.0-34.0	HRC	30-31	3	3	0
TENSILE STRENGTH	ASTM A325-07a	MIN 1200	ksi	139-141	2	2	0
PROOF LOAD	ASTM A325-07a	MIN 85.0	ksi	PASS	2	2	0
BOLT FINISH INSPECTION				INSPECTION : 2009/11/09			
SPECIFICATION : ASTM F2329-05				SAMPLING STANDARD : ASTM F1470-02			
CHARACTERISTIC	TEST METHOD	STANDARD	UNIT	TEST VALUE	SAMPLE	ACC	REJ
THICKNESS OF COATING	ASTM F2329-05	MIN 51.0	um	57-60	13	13	0
ADHESION TEST	ASTM F2329-05	NONE	N/A	PASS	2	2	0
BOLT APPEARANCE INSPECTION				INSPECTION : 2009/11/09			
SPECIFICATION : ASTM F2329-05				SAMPLING STANDARD : ASTM F1470-02			
CHARACTERISTIC	TEST METHOD	STANDARD	UNIT	TEST VALUE	SAMPLE	ACC	REJ
FINISHANCE FINISH	ASTM F2329-05	NONE	N/A	PASS	13	13	0
BOLT APPEARANCE INSPECTION				INSPECTION : 2009/11/09			
SPECIFICATION : ASTM F2329-05				SAMPLING STANDARD : ASME B18.2M-1987			
CHARACTERISTIC	TEST METHOD	STANDARD	UNIT	TEST VALUE	SAMPLE	ACC	REJ
GENERAL WORKMANSHIP	VISION	NONE	N/A	PASS	4	4	0
CHEMICAL ANALYSIS							
HEAT NO	C-x100 MN-x100 P-x1000 S-x1000 SI-x100 CU-x100 NI-x100 CR-x100 MO-x100 AL-x1000 B-x10000 V-x100						
2BT07	36 81 16 7 20				36	21	

\* Holes of steel, having the elements listed in section 5.4 of ASTM A325, intentionally added, were not used to produce the bolts.


**BOLT MARKING**

Remark : 1. Lab is accredited according to ISO/IEC 17025 requirements. This certificate is valid with signature of Yi-Sung Chen.  
 2. Samples testing conform to the requirements of specification. This test report is responsible for designated samples only.  
 3. This test report only relates to the items listed and tested, it's not allowed to be partially used.  
 4. The above composition is quoted from original mill certs which is not in the scope of Lab Accreditation.  
 5. Quality System conforms to ISO 9001 requirements and certified by TUV with certificate no. 01 100 0435931.  
 6. All fasteners meet the requirements of the PQA and records of compliance are on file.

Figure C.15 : Certificate of inspection for the bolts (continued)

**APPENDIX D – FINITE ELEMENT MODE SHAPES**

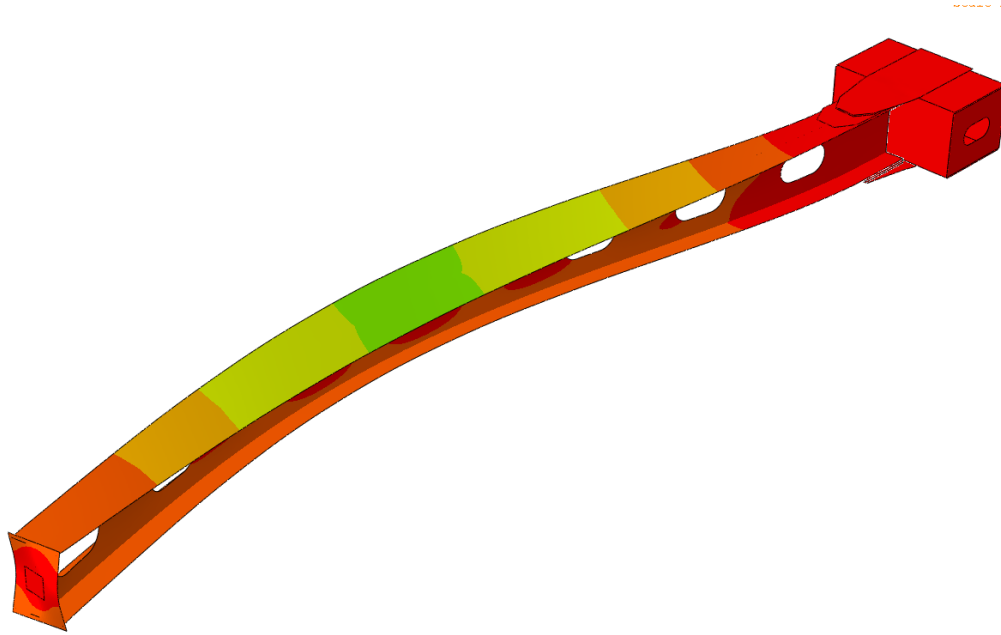


Figure D.1 : Laboratory vertical FEM mode shape 1

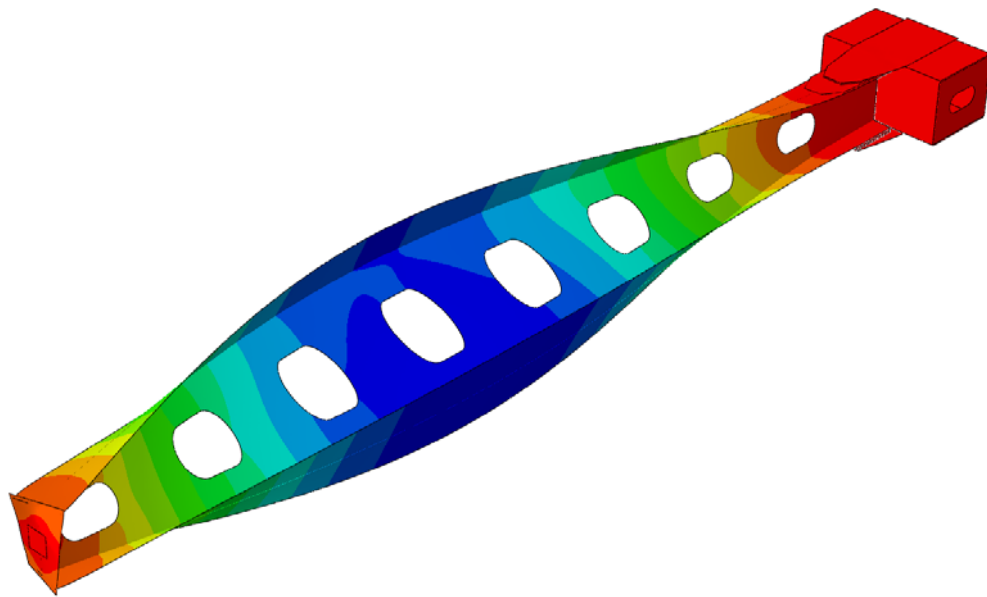


Figure D.2 : Laboratory vertical FEM mode shape 2

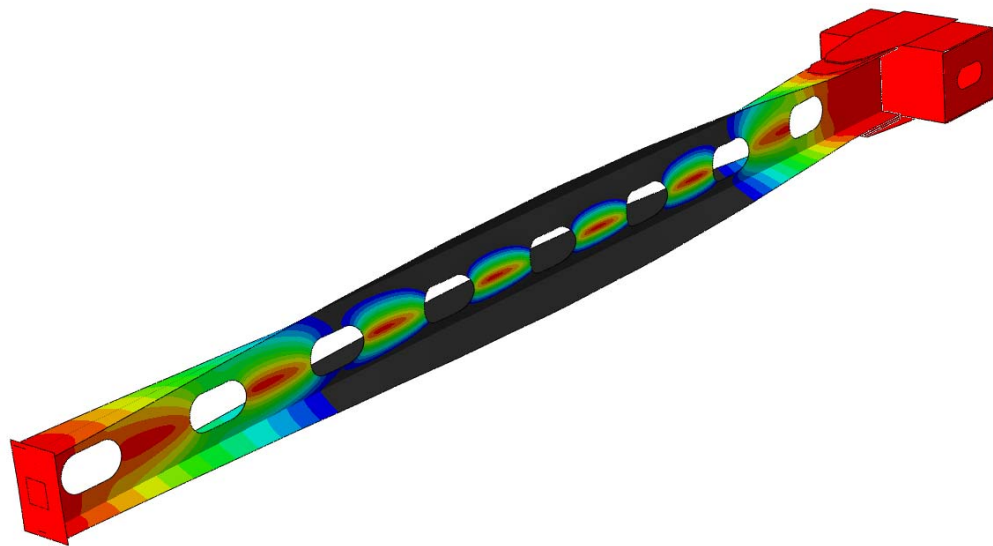


Figure D.3 : Laboratory vertical FEM mode shape 3

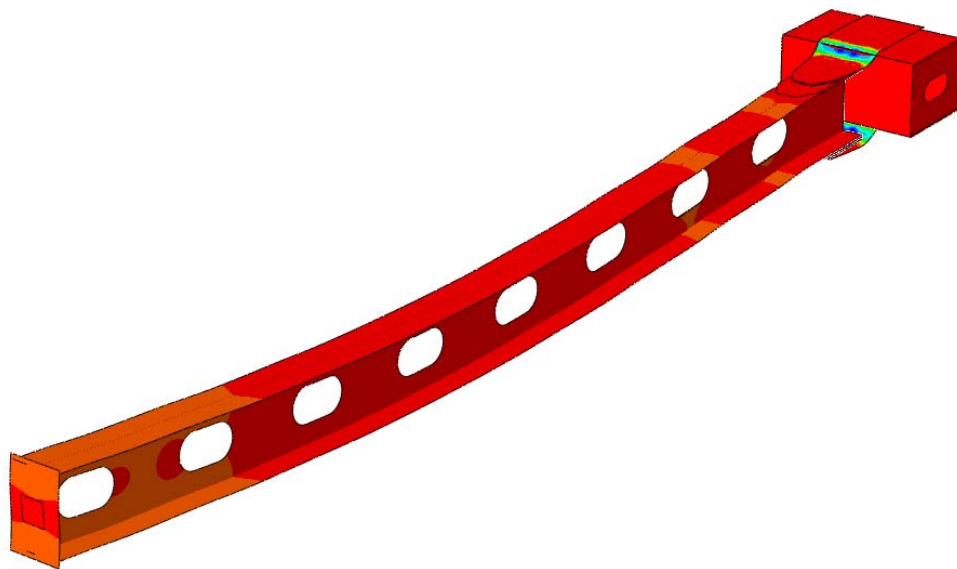


Figure D.4 : Laboratory vertical FEM mode shape 4

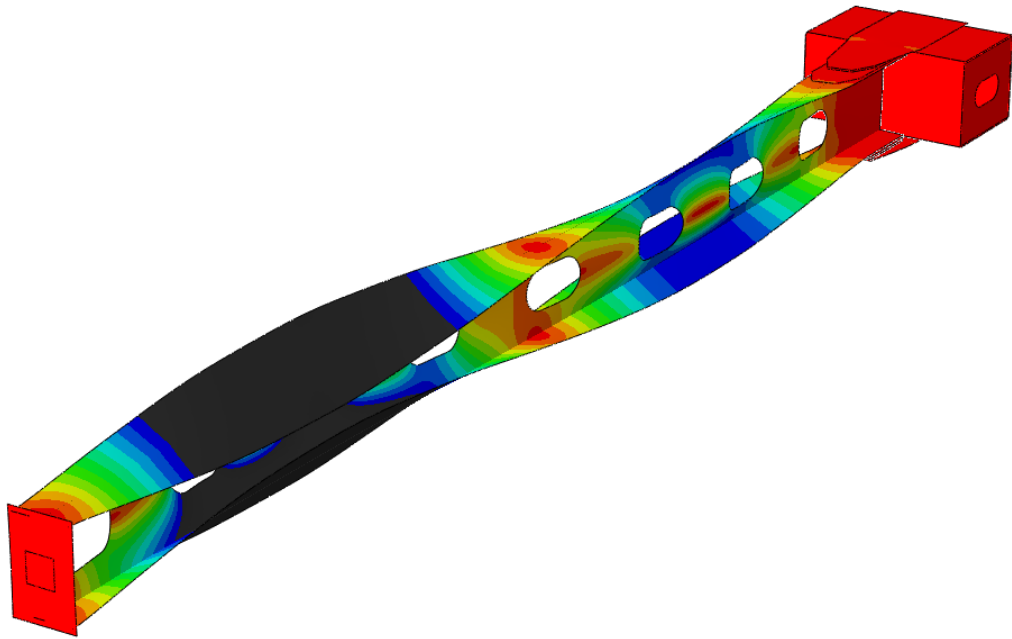


Figure D.5 : Laboratory vertical FEM mode shape 5

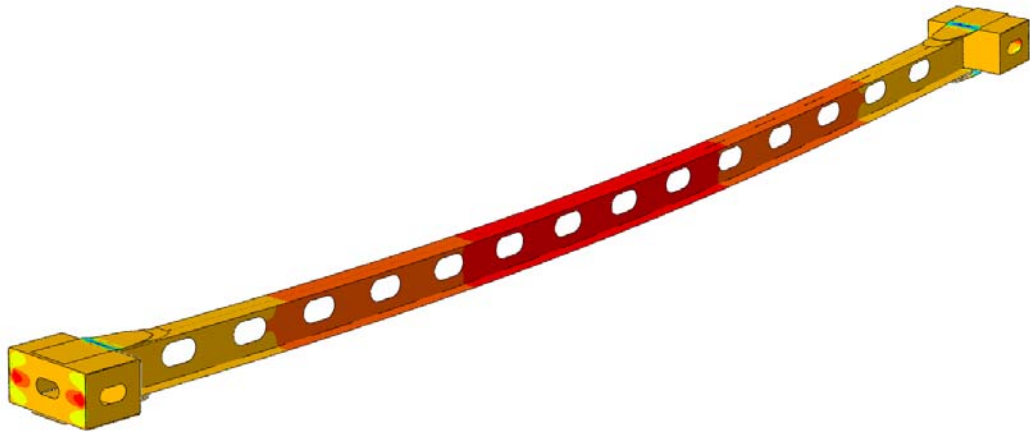


Figure D.6 : Bridge vertical (L13-M13) FEM mode shape 1

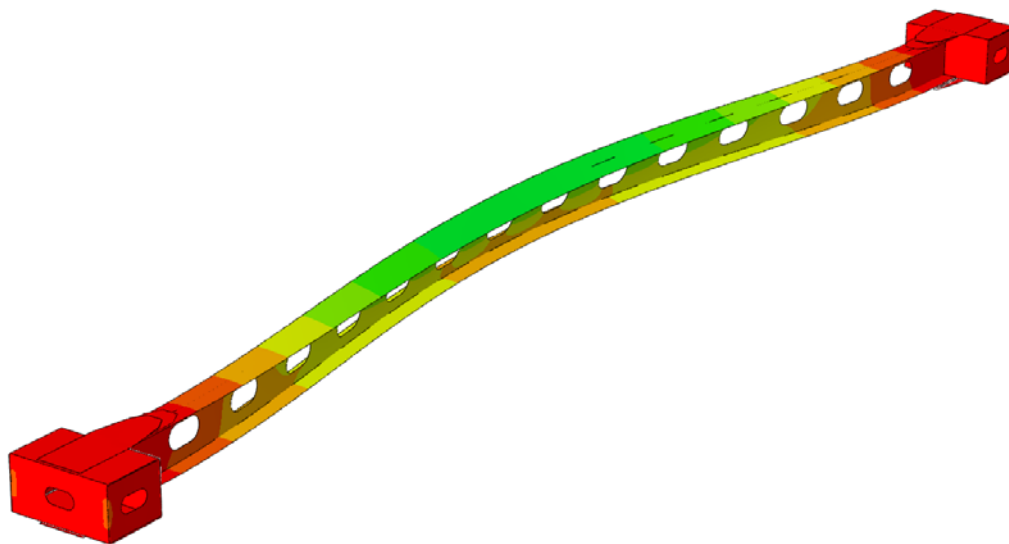


Figure D.7 : Bridge vertical (L13-M13) FEM mode shape 2

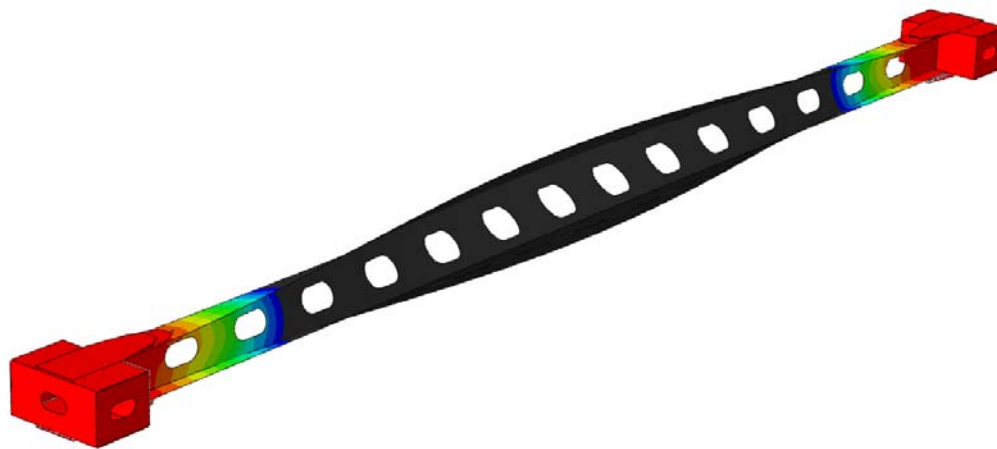


Figure D.8 : Bridge vertical (L13-M13) FEM mode shape 3



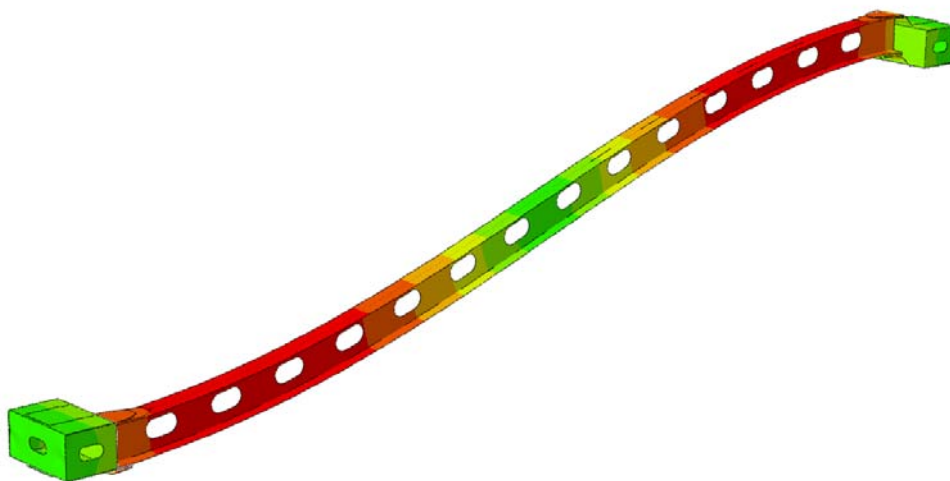


Figure D.9 : Bridge vertical (L13-M13) FEM mode shape 4

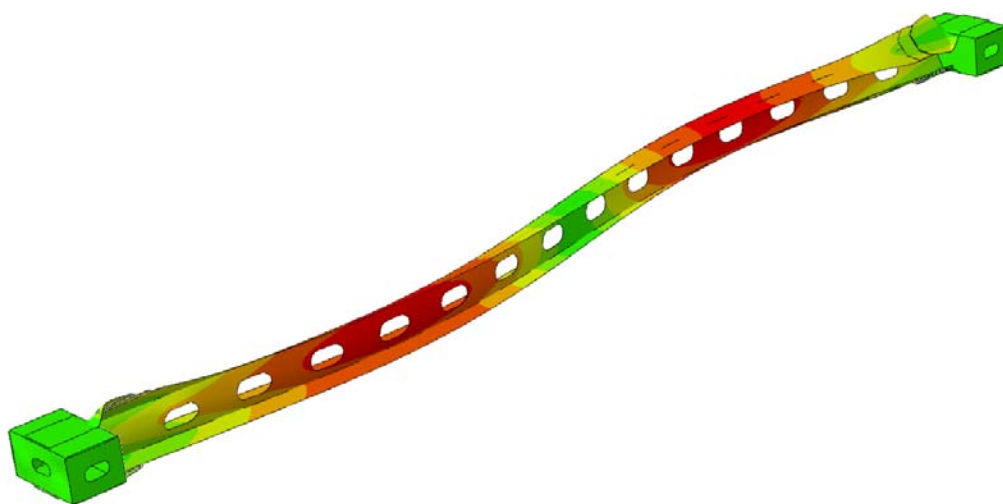


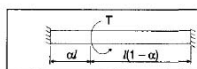
Figure D.10 : Bridge vertical (L13-M13) FEM mode shape 5

**APPENDIX E – SELECTED DESIGN EQUATIONS AND DESIGN  
CHARTS FROM THE AISC STEEL DESIGN GUIDE  
SERIES 9**

Case	$\theta$
6	<p><math>0 \leq z \leq \alpha l</math></p> $\theta = \frac{Ta}{(H+1)GJ} \left\{ H \times \left( \frac{1}{\sinh \frac{l}{a}} + \sinh \frac{\alpha l}{a} - \frac{\cosh \frac{\alpha l}{a}}{\tanh \frac{l}{a}} \right) + \left( \sinh \frac{\alpha l}{a} - \frac{\cosh \frac{\alpha l}{a}}{\tanh \frac{l}{a}} + \frac{1}{\tanh \frac{l}{a}} \right) \times \left[ \cosh \frac{z}{a} - 1.0 \right] - \sinh \frac{z}{a} + \frac{z}{a} \right\}$ <p><math>\alpha l \leq z \leq l</math></p> $\theta = \frac{Ta}{\left(1 + \frac{1}{H}\right)GJ} \left\{ \left[ \frac{\left( \cosh \frac{\alpha l}{a} - 1.0 \right)}{H \times \sinh \frac{l}{a}} + \frac{\left( \cosh \frac{\alpha l}{a} - \cosh \frac{l}{a} + \frac{l}{a} \times \sinh \frac{l}{a} \right)}{\sinh \frac{l}{a}} \right] + \right.$ $\left. \cosh \frac{z}{a} \left[ \frac{\left( 1.0 - \cosh \frac{\alpha l}{a} \right)}{H \times \tanh \frac{l}{a}} + \frac{\left( 1.0 - \cosh \frac{\alpha l}{a} \times \cosh \frac{l}{a} \right)}{\sinh \frac{l}{a}} \right] + \sinh \frac{z}{a} \left[ \frac{\left( \cosh \frac{\alpha l}{a} - 1.0 \right)}{H} + \cosh \frac{\alpha l}{a} \right] - \frac{z}{a} \right\}$ <p>where:</p> $H = \frac{\left[ \frac{\left( 1.0 - \cosh \frac{\alpha l}{a} \right)}{\tanh \frac{l}{a}} + \frac{\left( \cosh \frac{\alpha l}{a} - 1.0 \right)}{\sinh \frac{l}{a}} + \sinh \frac{\alpha l}{a} - \frac{\alpha l}{a} \right]}{\left[ \frac{\left( \cosh \frac{l}{a} + \cosh \frac{\alpha l}{a} \times \cosh \frac{l}{a} - \cosh \frac{\alpha l}{a} - 1.0 \right)}{\sinh \frac{l}{a}} + \frac{l}{a}(\alpha - 1.0) - \sinh \frac{\alpha l}{a} \right]}$

Figure E.1 : Equation for the rotation of Case 6 (AISC Steel Design Guide Series 9)

**Case 6**  $\theta \times \left( \frac{GJ}{T} \times \frac{1}{a} \right)$   
 $\alpha = 0.5$



Torsional End Restraints	
Left End	Right End
Fixed $\theta = \theta' = 0$	Fixed $\theta = \theta' = 0$

Concentrated torque at  
 $\alpha = 0.5$  on member with  
 fixed ends

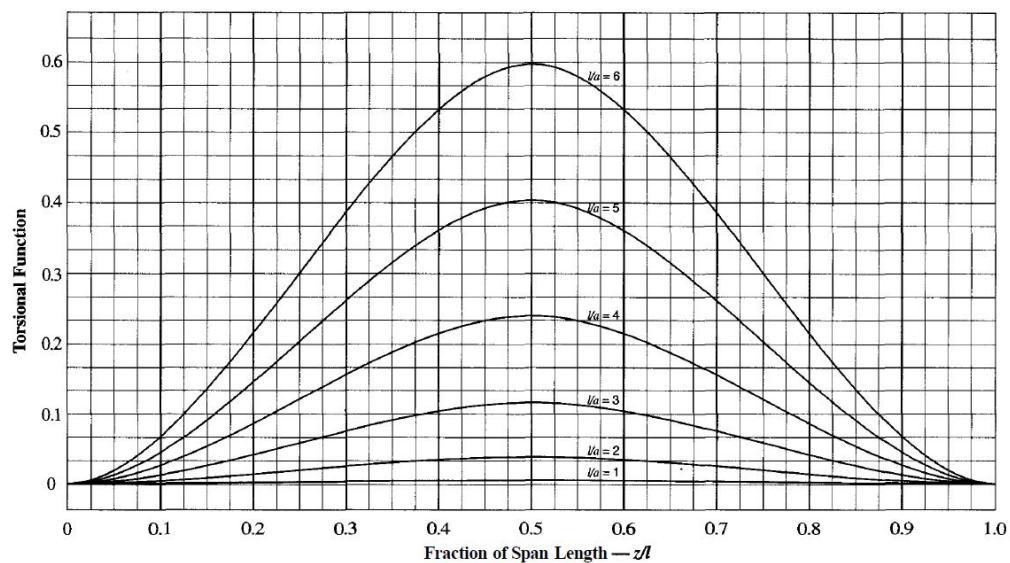
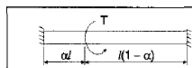


Figure E.2: Design chart for  $\theta$  Case 6 (AISC Steel Design Guide Series 9)

**Case 6**  $\theta' \times \left( \frac{GJ}{T} \right)$   
 $\alpha = 0.5$



Torsional End Restraints	
Left End	Right End
Fixed $\theta = \theta' = 0$	Fixed $\theta = \theta' = 0$

Concentrated torque at  
 $\alpha = 0.5$  on member with  
 fixed ends

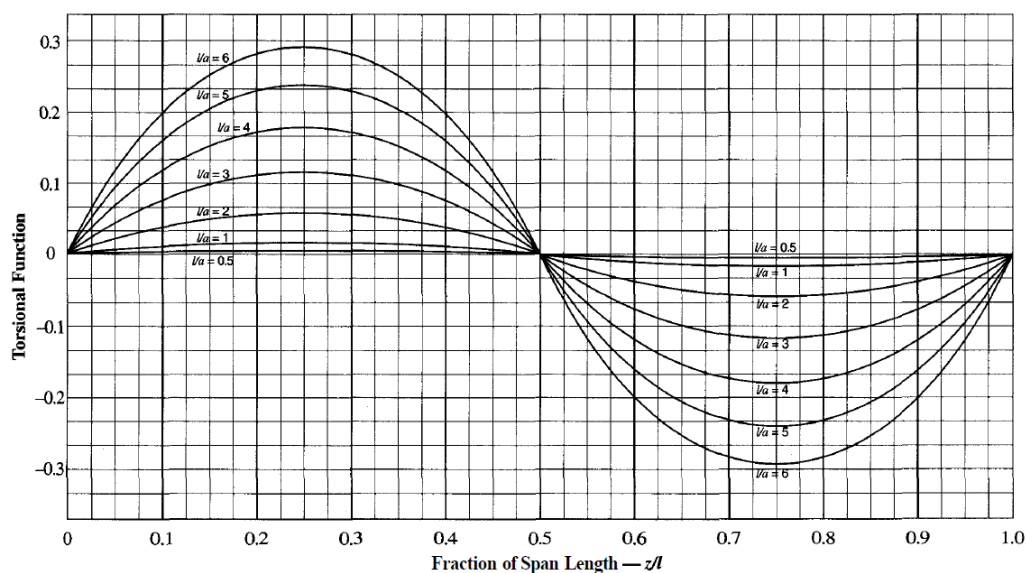
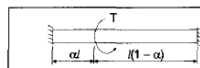


Figure E.3: Design chart for  $\theta'$  Case 6 (AISC Steel Design Guide Series 9)

**Case 6**  $\theta'' \times \left( \frac{GJ}{T} \times a \right)$   
 $\alpha = 0.5$



Torsional End Restraints			
Left End		Right End	
Fixed	$\theta = \theta' = 0$	Fixed	$\theta = \theta' = 0$

Concentrated torque at  $\alpha = 0.5$  on member with fixed ends

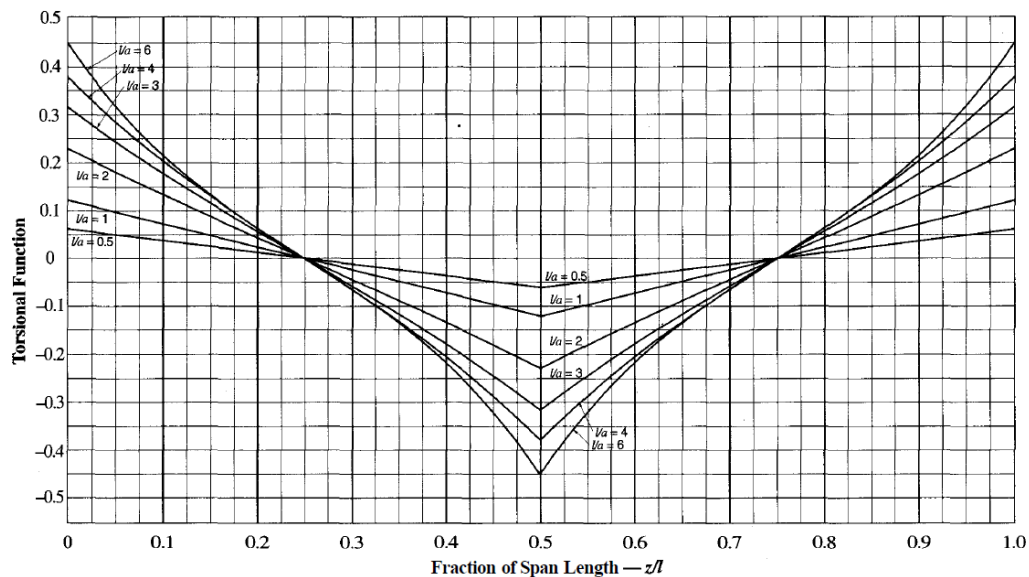
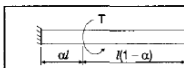


Figure E.4: Design chart for  $\theta''$  Case 6 (AISC Steel Design Guide Series 9)

**Case 6**  $\theta''' \times \left( \frac{GJ}{T} \times a^2 \right)$   
 $\alpha = 0.5$



Torsional End Restraints			
Left End		Right End	
Fixed	$\theta = \theta' = 0$	Fixed	$\theta = \theta' = 0$

Concentrated torque at  $\alpha = 0.5$  on member with fixed ends

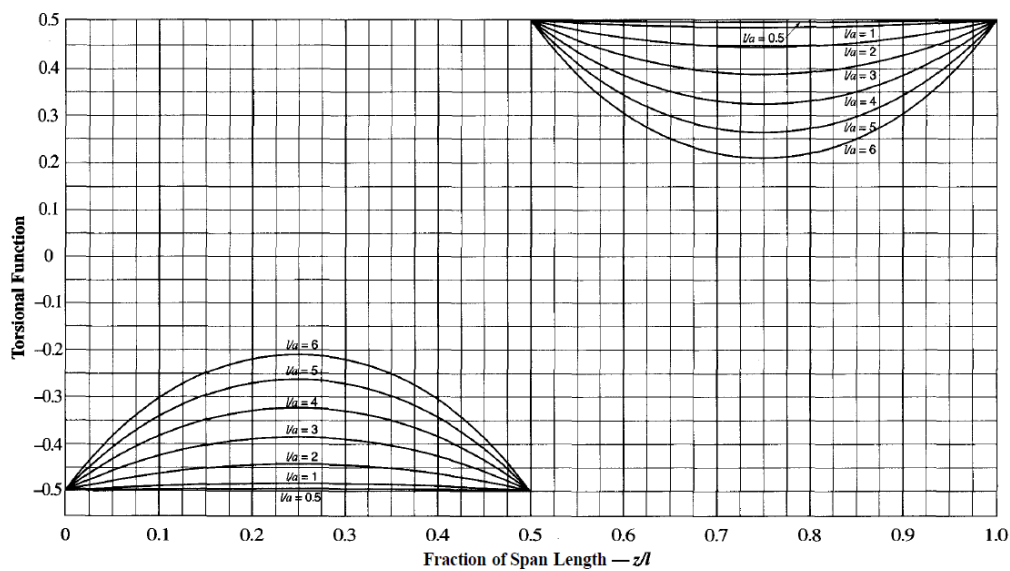
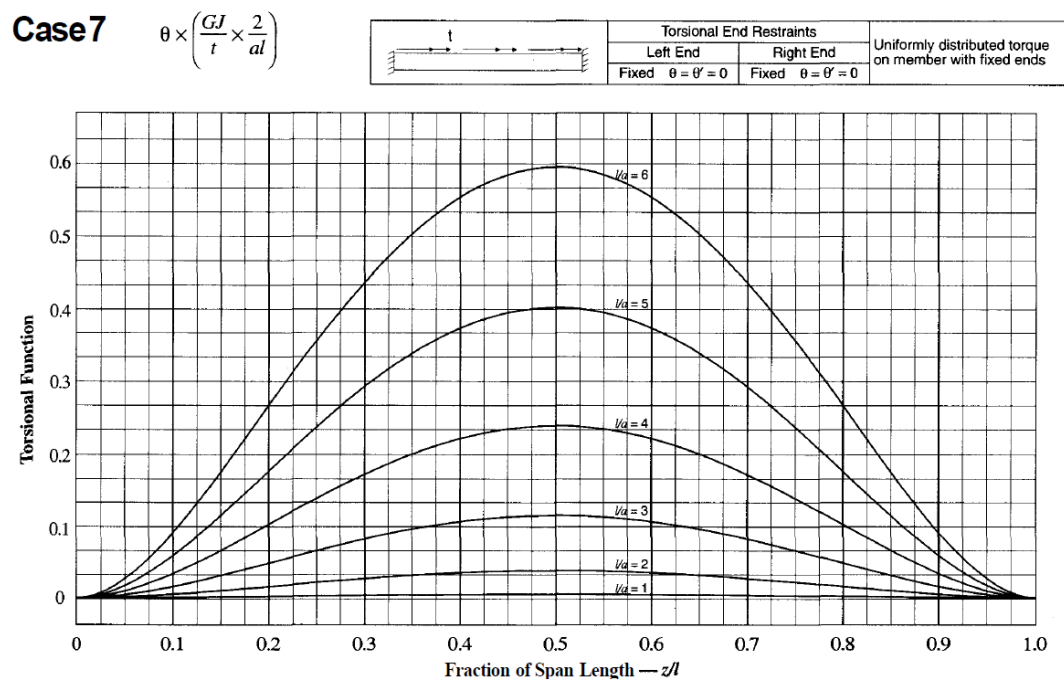


Figure E.5: Design chart for  $\theta'''$  Case 6 (AISC Steel Design Guide Series 9)

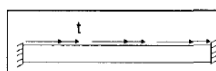
Case	$\theta$
7	$\theta = \frac{tla}{2GJ} \left[ \left( \frac{1 + \cosh \frac{l}{a}}{\sinh \frac{l}{a}} \right) \left( \cosh \frac{z}{a} - 1.0 \right) + \frac{z}{a} \left( 1 - \frac{z}{l} \right) - \sinh \frac{z}{a} \right]$

Figure E.6: Equation for the rotation of Case 7 (AISC Steel Design Guide Series 9)

Figure E.7: Design chart for  $\theta$  Case 7 (AISC Steel Design Guide Series 9)

**Case 7**

$$\theta' \times \left( \frac{GJ}{t} \times \frac{2}{l} \right)$$



Torsional End Restraints	
Left End	Right End
Fixed $\theta = \theta' = 0$	Fixed $\theta = \theta' = 0$

Uniformly distributed torque  
on member with fixed ends

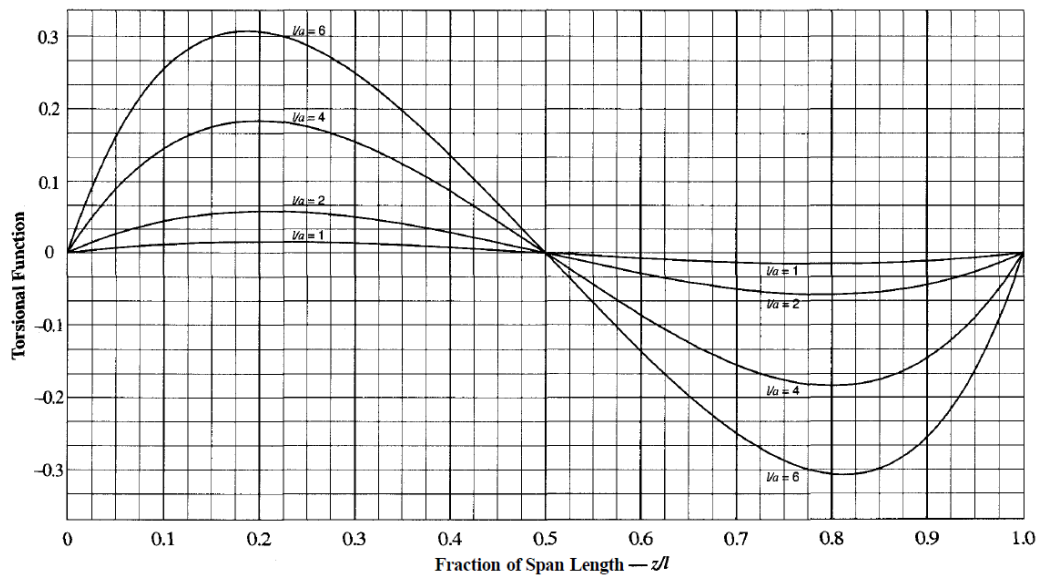
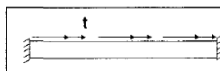


Figure E.8: Design chart for  $\theta'$  Case 7 (AISC Steel Design Guide Series 9)

**Case 7**

$$\theta'' \times \left( \frac{GJ}{t} \times \frac{2a}{l} \right)$$



Torsional End Restraints	
Left End	Right End
Fixed $\theta = \theta' = 0$	Fixed $\theta = \theta' = 0$

Uniformly distributed torque  
on member with fixed ends

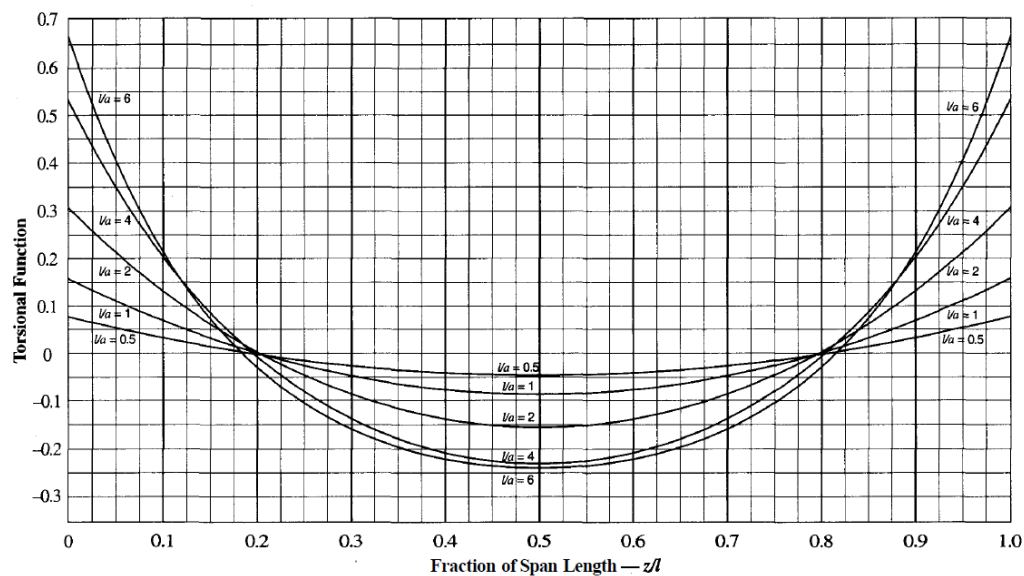


Figure E.9: Design chart for  $\theta''$  Case 7 (AISC Steel Design Guide Series 9)

**Case 7**  $\theta''' \times \left( \frac{GJ}{t} \times \frac{2a^2}{l} \right)$



Torsional End Restraints			
Left End		Right End	
Fixed	$\theta = \theta' = 0$	Fixed	$\theta = \theta' = 0$

Uniformly distributed torque on member with fixed ends

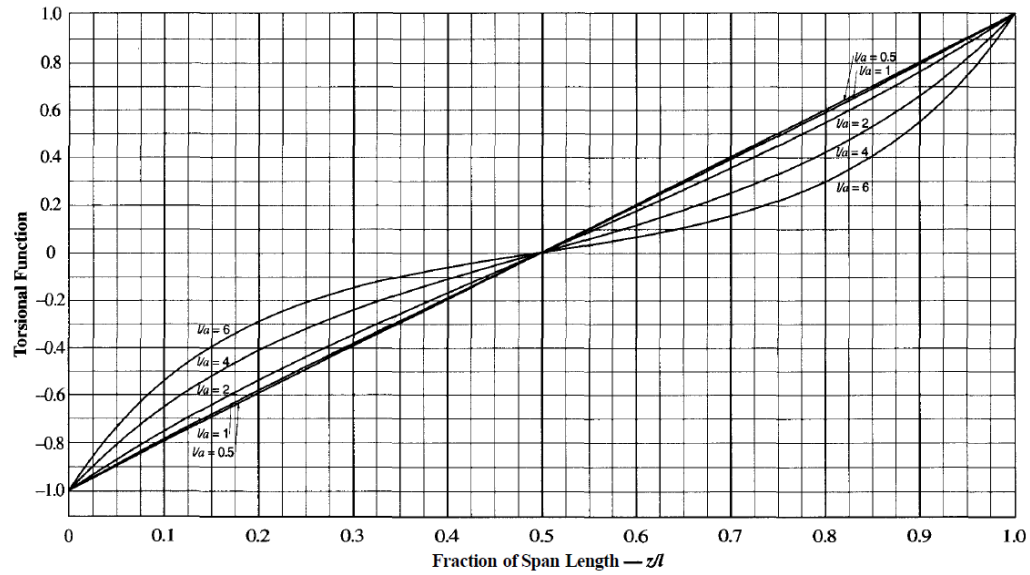
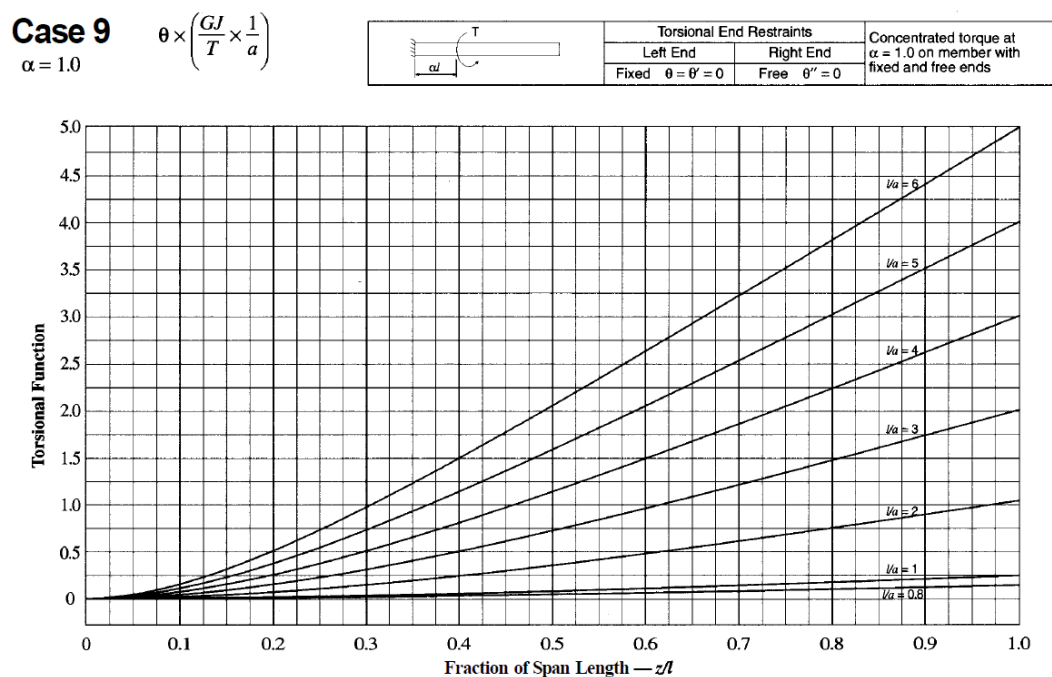


Figure E.10: Design chart for  $\theta'''$  Case 7 (AISC Steel Design Guide Series 9)

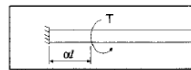


Case	$\theta$
9	$0 \leq z \leq \alpha l$ $\theta = \frac{Ta}{GJ} \left[ \left( \sinh \frac{\alpha l}{a} - \tanh \frac{l}{a} \times \cosh \frac{\alpha l}{a} + \tanh \frac{l}{a} \right) \left( \cosh \frac{z}{a} - 1.0 \right) - \sinh \frac{z}{a} + \frac{z}{a} \right]$ $\alpha l \leq z \leq l$ $\theta = \frac{Ta}{GJ} \left[ \left( \tanh \frac{l}{a} \times \cosh \frac{\alpha l}{a} - \tanh \frac{l}{a} - \sinh \frac{\alpha l}{a} \right) - \left( \cosh \frac{\alpha l}{a} - 1.0 \right) \left( \tanh \frac{l}{a} \times \cosh \frac{z}{a} \right) + \left( \cosh \frac{\alpha l}{a} - 1.0 \right) \times \sinh \frac{z}{a} + \frac{\alpha l}{a} \right]$

Figure E.11: Equation for the rotation of Case 9 (AISC Steel Design Guide Series 9)

Figure E.12: Design chart for  $\theta$  Case 9 (AISC Steel Design Guide Series 9)

**Case 9**  $\theta' \times \left( \frac{GJ}{T} \right)$   
 $\alpha = 1.0$



Torsional End Restraints		Concentrated torque at $\alpha = 1.0$ on member with fixed and free ends
Left End	Right End	
Fixed $\theta = \theta' = 0$	Free $\theta'' = 0$	

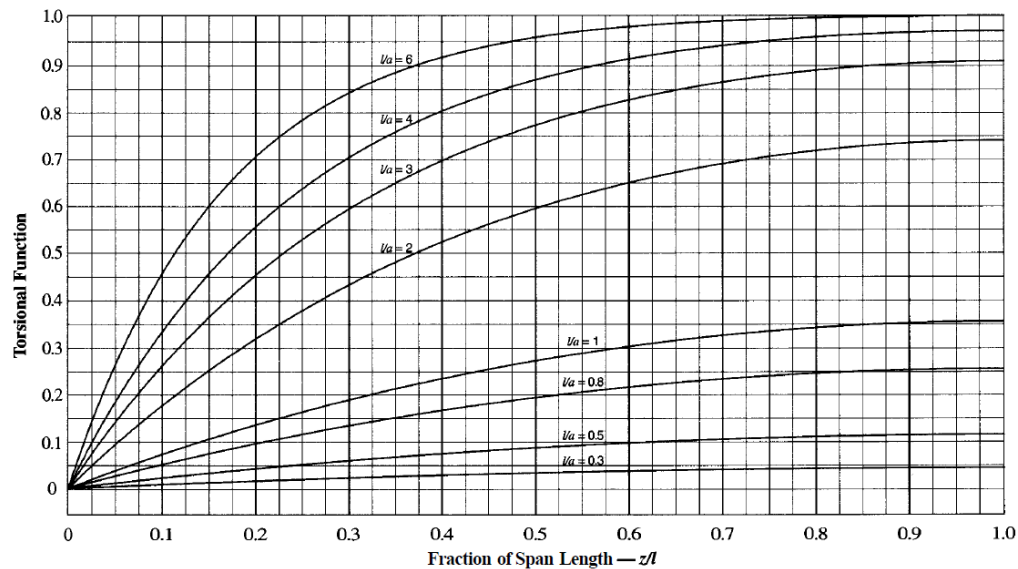
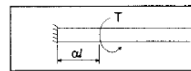


Figure E.13: Design chart for  $\theta'$  Case 9 (AISC Steel Design Guide Series 9)

**Case 9**  $\theta'' \times \left( \frac{GJ}{T} \times 5a \right)$   
 $\alpha = 1.0$



Torsional End Restraints		Concentrated torque at $\alpha = 1.0$ on member with fixed and free ends
Left End	Right End	
Fixed $\theta = \theta' = 0$	Free $\theta'' = 0$	

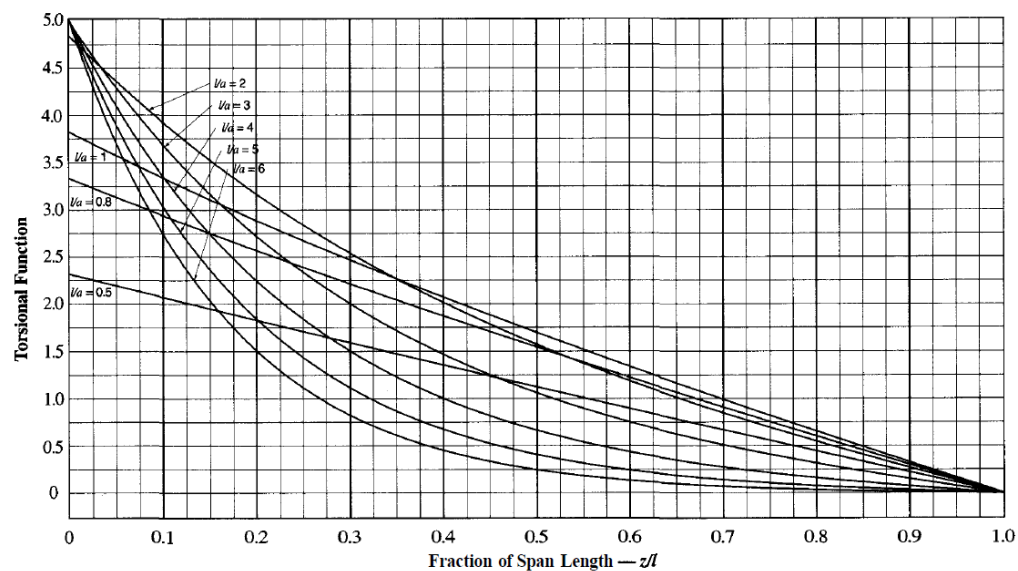
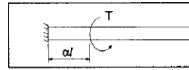


Figure E.14: Design chart for  $\theta''$  Case 9 (AISC Steel Design Guide Series 9)

**Case 9**  $\theta''' \times \left( \frac{GJ}{T} \times a^2 \right)$   
 $\alpha = 1.0$



Torsional End Restraints		Concentrated torque at $\alpha = 1.0$ on member with fixed and free ends
Left End	Right End	
Fixed $\theta = \theta' = 0$	Free $\theta'' = 0$	

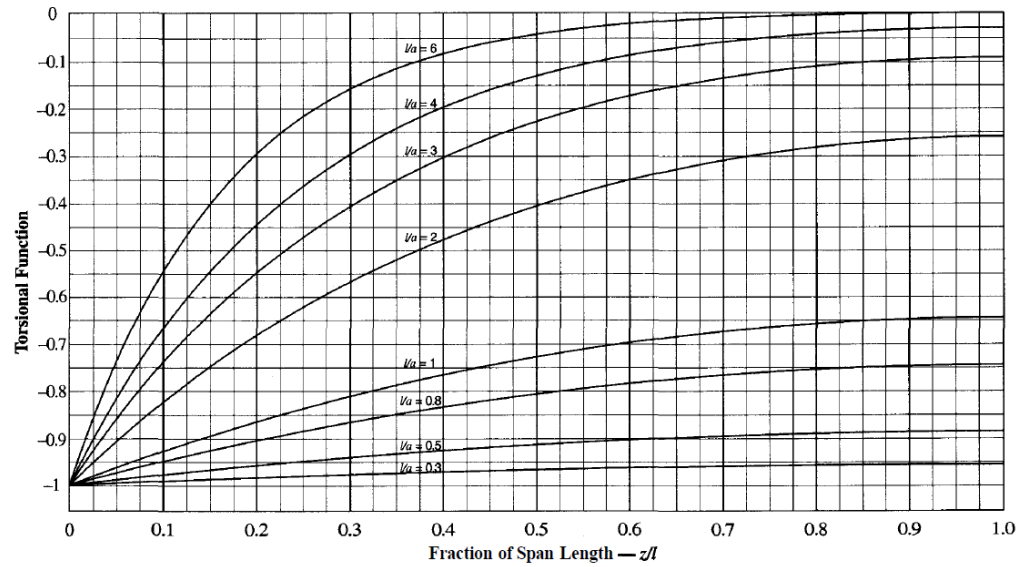


Figure E.15: Design chart for  $\theta'''$  Case 9 (AISC Steel Design Guide Series 9)

**APPENDIX F – TORSIONAL STIFFNESS OF AN I-SECTION**

Finite element calculations were run to determine the stiffness of an I-section with and without openings in the web. The cross section of the I-section was modeled with the same dimensions as the one used in the test setup. The length of the I-section matches the length of the vertical rebuilt for the tests in the laboratory. To determine the stiffness of the two different I-sections, zero plasticity in the material was assumed.

It must be mentioned that the web perforations did not have a great impact on the overall stiffness of the I-section. However, impacts of the boundary conditions were far greater. Therefore, the boundary conditions were chosen similar to those in the test setup. An endplate was placed onto one side of the I-section. The center point of the endplate and the I-section were located at the same place. At this location, the first boundary condition was placed (BC1). The displacements in all directions were restrained ( $U_x=0$ ,  $U_y=0$ ,  $U_z=0$ ; where  $U$  is the variable for displacement and the subscript is the axis in which the displacement is restrained), but the rotations were left unrestrained. On the other end of the I-section (BC2), the top and the bottom flange was restrained rigidly ( $U_x=0$ ,  $U_y=0$ ,  $U_z=0$ ;  $UR_x=0$ ,  $UR_y=0$ ,  $UR_z=0$ ; where  $UR$  is the variable for the rotational displacement and the subscript is the axis in which the rotation is restrained). The web was left unrestrained. A schematic drawing of the model is shown in Figure F.1.

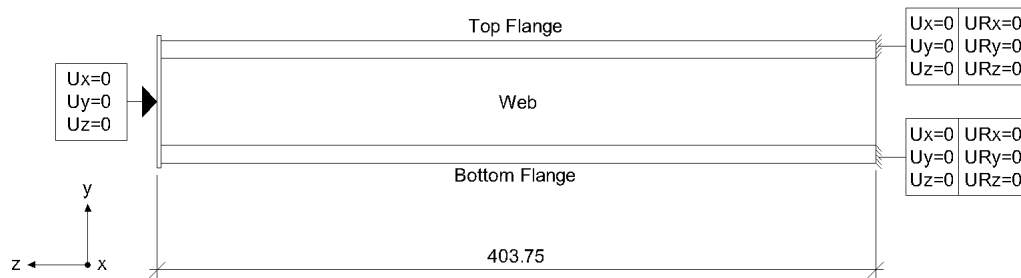


Figure F.1: Schematic drawing of the I-section boundary conditions

These boundary conditions were assumed to be close to the ones used in the test-setup.

To build these models steel was used as a material. All material properties are listed in Table F.1

Table F.1: Material properties used in the torsional stiffness of an I-section models

<b>Description:</b>	<b>Variable:</b>	<b>Value:</b>
Modulus of elasticity for steel	$E_s$	200000 MPa (29000 ksi)
Poisson's ratio for steel	$\nu_s$	0.3
Material properties for steel	$f_y / f_u$	N/A (elastic behavior)

All chosen dimensions are listed in Table 4.2. The decrease of the web area due to the perforations was calculated and is given in Table 4.2.

Table F.2: General sectional and overall dimensions of the experimental-setup FEA models

<b>Description:</b>	<b>Variable:</b>	<b>Dimension:</b>
Total length (with endplate)	$L_{setup}$	10255.3 mm / (403 $\frac{3}{4}$ in)
Length of the I-section	$L_{I-section}$	10236.2 mm / (403 in)
Total depth of I-section	$d_{I-section}$	657.2 mm / (25 $\frac{7}{8}$ in)
Flange width	$b_f$	406.4 mm / (16 in)
Flange thickness	$t_f$	12.7 mm / (1/2 in)
Web height	$h$	631.8 mm / (24 $\frac{7}{8}$ in)
Web thickness	$t_w$	7.9 mm / (5/16 in)
Endplate thickness	$t_{endplate}$	19.1 mm / (3/4 in)
Area of one perforation	$A_{perforation}$	150386.8 mm <sup>2</sup> / (233.1 in <sup>2</sup> )
Web area without perforations	$A_{web,tot}$	6467487.1 mm <sup>2</sup> / (10024.6 in <sup>2</sup> )
Web area with perforations	$A_{web,net}$	5264406.4 mm <sup>2</sup> / (8159.8 in <sup>2</sup> )
Decrease of web area	-	18.6 %

The model was loaded at the endplate, as was done in experimental testing. A moment of 50 kip-inches was applied at the center of the endplate and the rotation at this location was measured ( $UR_z$ ). The model without perforations is shown in Figure F.2, and the model with perforations in Figure F.3.

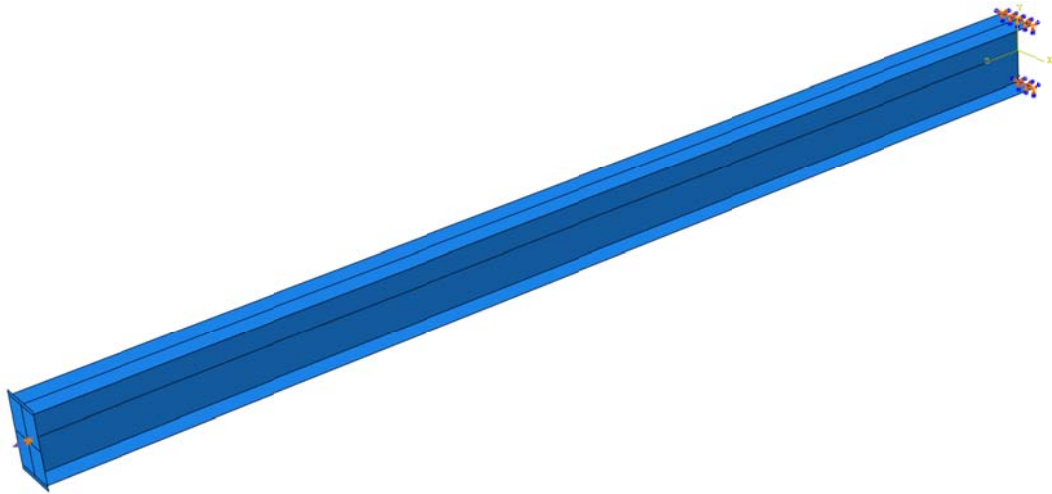


Figure F.2: FE model of an I-section without web perforations, used to determine beam stiffness

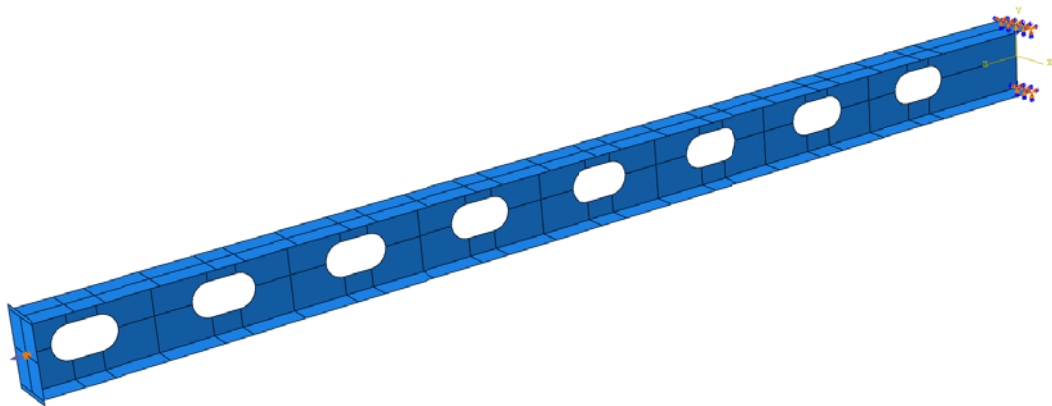


Figure F.3: FE model of an I-section with web perforations, used to determine beam stiffness

For the I-section without perforations, a torsional stiffness of 11.11 kN-m/rad (98.3 kip-in/rad) was found.

For the I-section with perforations, a torsional stiffness was determined to be 11.04 kN-m/rad (97.7 kip-in/rad) as. Therefore, the torsional stiffness of the I-section was reduced by 0.6 % by including the web perforations.



Considering these results, the finite element models for the experimental setup and the existing vertical could have been modeled without perforations in the I-section web. However, since the web perforations influence the natural frequency of the I-section, the perforations were included.